

RIGA TECHNICAL UNIVERSITY
Faculty of Civil Engineering
Department of Geomatics

Diana HARITONOVA
PhD Student of Doctoral Study Program “Construction”

**EVALUATION OF HIGH-PRECISION
TECHNIQUE APPLICATION FOR
OBSERVATIONS OF EARTH’S CRUST
MOVEMENTS IN LATVIA**

Doctoral Thesis

Scientific supervisor
Prof. Dr. phys. **J. BALODIS**

Riga 2016

ANNOTATION

The Doctoral Thesis focuses on geodynamic phenomena. Geodynamics covers a lot of processes operating continuously in the Earth's system. Within the frames of the Thesis the research on crustal motion, reference frames, postglacial rebound, and sea level variations has been carried out. To this end, the application of two principal space geodetic techniques – Global Navigation Satellite System (GNSS) and Satellite Laser Ranging (SLR) – has been particularly considered.

Two Latvian GNSS permanent networks: EUPOS[®]-Riga and LatPos, which have been operating since 2006, provide a distinct advantage for monitoring and data capture. The networks serve primarily as geodetic reference networks established for surveying and navigation purposes in the territory of Latvia. However, according to the worldwide experience and growing trends in space geodesy, it is commonly accepted to apply GNSS stations for the studies of geophysical processes as well.

The objective of the Thesis is to discover the geodynamic processes of the Earth's crust in the territory of Latvia, occurred due to Fennoscandian land uplift phenomenon at the coast of the Baltic Sea, by way of using the Latvian GNSS permanent station coordinate time series computed with reference to EUREF Permanent Network (EPN) and by obtaining the Earth's crust displacements, as well as to design an additional monitoring device for observations in relation to the International Laser Ranging Service (ILRS) network.

To achieve the stated objective the displacements of EUPOS[®]-Riga and LatPos stations obtained using continuous GNSS observations have been summarized for the period of eight years, or more precisely – from 2008 to 2015. For this purpose two solutions are distinctly presented: EUPOS[®] Combination Centre (ECC) cumulative weekly solution (2008–2014) and re-processed daily solution (2012–2015).

Latvia is located in the area exposed to ongoing relaxation of the Earth in response to the past ice mass loss, i.e., Glacial Isostatic Adjustment (GIA). The effect rates up to ~10 mm/yr in the vertical direction in northern Scandinavia. The comparison of obtained results from GNSS time series with the data retrieved from the deformation model NKG_RF03vel has been presented to support the Thesis.

Referring to the deformation model NKG_RF03vel, the vertical velocities of the Latvian GNSS stations have a range of 1.68 mm/yr, i.e., minimum +0.04 mm/yr and maximum +1.72 mm/yr. According to the daily solution, the vertical velocities of the Latvian western GNSS stations correlate to the data of NKG_RF03vel. The highest velocity differences in the

vertical component between the obtained results and values from the model are more pronounced in the case of the stations located in the south-eastern part of Latvia. However, the differences are less than 1 mm/yr. The horizontal velocities delivered by the weekly solution demonstrate comparatively adequate correlation to the NKG_RF03vel velocity field. This is the case study given in Chapter 3.

Such geodynamic effect as the ocean tide loading is commonly removed from GNSS measurements pursuant to the recommendations disclosed by IERS Conventions. At the same time, there is also the effect of non-tidal ocean loading variation having its own impact on geodetic observations. The Baltic Sea exhibits a number of remarkable phenomena. One of them is the sea level variations due to winds, complicated by the shape of gulfs and islands. Under this influence, the range of the sea level variations can reach 3 m on the coasts of gulfs. However, the tidal variations of the Baltic Sea range in the order of centimetres only. Chapter 4, provided herein, gives clear description of the water level variations of the Baltic Sea at the Latvian coast, which is potential enough to facilitate further research on the influence of the Baltic Sea loading on the GNSS coordinate time series.

To support this study, using hourly time series of the sea level records from seven Latvian coastal hydrological stations and employing spectral analysis, it has become feasible to identify diurnal and semi-diurnal tide existence both in the Gulf of Riga and the Baltic Sea at the Latvian coast. Totally, four main tidal constituents (O_1 , K_1 , M_2 and S_2) have been identified. Additionally, non-tidal frequency of five cycles per day has been detected in the sea level time series of the stations located in the Gulf of Riga.

The main results of the development of a universal satellite laser ranging device are interpreted in the last Chapter. In the capacity of a well-proven geodetic technique, SLR offers a significant potential to contribute to the scientific studies of the solid Earth, its ocean and atmospheric systems. As SLR enables the most accurate determination of the geocentric positions of the Earth satellites, it truly provides a reliable reference system to monitor the postglacial rebound, sea level and ice volume changes.

This Chapter aims to provide an overview of the observation methods and explicate the design of a new multi-purpose optical tracking system intended for both positional and laser ranging observations of near-Earth objects. Moreover, the key findings derived from the functionality tests of an astrometric subsystem have been interpreted here.

The Thesis includes 61 figure, 26 formulas, 9 tables, and 2 appendices. The total volume of the Thesis is 136 pages.

ANOTĀCIJA

Promocijas darbs fokusēts uz ģeodinamisko parādību izpēti. Ģeodinamika pēta vairākus procesus, kas nepārtraukti notiek sistēmā Zeme. Šajā darbā ir veikta izpēte par garozas kustībām, atbalsta sistēmām, pēcgliaciālo noregulēšanos un jūras līmeņa svārstībām. Ir apskatīts divu galveno kosmiskās ģeodēzijas tehnoloģiju pielietojums: Globālās Navigācijas Satelītu Sistēmas (GNSS) un Satelītu lāzerlokācijas (SLR).

Divi Latvijas pastāvīgās darbības GNSS tīkli: *EUPOS*[®]-*Riga* un *LatPos*, kas darbojas kopš 2006. gada, sniedz svarīgu iespēju novērošanai un datu iegūšanai. Šie tīkli, pamatā, ir ģeodēziskie atbalsta tīkli, kas ierīkoti uzmērīšanas un navigācijas mērķiem Latvijas teritorijā. Tomēr saskaņā ar pasaules pieredzi un augošām tendencēm kosmiskajā ģeodēzijā, ir vispārēji pieņemts izmantot GNSS stacijas arī ģeofizikālo procesu pētījumiem.

Darba mērķis ir izpētīt Zemes garozas ģeodinamiskos procesus Latvijas teritorijā, kas notiek Fennoskandijas zemes pacelšanās efekta ietekmē Baltijas jūras krastā, izmantojot Latvijas GNSS pastāvīgās darbības staciju koordinātu laika sērijas, aprēķinātas attiecībā pret *EUREF* pastāvīgās darbības tīklu (*EPN*), un iegūstot Zemes garozas pārvietojumus, kā arī uzprojektēt papildu monitoringa iekārtu, paredzētu novērojumiem Starptautiskā lāzerlokācijas servisa (*ILRS*) tīklā.

Izvirzītā mērķa sasniegšanai, *EUPOS*[®]-*Riga* un *LatPos* staciju pārvietojumi, kas iegūti no nepārtrauktiem GNSS novērojumiem, tika apkopoti astoņu gadu periodam – no 2008. līdz 2015. gadam. Šim nolūkam ir doti divi risinājumi: *EUPOS*[®] kombinēšanas centra (*ECC*) kumulatīvais iknedēļas risinājums (2008.–2014.) un pārrēķinātais ikdienas risinājums (2012.–2015.).

Latvija atrodas reģionā, kas pakļauts Zemes relaksācijas efektam, notiekošajam ledāja segas spiediena izzušanas ietekmē, t. i., glaciālajai izostatiskajai noregulēšanai (*GIA*). Šī efekta ātrums vertikālajā virzienā sasniedz līdz ~10 mm gadā Skandināvijas ziemeļu daļā. Promocijas darbā ir dots iegūto rezultātu no GNSS laika sērijām salīdzinājums ar datiem no deformācijas modeļa *NKG_RF03vel*.

Saskaņā ar deformācijas modeli *NKG_RF03vel* Latvijas GNSS staciju vertikālie ātrumi atrodas diapazonā 1,68 mm gadā, t. i., no +0,04 mm līdz +1,72 mm gadā. Saskaņā ar ikdienas risinājumu Latvijas rietumu daļas GNSS staciju vertikālie pārvietojumi atbilst *NKG_RF03vel* datiem. Vislielākās ātrumu starpības vertikālajai komponentei starp iegūtajiem rezultātiem un vērtībām no modeļa ir vairāk izteiktas to staciju gadījumā, kas atrodas Latvijas dienvidaustrumu daļā. Tomēr šīs starpības ir mazākas par 1 mm gadā. Salīdzinoši labi *NKG_RF03vel* ātrumu

laukam atbilst staciju horizontālie ātrumi, kas iegūti iknedēļas risinājumā. Šī pētījuma rezultāti ir apkopoti darba 3. nodaļā.

Tāds ģeodinamiskais efekts, kā okeānu plūdmaiņu spiediens, parasti tiek izslēgts no GNSS mērījumiem saskaņā ar *IERS* Konvenciju rekomendācijām. Bet pastāv vēl okeānu spiediena bezplūdmaiņu svārstību efekts, kuram ir sava ietekme uz ģeodēziskajiem novērojumiem. Baltijas jūrai ir raksturīgas vairākas ievērojamas parādības. Viena no tām ir jūras līmeņa svārstības vēju ietekmē, kas iespaidojas no līču un salu sarežģītām formām. Šo faktoru ietekmē jūras līmeņa svārstību diapazons var sasniegt 3 m līču krastos. Savukārt Baltijas jūras plūdmaiņu svārstības atrodas tikai dažu centimetru diapazonā.

4. nodaļā sniegts Baltijas jūras ūdens līmeņa svārstību Latvijas piekrastē raksturojums, kas ir potenciāli pietiekams, lai rosinātu turpmāko izpēti par Baltijas jūras spiediena ietekmi uz GNSS koordinātu laika sērijām.

Šā pētījuma ietvaros, izmantojot jūras līmeņa ierakstu stundu laika sērijas no septiņām Latvijas piekrastes hidroloģiskajām stacijām un pielietojot spektrālo analīzi, bija iespējams identificēt diennakts un pus-diennakts plūdmaiņu esamību gan Rīgas līcī, gan Baltijas jūrā Latvijas piekrastē. Kopumā tika identificēti četri galvenie plūdmaiņu viļņi (O_1 , K_1 , M_2 , S_2). Papildu frekvence – pieci cikli dienā, kas neatbilst plūdmaiņu frekvencei, tika identificēta jūras līmeņa laika sērijās stacijām, kas atrodas Rīgas līcī.

Pēdējā nodaļā ir aprakstīti unificētas satelītu lāzera tālmēra konstrukcijas izstrādes galvenie rezultāti.

Kā pārbaudītā ģeodēzijas tehnoloģija Satelītu lāzerlokācija (*SLR*) sniedz ievērojamu potenciālu zinātniskiem pētījumiem par cieto Zemi, tās okeānu un atmosfēras sistēmām. Satelītu lāzerlokācija ļauj visprecīzāk noteikt Zemes satelītu ģeocentriskās pozīcijas, tāpēc tā nodrošina stabilu atbalsta sistēmu pēcgliaciālās noregulēšanās, jūras līmeņa un ledus apjoma izmaiņu monitoringam.

Šīs nodaļas mērķis ir sniegt novērojumu metožu aprakstu un izklāstu par jaunas multifunkcionālās optiskās novērošanas sistēmas dizainu, kas paredzēta Zemei tuvo objektu pozicionāliem un lāzertālmēra novērojumiem, kā arī apkopot astrometriskās apakšsistēmas funkcionālu testu galvenos rezultātus.

Promocijas darbs ietver 61 attēlu, 26 formulas, deviņas tabulas un divus pielikumus. Darba kopējais apjoms ir 136 lappuses.

ACKNOWLEDGMENTS

This work was carried out at the Institute of Geodesy and Geoinformatics of the University of Latvia. First of all, I would like to express my special thanks to my scientific supervisor Professor Dr. phys. Janis Balodis, who has motivated me during all collaboration period through the years.

A number of people have been helpful during this work.

I would like to express my gratitude to Katerina Morozova and Izolde Jumare for their support in GNSS data management and processing. Regarding GNSS data analysis, I am grateful for all the help and support provided by Lotti Jivall from Lantmäteriet, Sweden.

I would like to thank Professor Dr. Bruno Meurers from the Department of Meteorology and Geophysics of the University of Vienna for wholesome progress advice during my stay in Vienna and provision of the executable code useful for the Earth tide effect analysis.

I am grateful for the financial support provided by the ESF project “Establishment of scientific group for development of universal satellite laser ranging device” and the project Fotonika-LV. Moreover, I would like to thank Ansis Zarins and Augusts Rubans for my involvement and guidance in the course of the project on the satellite laser ranging device, for their kind attitude and valuable support.

Riga, December 2016

Diana Haritonova

CONTENTS

ACRONYMS	9
INTRODUCTION.....	11
Subject topicality and formulation of the problem.....	11
Objective and tasks of the Doctoral Thesis	12
Scientific novelty of the Thesis	12
Practical relevance of the Doctoral Thesis	13
1. GEODYNAMICS	15
1.1. Recent crustal movements.....	15
1.2. Reference frame definition.....	16
1.3. Postglacial rebound	21
1.4. Effect of the ocean tides	25
2. GNSS.....	27
2.1. Introduction	27
2.2. GPS signal structure	30
2.3. Atmospheric effects.....	33
2.4. Multipath.....	34
2.5. Relative positioning.....	35
3. EARTH'S SURFACE MOVEMENTS AT THE LATVIAN GNSS STATIONS	37
3.1. Participation in EUPOS [®] ECC	37
3.2. Latvian GNSS networks.....	39
3.3. Network solution and data processing	41
3.4. Results and discussion.....	46
3.4.1. Velocity fields.....	46
3.4.2. GNSS time series and site-specific effects	53
3.5. Conclusions	56
4. SEA LEVEL VARIATIONS AT THE LATVIAN COASTAL HYDROLOGICAL STATIONS.....	57
4.1. Introduction	57
4.2. Data selection and processing	59
4.3. Results and discussion.....	61
4.4. Conclusions	66
5. DESIGN OF A NEW MULTI-PURPOSE OPTICAL TRACKING SYSTEM.....	67
5.1. Methods and their importance.....	67

5.1.1. CCD technology.....	67
5.1.2. Laser ranging	70
5.2. Design of the new instrument.....	71
5.2.1. Deformations of optical system's transmitting path	73
5.3. Control software main modules	75
5.4. Field tests of astrometric subsystem.....	78
5.4.1. Star image acquisition tests.....	78
5.4.2. Mount error model	81
5.5. Conclusions	86
MAIN CONCLUSIONS	87
APPENDICES.....	89
Appendix A	90
Appendix B	95
LIST OF REFERENCES OF THE THESIS.....	126
CONFIRMATION/APSTIPRINĀJUMS.....	136

ACRONYMS

BIFROST	Baseline Inferences for Fennoscandian Rebound, Sea level and Tectonics
CCD	Charge Coupled Device
CDMA	Code division multiple access
CIS	Conventional Inertial Reference System
CODE	Center for Orbit Determination in Europe
CPF	Consolidated Prediction Format
CTS	Conventional Terrestrial Reference System
DD	Double Difference
DGNSS	Differential GNSS
DORIS	Doppler Orbitography and Radiopositioning Integrated by Satellite
DTU	Technical University of Denmark
ECC	EUPOS [®] Combination Centre
EPN	EUREF Permanent Network
ETRF	European Terrestrial Reference Frame
ETRS	European Terrestrial Reference System
EUPOS	European Position Determination System
EUREF	Regional Reference Frame Sub-Commission for Europe
GALILEO	Europe's global navigation satellite system
GIA	Glacial Isostatic Adjustment
GLONASS	GLObalnaya NAVigatsionnaya Sputnikovaya Sistema, the Russian positioning system
GMF	Global Mapping Function
GNSS	Global Navigation Satellite System
GPS	Global Positioning System, the U.S. positioning system
IAG	International Association of Geodesy
IERS	International Earth Rotation and Reference Systems Service
IGS	International GNSS Service
ILRS	International Laser Ranging Service
ITRF	International Terrestrial Reference Frame
ITRS	International Terrestrial Reference System
IVS	International VLBI Service
LGM	Last Glacial Maximum

NAVSTAR	Navigation System by Timing and Ranging
NKG	Nordic Geodetic Commission
NOMAD	Naval Observatory Merged Astrometric Dataset
NOVAS	Naval Observatory Vector Astrometry Software
OTA	Optical Tube Assembly
PPP	Precise Point Positioning
PRN	Pseudorandom Noise
RINEX	Receiver INdependent EXchange format
RMS	Root Mean Square
SINEX	Solution (Software/technique) INdependent EXchange format
SLR	Satellite Laser Ranging
TWG	Technical Working Group
USB	Universal Serial Bus
VLBI	Very Long Baseline Interferometry

INTRODUCTION

Subject topicality and formulation of the problem

Geodesy, with its main task to measure the planet Earth, has experienced remarkable development over the past 60 years since 1957, when the first artificial Earth satellite was launched into the orbit. Thereafter, thousands of satellites of various shapes, weights and payloads have been launched into various orbits to accomplish different exploratory missions.

The NAVSTAR first Global Positioning System (GPS) satellite was launched in 1978. Based on the development of GPS satellite observations, a new international organization – International GPS Service – was established in 1991 for the purpose of collecting the GPS observation results from all around the world; currently – International GNSS Service (IGS) based on the multiple Global Navigation Satellite Systems. The International Laser Ranging Service (ILRS) and International Very Long Baseline Interferometry Service (IVS) were established as well.

On the basis of this international scientific cooperation, the International Terrestrial Reference Frame (ITRF) has been created, and now it is becoming the object of continuous monitoring. At present, the detailed studies of the territory of each country have become available by way of collecting and analysing the time series of continuous satellite observation data.

Nowadays, the satellite orbit measurement back coupling with the site position observations provides an excellent way to determine coordinates with millimetre accuracy. This allows discovering the shape of the Earth in details and to gather data required for the studies of its interior structure. Besides, repeatedly performed geodetic observations enable to detect significant changes occurring on the Earth, such as movements of continents, horizontal and vertical displacements of the Earth's surface, coastline displacements of the oceans and seas, as well as to identify other geodynamic processes.

The application of space geodetic techniques in the field of sciences dealing with the planet Earth furthers more and more practical benefits for people around the world. One of these benefits is the possibility of establishing a unified terrestrial reference frame. As the Earth's surface is divided into tectonic plates and is affected by the internal forces occurring therein, the coordinate frame undergoes a change. The most difficult task is to define changes in the height component of coordinates. This is mostly due to fact that the Earth's surface dynamics is closely associated with the gravitational attraction from the Sun, the Moon and

other objects, global and local mass redistribution, and global and seasonal climate changes as well. Therefore, the determination of height component and representation of its variations attract the scientific interest today.

Objective and tasks of the Doctoral Thesis

The objective of the Thesis is to discover the geodynamic processes of the Earth's crust in the territory of Latvia, occurred due to Fennoscandian land uplift phenomenon at the coast of the Baltic Sea, by way of using the Latvian GNSS permanent station coordinate time series computed with reference to EUREF Permanent Network (EPN) and by obtaining the Earth's crust displacements, as well as to design an additional monitoring device for observations in relation to the International Laser Ranging Service (ILRS) network.

To achieve the objective, the solution of the following tasks is proposed:

- 1) to compute EUPOS[®]-Riga and LatPos permanent station coordinates with reference to EUREF Permanent Network (EPN), considering different impact sources, and summarize the results for a whole observation period from 2008 to 2015, giving the station horizontal and vertical velocities;
- 2) to produce a catalogue containing information on EUPOS[®]-Riga and LatPos station location and their position time series;
- 3) to evaluate the correlation of the Latvian GNSS station displacements to the data of deformation model NKG_RF03vel;
- 4) to characterize the water level variations of the Baltic Sea at the Latvian coast on the basis of the sea level station observation data and by employing spectral analysis;
- 5) to design the experimental instrument of a new original multi-purpose optical tracking system intended for both positional and laser ranging observations of near-Earth objects.

Scientific novelty of the Thesis

The scientific novelty of the present Doctoral Thesis is based on the following achievements:

- 1) the data on the Latvian GNSS station horizontal and vertical velocity fields has been formalized for the first time as a basis for the high-precision coordinate determination;

- 2) the catalogue containing information on EUPOS[®]-Riga and LatPos station location and their position time series has been prepared. In this context, the verification of GNSS station stability is given;
- 3) the correlation of the Latvian GNSS station displacements with the data of the deformation model NKG_RF03vel has been efficiently evaluated;
- 4) the description of the sea level variations at the Latvian coast has been given. It complements the earlier results concerning the dynamics of the Baltic Sea in this region, as it is based on the observations obtained along all Latvian coastal zone, as well as it is potential enough to facilitate further research on the influence of the Baltic Sea loading on GNSS coordinate time series;
- 5) the innovative and universal satellite laser ranging device with original optical scheme with three optical channels, i.e., one transmitter and two receivers, has been designed. The one of the twin optical systems is fitted with a CCD and used for astrometric purposes, but the other is fitted with a reflected light pulse detector and will be used for SLR pulse processing. The new satellite laser ranging device provides an efficient way to collect relevant geodynamic data for the vertical movement studies in the global ILRS network.

Practical relevance of the Doctoral Thesis

In the same way as other Member states of the European Union, the Latvian Geospatial Information Agency (LGIA) from Latvian side in cooperation with IAG Regional Reference Frame Sub-Commission for Europe (EUREF) tends to focus on the realization of a modern and precise continental reference frame in Europe through the establishment and maintenance of European Terrestrial Reference System (ETRS89) and European Vertical Reference System (EVRS). ETRS89 provides geocentric three-dimensional positions with millimetre accuracy in the homogeneous reference system for the whole Europe, and EVRS does the same for the height component. These systems provide a basis for geo-referencing in Europe. ETRS89 is commonly used for modern mapping and Earth science applications. EUREF Permanent Network (EPN), as a key instrument in maintaining ETRS89, empowers conditions for the European cooperation in the International GNSS Service (IGS) and contributes to the realization of the International Terrestrial Reference System (ITRS), as well as to the monitoring of tectonic deformations in Europe, long-term climate monitoring and development of the standards and the operational means to disseminate GNSS data (EUREF, 2008).

The main practical gain as a result of reaching the objective of the Doctoral Thesis is the data on the Latvian GNSS station horizontal and vertical velocity fields, which gives an understanding of the geodynamic processes having occurred due to Fennoscandian land uplift phenomenon in the territory of Latvia, and serves as a basis for the high-precision coordinate determination.

The verification of GNSS station stability given in the Thesis according to the data of the produced catalogue and the station residual position RMS values could be taken into account during selection of a new site for the GNSS station installation.

The given description of the sea level variations at the Latvian coast could facilitate further research on the influence of the Baltic Sea loading on GNSS coordinate time series.

The demanding accuracy requirements in determining the geodetic and geodynamic parameters, as well as continuous improvements in the field of geopotential models, nutation and loading phenomenon models, have strongly necessitated the scientific examination of the comparative analysis of different strategies applied for the monitoring procedure. As each of the space geodetic techniques (GNSS, SLR, etc.) enjoys its own features and advantages in parameter determination, it is highly relevant through the optimal way to combine all observation resources.

The developments in the Thesis are the necessary base for further implementation of the GNSS and SLR observations in one combination. Furthermore, as the designed new satellite laser ranging device can be mobile, it provides the possibility of performing the observations at different sites, in that way contributing to the densification of the International Laser Ranging Service (ILRS) network.

1. GEODYNAMICS

Geodynamics is a science dealing with the processes operating in the Earth's system. Geodynamics can be divided into: core dynamics, mantle dynamics, lithosphere dynamics, hydrosphere dynamics, atmospheric dynamics and dynamics of the space environment surrounding Earth. Within this Chapter the topics on crustal motion, reference frames, postglacial rebound and ocean tides are summarized.

1.1. Recent crustal movements

The increasing accuracy of the satellite-based geodetic positioning techniques makes it possible to derive the information on the crustal motions from repeated or continuous observations. The following main fields of the application for crustal motion monitoring can be identified (Seeber 2003):

- a) global and continental plate motion and deformation analysis,
- b) regional crustal motion analysis, and
- c) local monitoring of deformation and subsidence.

The first group (a) shows very impressive results after a couple of years of observations. The comparisons between GPS and other space techniques like VLBI and SLR demonstrate an agreement at the centimetre level, and hence prove the capability of GPS for global geodynamics (Boucher *et al.* 1999).

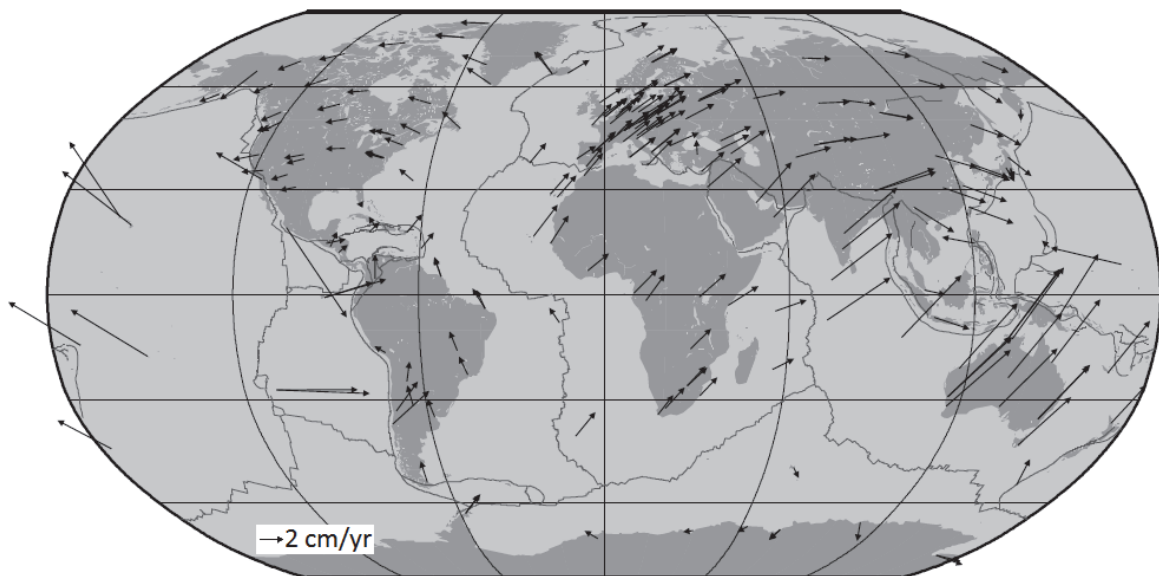


Figure 1.1. Velocity field obtained from the weekly coordinate solutions at CODE within the years 2002 to 2006 (Beutler *et al.* 2007)

A major break-through came with the establishment of the International GNSS Service (IGS). More than 300 globally distributed stations deliver data on a permanent basis and as such provide a continuous monitor of deformation. The station velocities can be used to compute global stress maps and to determine a kinematic model of the individual plate rotation vectors. Figure 1.1 shows the global velocity field obtained from the weekly coordinate solutions at the Center for Orbit Determination in Europe (CODE) within the years 2002 to 2006.

The projects of the second group (b) have already shown significant results. The analysis and continuous measurements have been started in nearly all tectonically active parts of the world.

The projects of the third group (c) belong in most cases to the field of deformation analysis in engineering surveying. The potential application areas involve monitoring of land subsidence, e.g. in mining areas and oil fields, hang sliding, and local geotectonics (Seeber 2003).

1.2. Reference frame definition

A reference frame means the practical realization of a reference system through observations. It consists of a set of identifiable fiducial points on the sky (e.g. stars, quasars) or on the Earth's surface (e.g. fundamental stations). It is described by a catalogue of precise positions and motions at a specific epoch. In satellite geodesy two fundamental systems are required:

- a) a space-fixed, Conventional Inertial Reference System (CIS) for the description of satellite motion, and
- b) an Earth-fixed, Conventional Terrestrial Reference System (CTS) for the positions of the observation stations and for the description of results from satellite geodesy.

A suitable Earth-fixed reference system must be connected in a well-defined way to the Earth's crust. Such CTS can be realized through a set of Cartesian coordinates of fundamental stations or markers within a global network.

The conventional terrestrial reference system, established and maintained by the International Earth Rotation and Reference Systems Service (IERS) and nearly exclusively used for today's scientific and practical purposes, is the International Terrestrial Reference System (ITRS); its realization is the International Terrestrial Reference Frame (ITRF).

Each new ITRF is realized based on new observations with space geodetic techniques such as DORIS, GPS, SLR and VLBI. The result is published under the denomination ITRF_{yy}, where yy means the last digits of the year, whose data were used in the formation of the frame (Seeber 2003).

Figure 1.2 displays ITRF2008, which is composed of 934 stations located at 580 sites with an imbalanced distribution between the northern (463 sites) and the southern hemisphere (117 sites).

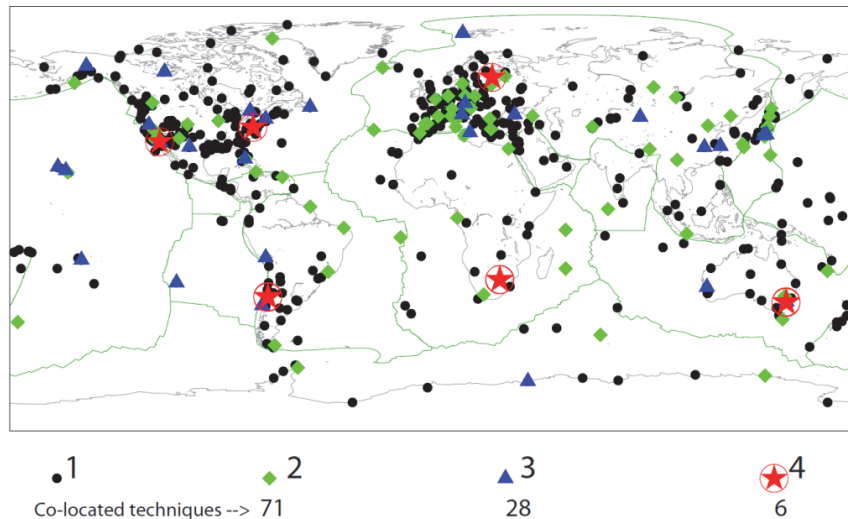


Figure 1.2. ITRF2008 sites and co-located techniques: 1 technique is marked with a circle (475), 2 co-located techniques – with a diamond (71), 3 – with a triangle (28) and 4 – with a star (6) (Petit and Luzum 2010)

Since today's geodetic space techniques provide station coordinates at the 1-cm or sub-centimetre level, it is necessary to model the various deformations at the millimetre level. The main influences are

- a) global plate tectonics,
- b) solid Earth tides,
- c) ocean and atmospheric loading effects,
- d) polar tides,
- e) regional and local effects.

The detailed models and algorithms for these effects are given in the IERS Conventions (Petit and Luzum 2010).

According to Boucher *et al.* (1992), one can derive from each annual ITRF_{yy} a corresponding frame in ETRS89, which will be itself labelled ETRF_{yy} and is a regional realization of the ITRS for Europe.

In order to harmonize future realizations of the ETRS89 overall Europe, the EUREF Technical Working Group (TWG) recommends not to use the ETRF2005 and rather to adopt the ETRF2000 as a conventional frame of the ETRS89 system. This decision was taken by the TWG, noticing that the coordinate shifts at epochs posterior to 1989.0 occur between ETRFyy frames which are originally due to the equivalent shifts between the global ITRF frames. This is the example of coordinate shifts at epochs posterior to 1989.0 between ETRF2000 and ETRF2005. These shifts are due to the Z-translation rate of 1.8 mm/yr between ITRF2000 and ITRF2005, as well as the refined rotation rate values (\dot{R}_{YY}). Therefore the adoption of the ETRF2000 as a conventional frame of the ETRS89 realization will minimize the coordinate shifts at epochs posterior to 1989.0 between different implementations of the ETRS89 in different European countries. Consequently, the European countries which will adopt the ETRS89 or want to redefine their national systems are encouraged to adopt the ETRF2000 frame and express their station coordinates in that frame (Boucher and Altamimi 2011).

The general procedure consists of two-step transformation:

- 1) transform ITRFyy coordinates at the central epoch of the used observations into ITRF2000 using the IERS/ITRF published values;
- 2) apply the usual transformation formula allowing transformation from ITRF2000 to ETRF2000.

In fact the two-step transformation procedure could be performed in one step using 14 transformation parameters. Table 1.1 lists 14 parameters to be used in transformation from ITRF2008 into ETRF2000.

Table 1.1

Transformation parameters from ITRF2008 to ETRF2000 at epoch 2000.0 and their rates/yr

	$T1$ mm	$T2$ mm	$T3$ mm	D 10^{-9}	$R1$ mas	$R2$ mas	$R3$ mas
ITRF2008	52.1	49.3	-58.5	1.34	0.891	5.390	-8.712
Rates	0.1	0.1	-1.8	0.08	0.081	0.490	-0.792

These parameters are computed by the summation of the transformation ITRF2008-to-ITRF2000 and ITRF2000-to-ETRF2000. The transformation ITRF2000-to-ETRF2000 consists of the translation parameters and the rotation rates, whereas the rotation parameters at epoch 2000.0 are computed by multiplying the rotation rates by 11 (i.e., 2000.0 – 1989.0).

The transformation parameters listed in Table 1.1 are expressed at epoch 2000.0. Since the transformation should be performed at the central epoch (t_c) of the used observations, then these transformation parameters should be propagated at epoch t_c , using:

$$P(t_c) = P(2000.0) + \dot{P} \cdot (t_c - 2000.0), \quad (1.1)$$

where \dot{P} designates the rate of any one of the 7 parameters. Therefore 7 parameters propagated at epoch t_c should be used to transform GNSS coordinates from ITRF2008 to ETRF2000 (Boucher and Altamimi 2011).

The general model for transformation from a system A to a system B is

$$\begin{pmatrix} X_B \\ Y_B \\ Z_B \end{pmatrix} = \begin{pmatrix} X_A \\ Y_A \\ Z_A \end{pmatrix} + \begin{pmatrix} T1_{A,B} \\ T2_{A,B} \\ T3_{A,B} \end{pmatrix} + \begin{pmatrix} D_{A,B} & -R3_{A,B} & R2_{A,B} \\ R3_{A,B} & D_{A,B} & -R1_{A,B} \\ -R2_{A,B} & R1_{A,B} & D_{A,B} \end{pmatrix} \cdot \begin{pmatrix} X_A \\ Y_A \\ Z_A \end{pmatrix}. \quad (1.2)$$

For example, the residual position time series of Latvian IGS station RIGA, which has been classified as a class A station by EUREF, in ITRF2008 and ETRF2000 are shown:

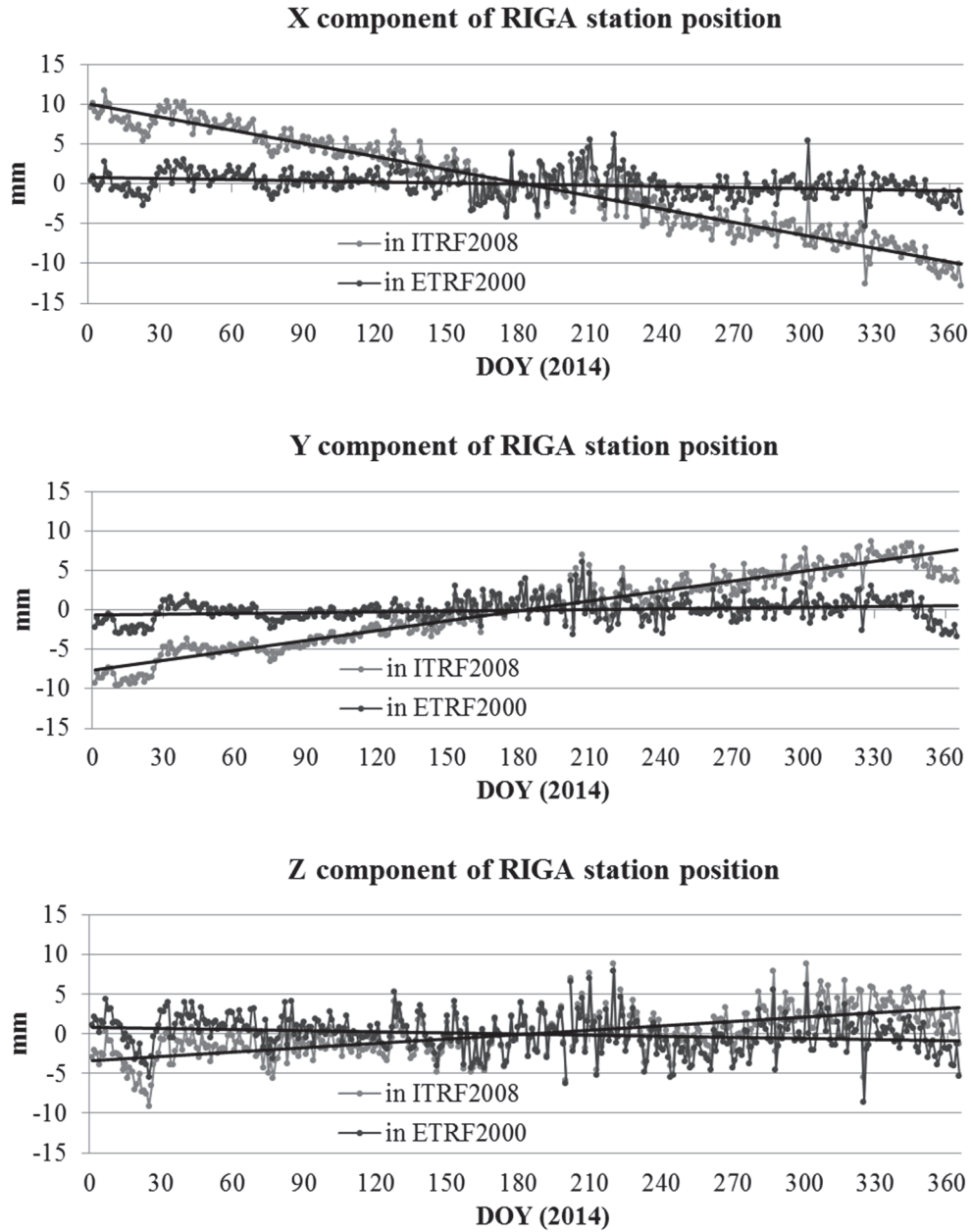


Figure 1.3. Daily time series of RIGA station position in X, Y and Z components (in mm) in ITRF2008 and ETRF2000 obtained with *Bernese GNSS Software v 5.2* for the year 2014: DOY – day of year (prepared by author)

1.3. Postglacial rebound

In Fennoscandia and Canada, the crust has been continuously rising since the deloading of the ice sheets at the end of the Ice Age (see Figure 1.4); a small contribution also comes from the deloading of sea water due to the crustal uplift itself. This phenomenon is well known as the postglacial rebound or the postglacial land uplift. It is mainly an isostatic rebound governed by the viscous properties of the mantle, to some extent modified by the presence of the elastic crust (Kakkuri 1993).

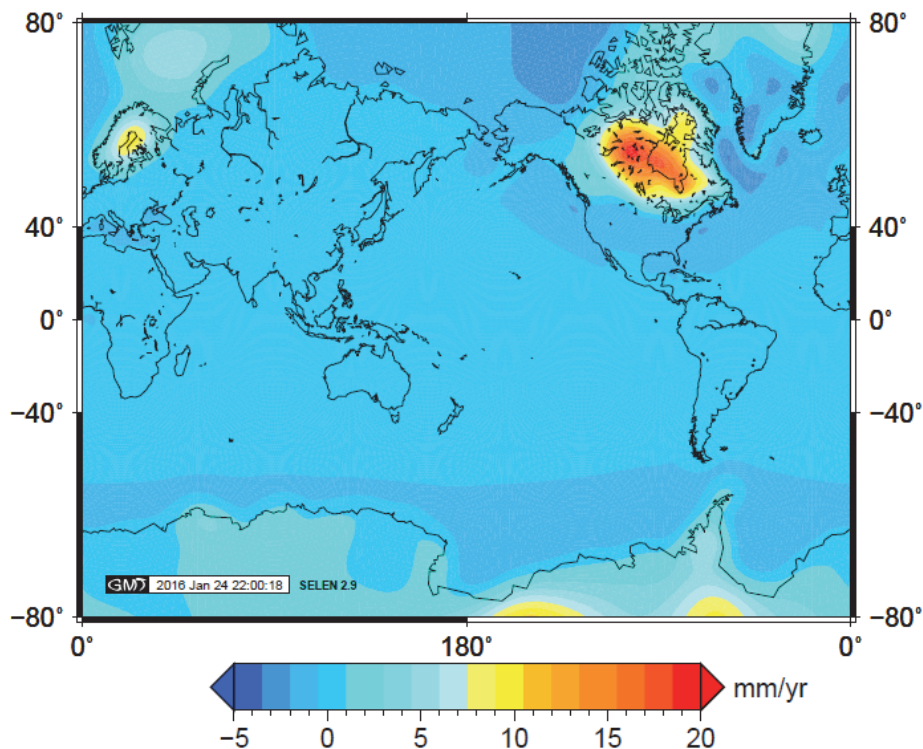


Figure 1.4. Global map of the GIA-induced rate of vertical displacement today: from -3.5 to $+19.2$ mm/yr (Spada and Melini 2013)

Land uplift is the only one of the processes related to Glacial Isostatic Adjustment (GIA), which is the response of the solid Earth to the changing mass of glaciers and ice sheets. The study of GIA is multi-disciplinary. GIA leads to changes in the gravity field, Earth rotation, and the stress in the crust, which can affect the sea level (Poutanen and Steffen 2014). Figure 1.5 represents the interaction between the effects involved. The GIA research includes the collection of high-quality datasets for its description, the development of glaciation histories in time and space, and the construction of Earth models (Steffen and Wu 2011).

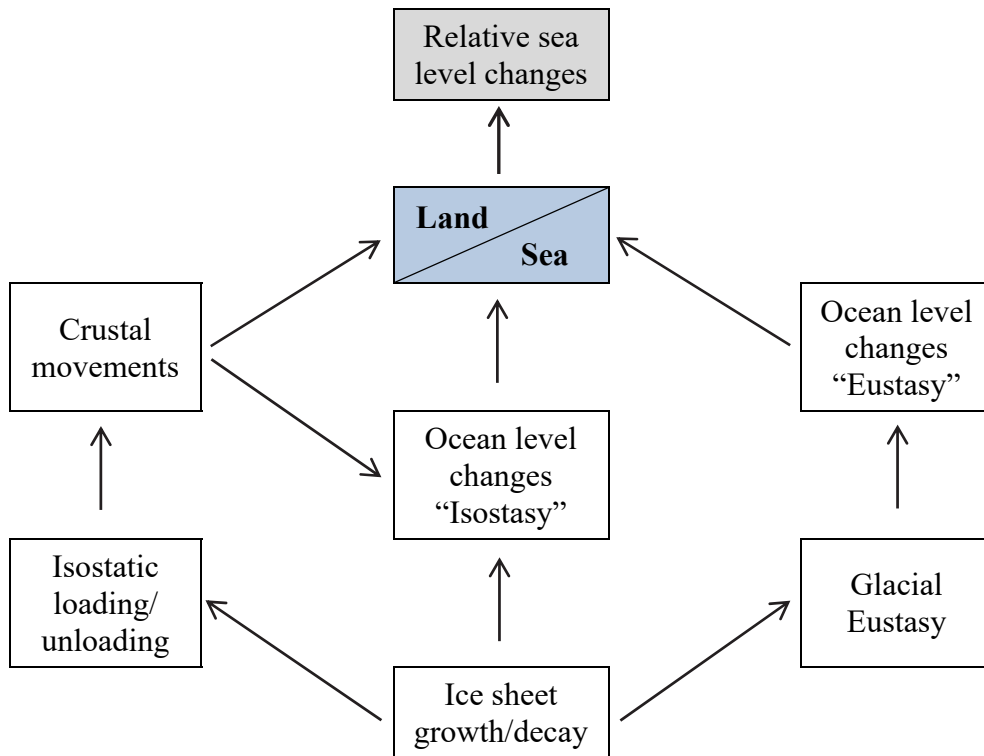


Figure 1.5. GIA and relative sea-level change (Steffen 2015)

Land uplift is the most notable geodynamic process in Fennoscandia (Poutanen and Steffen 2014). The source of land uplift today goes back to the times, when northern Europe was covered with a huge ice sheet. The Last Glacial Maximum (LGM), the time of maximum ice coverage in Fennoscandia, occurred about 20000 years ago. The ice thickness was about 2500–3000 m, and its weight pressed the crust down by 500–900 m. The melting period started 18000 years ago, and the central Gulf of Bothnia was ice-free about 10500 years ago (Peltier 1994; Berglund 2004).

The land uplift maximum is near the city of Umeå (Steffen and Wu 2011), where the current absolute uplift is about 10 mm/yr, and during the last century the uplift rate relative to the sea reached almost 9 mm/yr (Poutanen and Steffen 2014).

There are three different cases of land uplift: absolute, apparent and relative. Referring to the GNSS time series, one obtains the absolute uplift: height change of the crust relative to the mass centre of the Earth. By means of a tide gauge, one observes the apparent uplift; change of the shoreline relative to the mean sea level. Between the two tide gauges one can observe the uplift difference, the relative uplift. The apparent uplift differs from the absolute uplift due to the global eustatic sea level rise, the rise of the geoid, as well as steric effects (salinity and density changes due to the thermal expansion) (Nordman *et al.* 2014). The relation is, as follows

$$\dot{h} = \dot{H}_a + \dot{H}_e + \dot{N} + \dot{H}_s, \quad (1.3)$$

where

\dot{h} – absolute uplift;

\dot{H}_a – apparent uplift;

\dot{H}_e – eustatic rise of the sea level;

\dot{N} – rise of the geoid;

\dot{H}_s – possible changes in steric effects (often neglected).

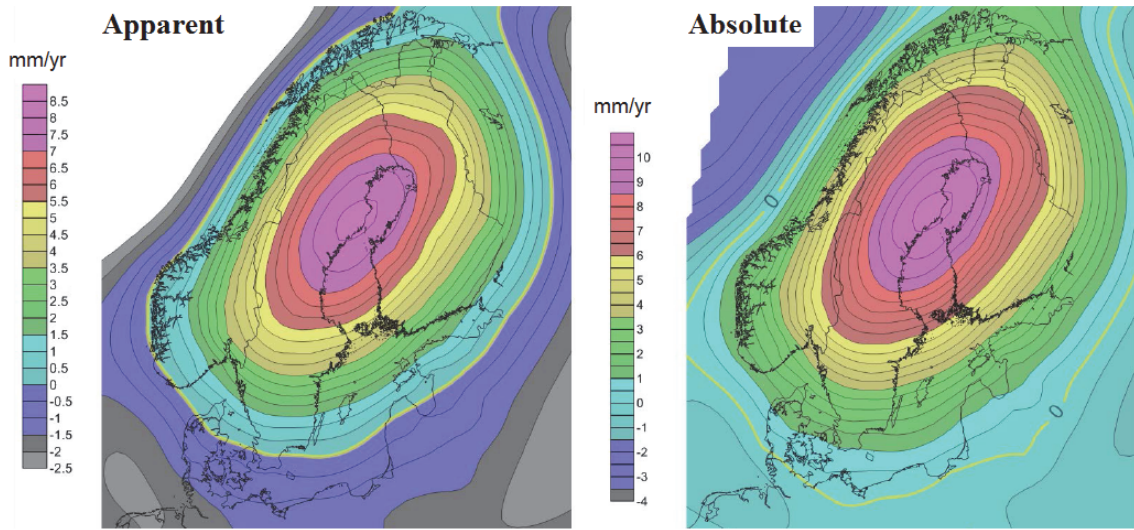


Figure 1.6. Apparent and absolute land uplifts from NKG2014LU_test (Vestøl *et al.* 2014)

Figure 1.6 represents the test model for Fennoscandian uplift, where the apparent (left) and absolute land uplifts (right) are shown.

Referring to relatively short (less than 10 years) time series of GNSS observations, the absolute uplift rate can be obtained more accurately than by means of a 100 year history of repeated precise levelling. For longer time scales, up to the LGM, indirect methods may be used, namely, the timing of ancient shorelines and geophysical modelling (Poutanen and Steffen 2014).

The thorough analysis of GNSS data provides the velocity field, which can indicate the uplift center and horizontal crustal motions due to the rebound. For this, the project BIFROST (Baseline Inferences for Fennoscandian Rebound Observations, Sea Level, and Tectonics) was initiated in 1993. Initially tens of permanent GPS stations separated by a few hundreds of km in Finland and Sweden were included in the network. Since then more stations in other countries have been included. The present-day rates of vertical and horizontal motion at the stations are averaged over the period of data collection to yield estimates accurate to a few tenths of mm/yr.

The uplift maximum and the shape has changed over time depending on the number of stations and especially on the time span of each GPS station, and thus the average time span of the network (Steffen and Wu 2011).

The latest Nordic uplift model NKG2005LU (Vestøl 2006; Ågren and Svensson 2007) is based on levelling, tide gauges and geophysical modelling. It was initiated and computed in the NKG working group for the height determination. The observations used for the model stem mainly from two sources; tide gauge and levelling values are taken from Ekman (1996) and GNSS values are from Lidberg (2004) and Lidberg *et al.* (2007). The data has been used to interpolate and extrapolate a continuous surface for the land uplift. In case of areas where observations are sparse or missing, the GIA model values from Lambeck *et al.* (1998) have been used, e.g. for the Russian Karelian area behind the east border of Finland (Nordman *et al.* 2014).

The North- and East-components of the deformation model NKG_RF03vel (see Figure 1.7) origin from the GIA model presented in Milne *et al.* (2001). The velocity field from this model has been transformed to the GPS-derived velocity field in Lidberg (2004) (Jivall 2014). Thus, the horizontal velocity field describes the horizontal displacements relative to stable Eurasia as defined by the ITRF2000 and its rotation pole for Eurasia (Altamimi *et al.* 2003).

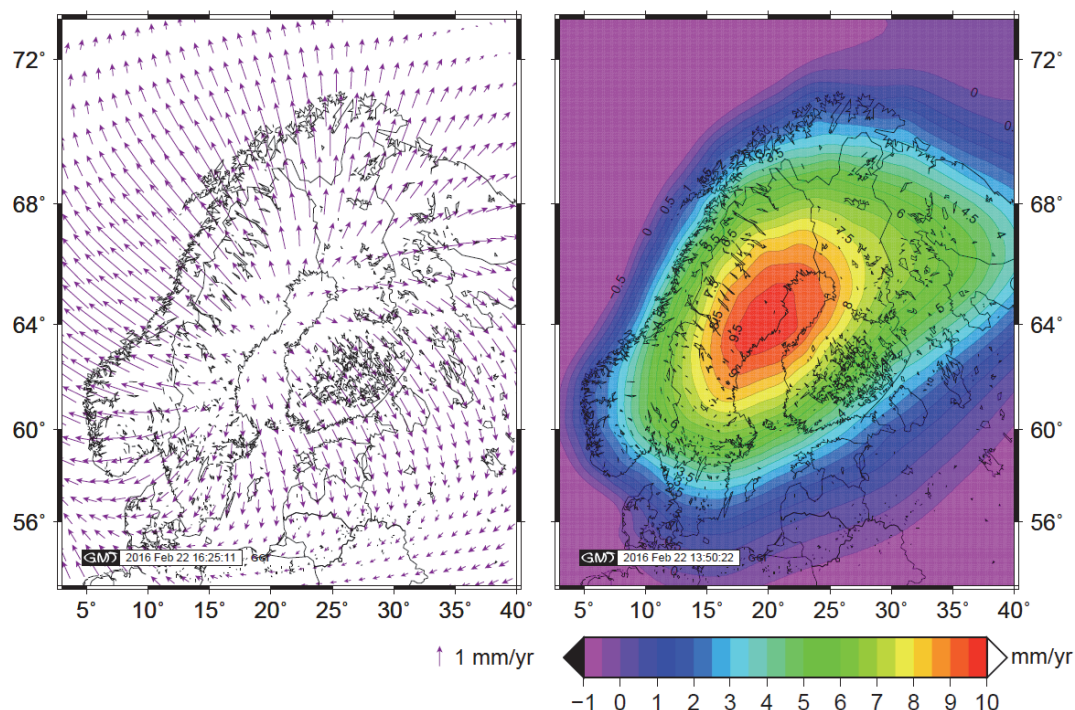


Figure 1.7. The deformation model NKG_RF03vel: horizontal velocities according to Lidberg (2004) (left) and vertical velocities from the NKG2005LU(ABS) model (right) (visualized by author)

New Nordic uplift models are currently in preparation; they take into account the latest advances in observation techniques and modelling (Poutanen and Steffen 2014).

1.4. Effect of the ocean tides

The ocean tides are generated by the same gravitational forces as the solid Earth tides, but the ability of the ocean to redistribute the mass shapes own dynamics to the ocean tides. The ocean tide behaviour in any spot of the coast is strongly affected by the shape of the coastline and the seabed profile. Therefore, the ocean tides have the same spectrum as the solid Earth tides but different amplitude and phase (Doan and Brodsky 2006).

The ocean tide models are required to calculate the loading response at a point. Some of them are based on the hydrodynamic modelling, and others – on the satellite altimetry observations. In general, the satellite altimetry based ocean tide models are best in the open ocean areas, while the models based on the tide gauge data and hydrodynamic modelling are best near the coastal areas (Khan 2005).

The ocean tide models are typically developed and distributed as the gridded maps of the tide height amplitudes. These models provide in-phase and quadrature amplitudes of the tide heights for main tidal frequencies on a variable grid spacing over the oceans (Petit and Luzum 2010).

Table 1.2

Main tidal constituents with their periods and frequencies: h – hours, m – minutes, d – days, y – years, cpd – cycles per day

Tidal constituent	Period	Frequency, cpd
K ₂	11 h 58 m	2.006
S ₂	12 h 00 m	2.000
M ₂	12 h 25 m	1.933
N ₂	12 h 39 m	1.897
K ₁	23 h 56 m	1.003
P ₁	24 h 04 m	0.997
O ₁	25 h 49 m	0.930
Q ₁	26 h 52 m	0.893
M _f	13.66 d	0.073
M _m	27.55 d	0.036
S _{sa}	0.5 y	0.011

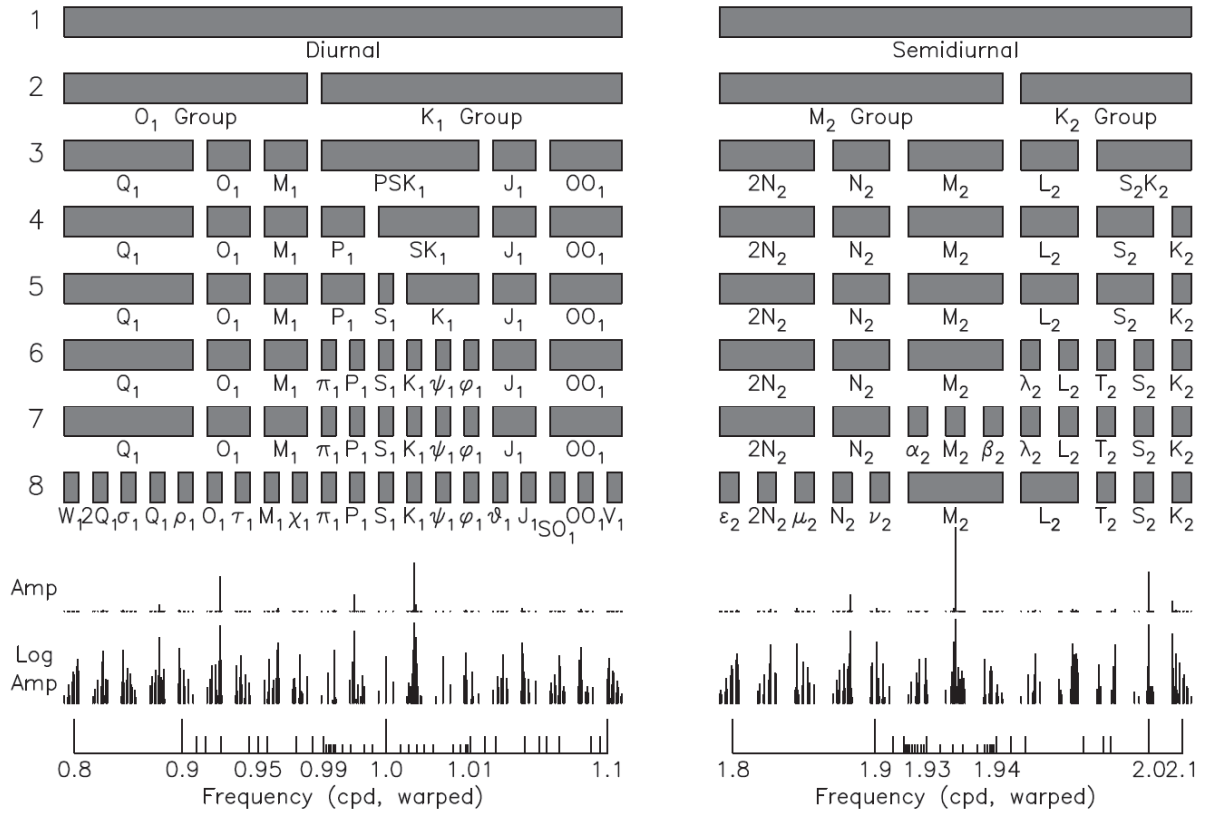


Figure 1.8. Diurnal and semi-diurnal tidal groups shown with the frequency axis warped to make each of the groups equal in size; the two lines below the groups show the amplitude spectrum of tidal harmonics in both linear and logarithmic amplitude (Agnew 2013)

The ocean tide model can be represented as a sum of harmonic constituents, which are determined by their frequencies ω_i , amplitudes A_i and phases φ_i . The total tidal variation is a sum of all the tidal harmonics. The ocean tide height can be defined as

$$H_{ot} = \sum_{i=1}^N H_{i,ot} = \sum_{i=1}^N A_i \cos(\omega_i t + \varphi_i), \quad (1.4)$$

where N is the total number of tidal constituents.

Table 1.2 gives the name, period and frequency of the main diurnal (Q_1 , O_1 , P_1 , K_1), semi-diurnal (N_2 , M_2 , S_2 , K_2) and long period (S_{sa} , M_m , M_f) constituents.

Figure 1.8 shows the decomposition of diurnal and semi-diurnal constituents and their amplitude spectrum. The spectrum of tidal amplitudes on a linear scale indicates higher amplitudes for the mentioned 11 tidal constituents. Other constituents can be separated precisely only with the large amount of data and low noise.

2. GNSS

GNSS includes the U.S. NAVSTAR (Navigation System by Timing and Ranging) Global Positioning System (GPS), the Russian GLObalnaya NAvigatsionnaya Sputnikovaya Sistema (GLONASS), and, in the future, also the European system – Galileo, etc.

The very high accuracy potential associated with comparatively easily transportable equipment makes GNSS a suitable technique for determining recent crustal movements. Due to availability of fully automatic, low power consumption GNSS receivers and the capacity to transfer data over large distances, continuous observations at permanent installations are more and more applied (Seeber 2003).

This Chapter gives an overview of GNSS positioning and provides an introduction to the correction concepts.

2.1. Introduction

Four simultaneously measured pseudoranges are needed to solve for the four unknowns at any time epoch; these are the three components of position and the clock bias. Geometrically, the solution is accomplished by a sphere being tangent to the four spheres defined by the pseudoranges. The center of this sphere corresponds to the unknown position (P) and its radius is the range correction ($\Delta\varrho$) caused by the receiver clock error (Hofmann-Wellenhof *et al.* 2008). This scenario for the two-dimensional case is shown in Figure 2.1.

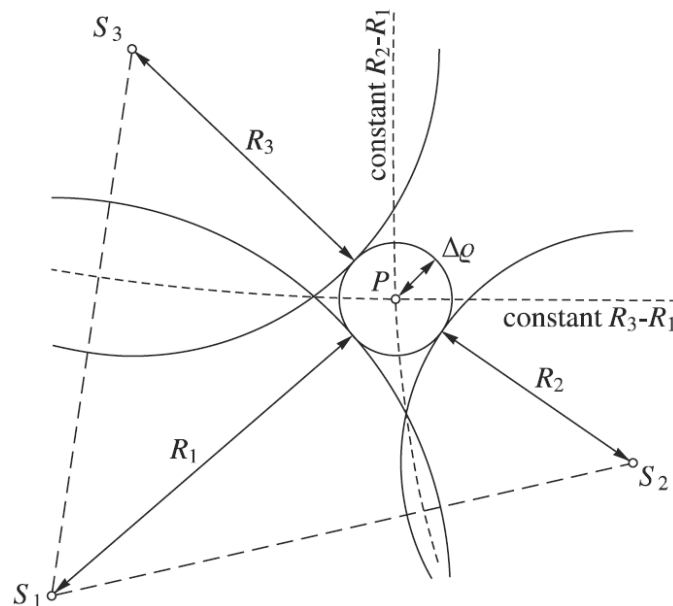


Figure 2.1. Two-dimensional pseudorange positioning (Hofmann-Wellenhof *et al.* 2008)

The fundamental equation of satellite geodesy can be formulated as (see Figure 2.2)

$$\mathbf{r}_S(t) = \mathbf{r}_B(t) + \boldsymbol{\rho}(t) \quad (2.1)$$

or

$$\mathbf{r}_j(t) = \mathbf{r}_i(t) + \Delta \mathbf{r}_{ij}(t) . \quad (2.2)$$

To solve the equation (2.2) it is necessary to establish a relation between the observations, characterized by the vector $\Delta \mathbf{r}_{ij}(t)$, and the parameters which describe the satellite position $\mathbf{r}_j(t)$ and the location of the observation station $\mathbf{r}_i(t)$. In the estimation process either all parameters can be treated as unknown, or some of the parameters are considered to be known, in order to stabilize and simplify the solution.

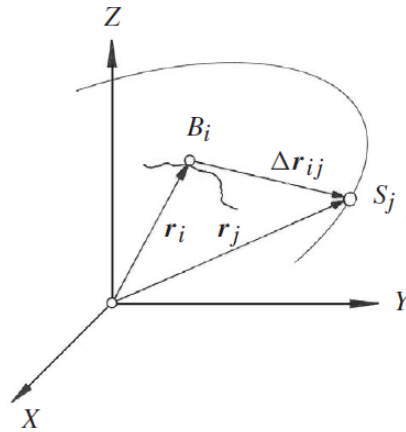


Figure 2.2. Basic relations for satellite observations (Seeber 2003)

In general, a nonlinear observation equation model between the observations and the parameters is introduced:

$$\mathbf{L} + \mathbf{v} = \boldsymbol{\Phi}(\mathbf{X}) , \quad (2.3)$$

with

\mathbf{L} – the vector of the observations;

\mathbf{X} – the vector of the unknown parameters;

$\boldsymbol{\Phi}$ – a nonlinear vectorial function;

\mathbf{v} – the vector of the residuals, containing the unmodeled components of the total estimation process.

The observation equation (2.3) can be linearized when the approximate values \mathbf{X}_0 are introduced for the unknown parameters. With

$$\mathbf{L}_0 = \boldsymbol{\Phi}(\mathbf{X}_0) \quad (2.4)$$

it follows that the vector of residual observations

$$l = L - L_0 \quad (2.5)$$

and the vector of residual parameters

$$x = X - X_0 . \quad (2.6)$$

The linear form of (2.3) is then

$$l + v = Ax . \quad (2.7)$$

The design matrix A contains the partial derivatives of the observations with respect to the parameters, developed around the approximate point of expansion X_0 :

$$A = \left(\frac{\partial \Phi(X)}{\partial X} \right)_0 . \quad (2.8)$$

The system of equations (2.7) can be solved in a least-squares adjustment process, based on the minimization of the function

$$v^T W v \rightarrow \text{minimum} , \quad (2.9)$$

and yields a best estimate \hat{X} of the unknown parameters. W denotes the weight matrix of the observations (Seeber 2003).

The satellite and the observation point are both the functions of time, in other words, the equation (2.1) contains the time dependent effects, which can be subdivided into three main groups.

The first group considers the geocentric motion of the observation point and geodynamic parameters giving the relation between the Conventional Terrestrial Reference System and the Conventional Inertial Reference System. This group includes Earth rotation, polar motion, solid Earth tide, ocean tide loading, etc.

The second group can be related to the satellite orbit motions. The satellite motions are perturbed from “pure” Keplerian motions by the so-called “perturbing forces”. These forces must be applied to the equation of motion to obtain highly accurate satellite orbits.

The third group considers clock parameters and effects, which delay the signal propagating from the satellite to the GNSS receiver. The main “signal delaying” effects here are the tropospheric and the ionospheric delays. The different types of software often estimate the bias parameters to take these effects into consideration (Khan 2005).

In the event of observations from a single station the parameter estimation process is usually restricted to the determination of the station coordinates only. The number of parameters

can be increased when simultaneous observations are available from several stations; then the corrections to the satellite orbit and observation biases may be estimated. For the solution of a general and global parameter estimation problem, the observations of a large number of different satellites are required from many globally distributed stations. Figure 2.3 contains a schematic representation concerning the process of observation and parameter estimation (Seeber 2003).

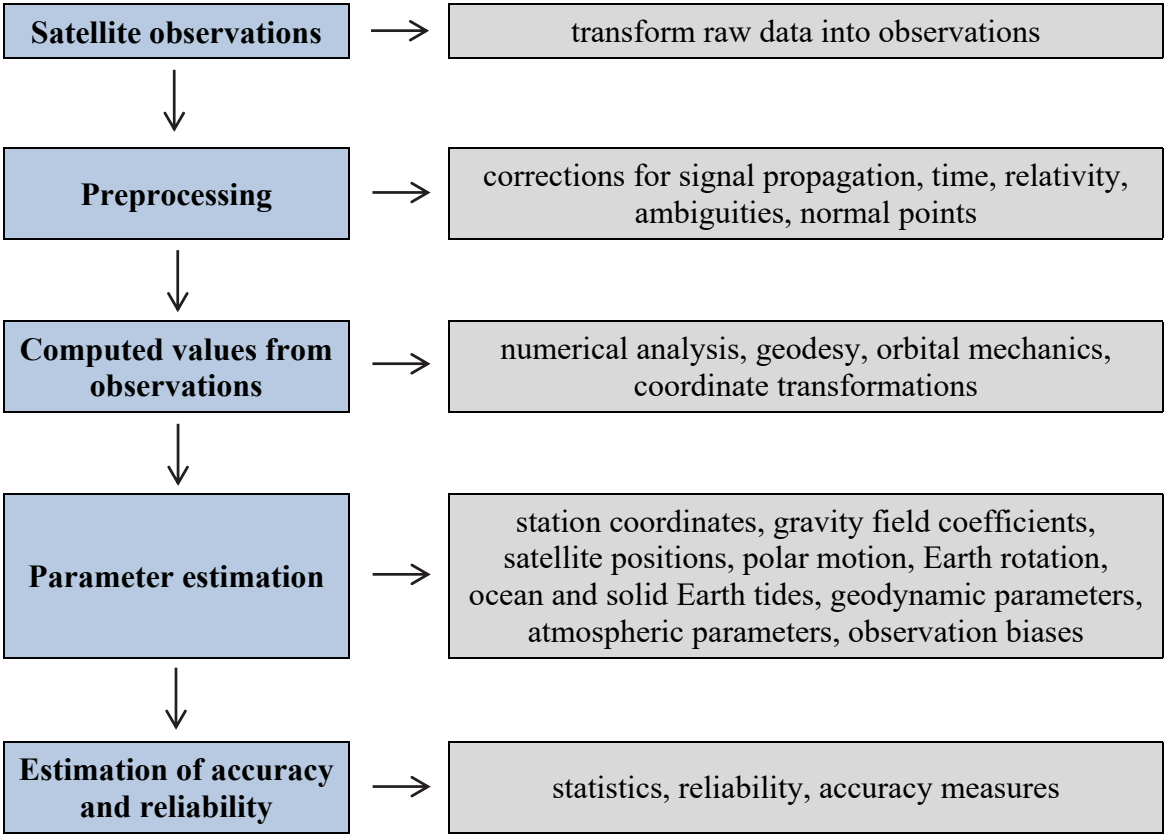


Figure 2.3. Functional scheme for the use of satellite observations (Seeber 2003)

2.2. GPS signal structure

GPS signals must provide a means for determining positions in real-time. This is achieved by modulating the carriers with pseudorandom noise (PRN) codes (see Figure 2.4). These are sequences of binary values (zeros and ones, or +1 and -1), which appear to have a random character, but which can be identified unequivocally. Their most important property is a low autocorrelation value for all delays, except those, that coincide exactly.

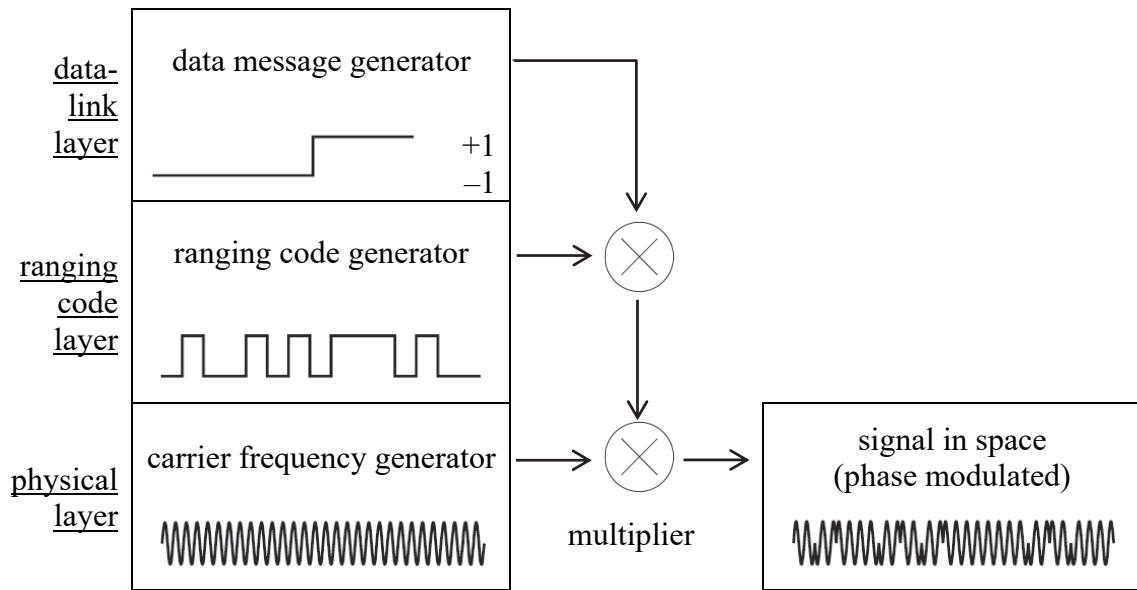


Figure 2.4. Composition of the navigation satellite signal (Hofmann-Wellenhof *et al.* 2008)

The pseudoranges are derived from the travel time of an identified coded PRN signal. Two different codes are in use, the P-code and the C/A-code. P means precision or protected, and C/A means clear/acquisition (Seeber 2003).

Table 2.1

Components of the satellite signal (Beutler *et al.* 2007)

Component	Frequency (MHz)	
Fundamental frequency	f_0	= 10.23
Carrier L_1	$f_1 = 154 f_0$	= 1575.42 ($\lambda_1 = 19.0$)
Carrier L_2	$f_2 = 120 f_0$	= 1227.60 ($\lambda_2 = 24.4$)
P-code $P(t)$	f_0	= 10.23
C/A-code $C(t)$	$f_0/10$	= 1.023
Navigation message $D(t)$	$f_0/204600$	= $50 \cdot 10^{-6}$

The P-code has a frequency of 10.23 MHz (see Table 2.1), i.e., a sequence of 10.23 million binary digits or chips per second. This frequency is also referred to as the chipping rate of the P-code. The corresponding “wavelength” of one chip is about 30 m. The P-code sequence repeats after 266 days (= 38 weeks). Portions of seven days are assigned to the various satellites. As a result, all satellites can transmit on the same frequency and can be identified by their unique one-week PRN-segment. This technique is also called the code division multiple access (CDMA). The code segments are set back to zero each week at midnight (0^h UT) from Saturday

to Sunday. The P-code is the principle code for navigation and available on both carrier frequencies L_1 and L_2 .

The C/A-code has a length of only one millisecond and is generated at a chipping rate of 1.023 MHz. The corresponding wavelength is about 300 m. The C/A-code is currently only transmitted on the L_1 carrier.

To determine the signal propagation time, the user needs a copy of the code sequence in the receiver. This code sequence is phase-shifted in time step by step, and correlated with the received code signal until maximum correlation is achieved. The necessary phase shift in the two sequences of codes is a measure of the signal travel time between the satellite and receiver antennas. This technique can be described as the code phase observation.

For precise geodetic applications the pseudoranges have to be derived from phase measurements on the carrier signals because of the much better resolution (Seeber 2003).

The L_1 signal can be described as (Spilker 1980; Wübbena 1991):

$$S_{L1}(t) = A_p P_i(t) D_i(t) \sin(\omega_1 t) + A_c C_i(t) D_i(t) \cos(\omega_1 t), \quad (2.10)$$

where

- i – denotes the i 'th satellite;
- A_p – amplitude of the P-code;
- $P_i(t)$ – P-code sequence with state ± 1 ;
- $D_i(t)$ – data stream with state ± 1 ;
- A_c – amplitude of the C/A-code;
- $C_i(t)$ – C/A-code sequence with state ± 1 ; and
- $A \sin(\omega_1 t)$ – carrier signal.

The L_2 signal has a much simpler structure because it does not contain the C/A-code:

$$S_{L2}(t) = B_p P_i(t) D_i(t) \sin(\omega_2 t), \quad (2.11)$$

where B_p is the P-code amplitude. The epochs of both codes and carriers are synchronized (Seeber 2003).

The GPS signals, when propagating from the satellite antenna to the user antenna, are subject to the following propagation effects (Seeber 2003):

- a) propagation delay in the ionosphere,
- b) propagation delay in the troposphere and
- c) multipath propagation at the satellite and in the vicinity of the receiver antenna.

The overview of these effects is given in the next two Sections.

2.3. Atmospheric effects

The structure of the atmosphere can be described as a set of concentric spherical shells with different physical and chemical properties.

With respect to signal propagation a subdivision into troposphere and ionosphere is advisable, because the particular propagation conditions are quite different (Seeber 2003).

The ionosphere, which extends from approximately 50 to 1000 km above the surface of the Earth, consists of gases that have been ionized by solar radiation. The ionization produces clouds of free electrons that act as a dispersive medium for GNSS signals, in which propagation velocity is a function of frequency. A particular location within the ionosphere is alternately illuminated by the Sun and shadowed from the Sun by the Earth in a daily cycle; consequently the characteristics of the ionosphere exhibit a diurnal variation, in which the ionization is usually maximum late in mid-afternoon, and minimum – a few hours after midnight. Additional variations result from changes in solar activity (Grewal *et al.* 2007).

GNSS satellites transmit two frequencies. Since the two frequencies will experience different delays, it is possible to correct for the first-order ionospheric signal delay (Khan 2005).

The lower part of the Earth's atmosphere is composed of dry gases and water vapor, which lengthen the propagation path due to refraction. The magnitude of the resulting signal delay depends on the refractive index of the air along the propagation path and typically varies from about 2.5 m in the zenith direction to 10–15 m at low satellite elevation angles. The troposphere is nondispersive at the GNSS frequencies, so that delay is not frequency dependent. In contrast to the ionosphere, the tropospheric path delay is the same for both code and carrier signal components. Therefore, this delay cannot be measured by utilizing L_1 and L_2 pseudorange measurements, and either models and/or differential positioning must be used to reduce the error (Grewal *et al.* 2007).

In order to describe the influence of the ionosphere and the troposphere, the basic observation equations are used (Beutler *et al.* 2000; Gregorius 1996):

$$L_{Fk}^i = \varrho_k^i - \Delta\varrho_{Fk,ion}^i + \Delta\varrho_{k,trop}^i + c\delta_k - c\delta^i + \lambda_F n_{Fk}^i, \quad (2.12)$$

$$P_{Fk}^i = \varrho_k^i + \Delta\varrho_{Fk,ion}^i + \Delta\varrho_{k,trop}^i + c\delta_k - c\delta^i. \quad (2.13)$$

The equation (2.12) is the basic observation equation for the L_1 and L_2 carrier phases and the equation (2.13) is the basic observation equation for the P_1 and P_2 code measurements. The index F is 1 or 2 corresponding to the two frequencies,

ρ_k^i – geometric distance between the receiver k and the satellite i ;

$\Delta Q_{Fk,ion}^i$ – ionospheric delay;

$\Delta Q_{k,trop}^i$ – tropospheric refraction;

$c\delta_k$ – receiver clock error, where c is the velocity of light;

$c\delta^i$ – satellite clock error;

λ_F – wavelength of the L_F carrier;

n_{Fk}^i – unknown integer of cycles, also called phase ambiguity.

Some of the biases and errors can be eliminated or, at least, reduced by forming differences between the observation equations (Khan 2005).

2.4. Multipath

The multipath propagation means that one or more reflected signals reach the antenna in addition to the direct signal. Under particular circumstances only the reflected signal may reach the antenna.

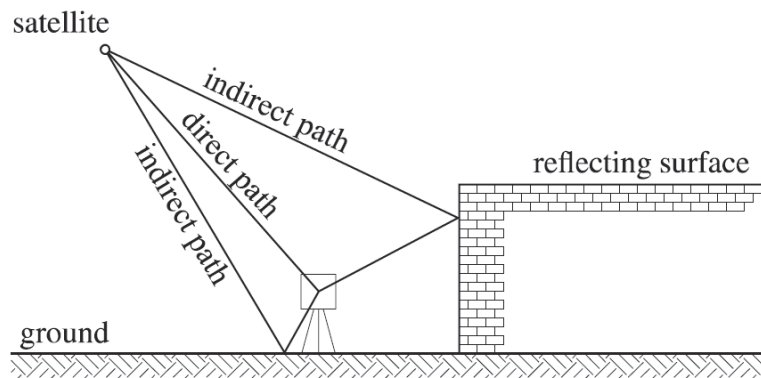


Figure 2.5. Multipath effect (Hofmann-Wellenhof *et al.* 2008)

There can be reflections off horizontal, vertical and inclined surfaces (see Figure 2.5); possible examples are streets, buildings, waterways and vehicles. This should be considered when selecting observation sites, in particular for the permanent reference stations (Seeber 2003).

The multipath propagation affects both the code and carrier measurements. The effect on P-code observations is two orders of magnitude larger than on carrier phase observations,

and can reach decimeters to meters. The effect on C/A-code observations is at the order of several meters, and can even reach, in extreme situations, 100 m or more (Braasch 1996).

The effect on carrier phase produces the phase shift, which is seen as a periodic bias. The error in the carrier phase signal is given by (Seeber 1993)

$$\Theta = \arctan\left(\frac{\sin \Phi}{\alpha^{-1} + \cos \Phi}\right) \quad (2.14)$$

with amplitude

$$B = A\sqrt{1+\alpha^2 + 2\alpha \cos \Phi}, \quad (2.15)$$

where Φ is the phase shift of the reflected signal with respect to the phase of the direct signal and α is a damping factor between 0 (= no reflection) and 1 (= reflected and not reflected signals are equally damped) (Khan 2005).

Due to the changing satellite geometry, the multipath effect in carrier phases shows a cyclic behavior. The typical periods are between 15 and 30 minutes, depending also on the local reflectors (Seeber 2003).

2.5. Relative positioning

The objective of relative positioning is to determine the coordinates of an unknown point with respect to a known point, which usually is stationary, i.e., relative positioning aims at the determination of the vector between the two points, which is often called the baseline vector or baseline (see Figure 2.6).

Let A denotes the known point, B – the unknown point, and \mathbf{b}_{AB} – the baseline vector. Introducing the corresponding position vectors $\mathbf{X}_A, \mathbf{X}_B$, the relation

$$\mathbf{X}_B = \mathbf{X}_A + \mathbf{b}_{AB} \quad (2.16)$$

may be formulated, and the components of the baseline vector \mathbf{b}_{AB} are

$$\mathbf{b}_{AB} = \begin{bmatrix} X_B - X_A \\ Y_B - Y_A \\ Z_B - Z_A \end{bmatrix} = \begin{bmatrix} \Delta X_{AB} \\ \Delta Y_{AB} \\ \Delta Z_{AB} \end{bmatrix}. \quad (2.17)$$

The coordinates of the reference point must be given. More often the coordinates are precisely known based upon GNSS or other methods.

Relative positioning can be performed with the code ranges or phase ranges. The solutions based on phase ranges are far more accurate.

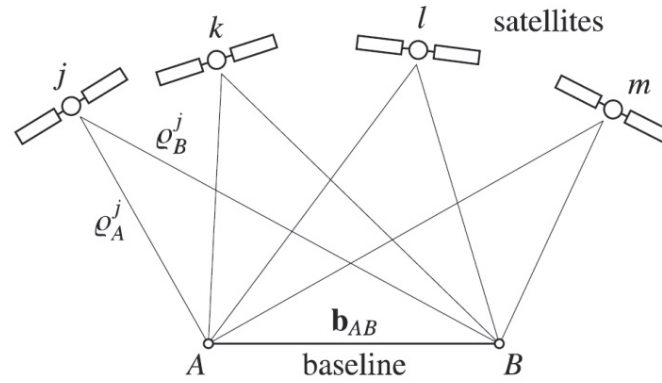


Figure 2.6. Basic concept of relative positioning (Hofmann-Wellenhof *et al.* 2008)

Relative positioning requires simultaneous observations at the reference and unknown points. Assuming such simultaneous observations, the linear combinations can be formed leading to single-differences, double-differences and triple-differences (Hofmann-Wellenhof *et al.* 2008).

The single-differences can be performed between two receivers or two satellites. The double-differences are performed between the pair of receivers and the pair of satellites. This eliminates the receiver clock errors and the satellite clock errors. Furthermore, the triple-differences, which are the differences of double-differences at two different epochs, are performed to eliminate phase ambiguities within given intervals (Khan 2005).

The method of double-differences is widely used. In the computation, a network is formed, which consists of reference (fiducial) stations and stations with unknown coordinates. The advantage of a network is that almost all errors common to the network cancel each other out either partially or totally; these errors include troposphere, ionosphere, tidal and non-tidal loading (Nordman 2010).

Instead of “relative positioning” the term “differential positioning” is often used, however, the two methods are different. Differential positioning is rather an improved single-point positioning technique and is based on applying predicted corrections to pseudoranges measured at an unknown site. The technique provides instantaneous (real-time) solutions, where improved accuracies with respect to a reference station are achieved. In the case of relative positioning, in contrast to differential positioning, the measurements taken at both sites are directly combined, what improves the position accuracy but prevents instantaneous solutions (Hofmann-Wellenhof *et al.* 2008).

3. EARTH'S SURFACE MOVEMENTS AT THE LATVIAN GNSS STATIONS

The vertical and horizontal displacements of the Earth's surface can be measured to a high degree of precision by using GNSS. In Latvia, there are two permanent GNSS networks – LatPos and EUPOS[®]-Riga in operation to provide continuous observations. The time series of GNSS station positions from both networks are developed at the Institute of Geodesy and Geoinformatics of the University of Latvia (LU GGI) applying scientific post-processing software package.

The local surface displacements obtained from the Latvian GNSS station position time series are under discussion in this study. As Latvia is located in the region that is under the effect of the ongoing relaxation of the Earth in response to the past ice mass loss, the comparison of obtained results with the data from the deformation model NKG_RF03vel is presented.

3.1. Participation in EUPOS[®] ECC

The EUPOS[®] initiative represents an international expert group of the public organisations coming from the field of geodesy, geodetic survey and cadastre (EUPOS[®] home page). The partners from Central and Eastern Europe work on the provision of compatible spatial reference infrastructures by using the Global Navigation Satellite Systems GPS, GLONASS and as soon as it is available Galileo by operating Differential GNSS EUPOS[®] reference station services (Rosenthal 2008).

EUPOS[®] provides the following EUPOS services for Differential GNSS applications (EUPOS[®] ISC 2013):

- a) EUPOS DGNSS for real-time applications by single-frequency pseudorange or pseudorange and carrier phase measurements with sub-metre to decimetre level accuracy;
- b) EUPOS Network RTK for real-time applications by multi-frequency carrier phase measurements with centimetre accuracy;
- c) EUPOS Geodetic for post-processing applications by the code and carrier phase measurements in static or kinematic mode with decimetre up to sub-centimetre accuracy.

In order to further strengthen the national EUPOS[®]/ETRS89 realizations and ensure the homogeneity of the national EUPOS[®] services the FÖMI Satellite Geodetic Observatory (SGO) proposed at the EUPOS[®] Conference 2010 the idea to establish EUPOS[®] Combination Centre

(ECC). The main task of the ECC is the combination of the weekly national EUPOS[®] SINEX solutions into a single weekly EUPOS[®] solution. This activity is analogous to the EUREF Permanent Network (EPN) data analysis and combination approach, and the EUPOS[®] combined solution may be regarded as the densification of the EPN, namely the further densification of the actual ETRS89 realization. The EPN analysis standards should also be followed, therefore ECC can only handle SINEX solutions computed by a scientific post-processing software package. The detailed description of analysis can be found at the Guidelines for the EPN Analysis Centres published by the EPN Coordination Group and the EPN Central Bureau (2013).

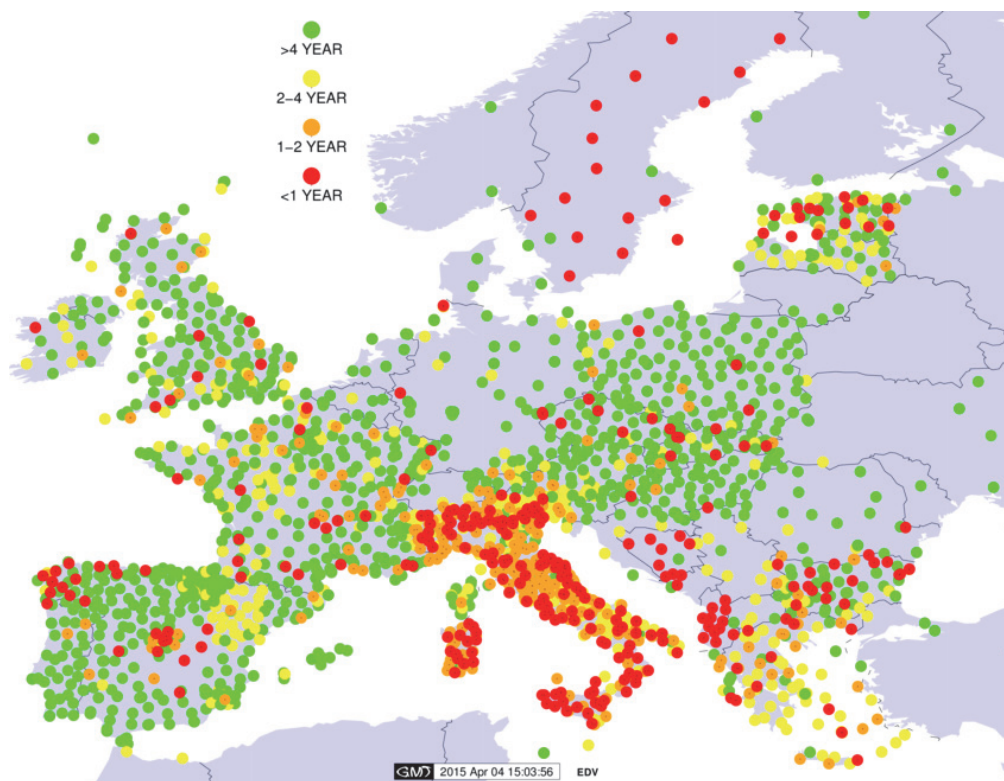


Figure 3.1. GNSS station observation availability for the EUPOS[®] combined solution shown with time intervals (status on April 2015)

The Institute of Geodesy and Geoinformatics (GGI) calculates and submits the Latvian SINEX solutions to ECC regularly (Balodis *et al.* 2013; Haritonova *et al.* 2013a; 2013b; Haritonova *et al.* 2014a; 2014b; Janpaule *et al.* 2015). Currently ECC activities are very successful and the study area covers almost all the Europe (Kenyeres 2014). The result of ECC activities is depicted in Figure 3.1.

3.2. Latvian GNSS networks

The first GPS measuring campaign was carried out in 1992. There were no any GPS receivers in Latvia at this time and Latvian surveyors were facing great difficulties in connection with a coming land reform. The Latvian coordinate information in Soviet time was top secret and it was governed by Soviet army officials. Just local reference systems for towns and cities were used by civil engineering under the strong control of GUGK (the main governance office for geodesy and cartography). However, no reference network information was available for citizens and services throughout the country (Balodis *et al.* 2015a).

The EUREF 92 GPS campaign was initiated by the General Directors of Nordic Geodetic and Mapping Authorities at a meeting in Tallinn, May 1992, as a contribution to the establishment of a new geodetic reference network (Madsen, F. and Madsen, B. 1993). The campaign was organised by Nordic Geodetic Commission (NKG) and the results were computed by NKG people. Four reference points in Latvia were positioned in ETRS89 system with EUREF accuracy estimates of class C. The GPS network in Latvia was densified by the State Land Service (SLS) and by the Latvian Geospatial Information Agency (LGIA). Two times more NKG GPS campaigns were performed, where Latvian 4 points were included and Latvian own receivers were used by Latvian surveyors in those last campaigns. The first one was performed in 2003, and results are published by Jivall *et al.* (2007). No results have been published on the campaign of 2008.

Within the framework of EUPOS[®] regional development project, two GNSS permanent station networks have been developed in Latvia – LatPos (Zvirgzds 2007; Zvirgzds 2012) and EUPOS[®]-Riga (Abele *et al.* 2008), which have been operating since 2006.

The sites were selected as specified in EUPOS[®] ISC (2013) so that:

- a) the horizon at the location of GNSS antenna is free from obstructions;
- b) reflective surfaces are located as far as possible, so that the far-field and near-field multipath effects on satellite signals would be minimized or avoided;
- c) long-term stability of the GNSS antennas is ensured.

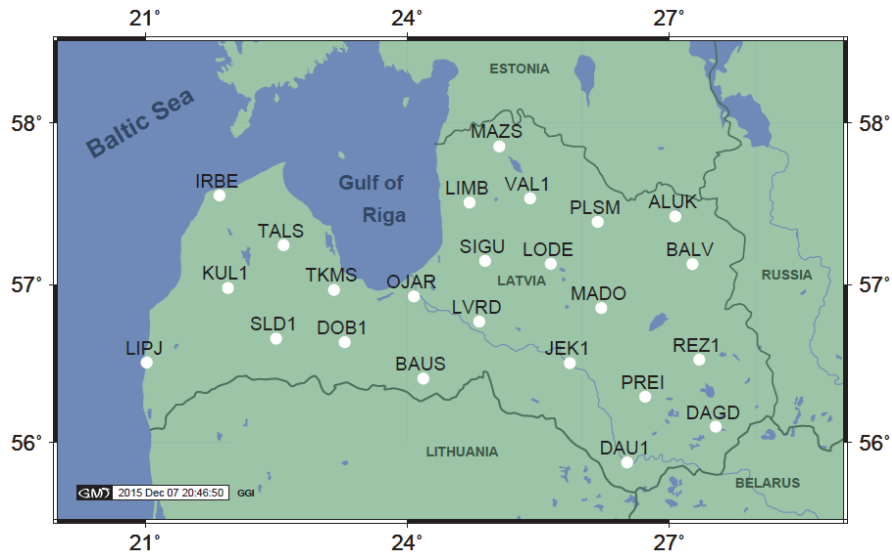


Figure 3.2. Actual LatPos network with 24 continuously operating GPS/GNSS stations

At present, the LatPos network includes 24 permanent stations, as shown in Figure 3.2 (LatPos and LGIA home pages). Some of the initial stations have been renamed and removed within relatively small areas during the whole period of operation, thus causing discontinuities in the site position time series.

EUPOS[®]-Riga network consists of 5 stations, which are located in Riga and its surroundings (EUPOS[®]-Riga home page). This network has been once modified in 2012, when two stations were moved to Riga surrounding area. EUPOS[®]-Riga stations are shown in Figure 3.3. The location of RIGA station from the IGS and EPN networks is shown as well.

The information on Latvian GNSS station location and monumentation is given in Appendix B (information on LatPos GNSS antennas mounting: site type and installation year, is given according to LGIA National Geodetic Network Database).

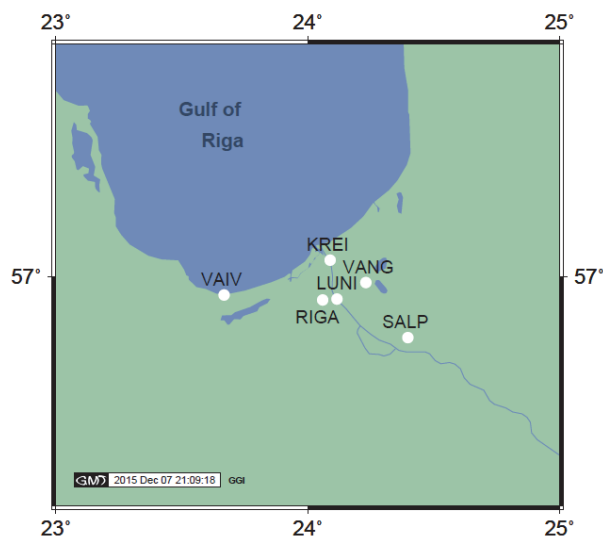


Figure 3.3. EUPOS[®]-Riga and IGS/EPN station RIGA

EUPOS[®]-Riga and LatPos networks are primarily geodetic reference networks established for surveying and navigation purposes in the territory of Latvia. However, according to the worldwide experience and growing trends in space geodesy, it is commonly accepted to apply GNSS stations for the studies of geophysical processes as well (Haritonova *et al.* 2015a).

3.3. Network solution and data processing

The time series of GNSS station positions of both EUPOS[®]-Riga and LatPos networks have been computed by *Bernese* software developed at the University of Bern, Switzerland. Applying *Bernese GPS Software version 5.0* (Beutler *et al.* 2007), the station diurnal coordinates have been obtained for 7-year long observation period – from 2008 to 2014. Since 2015, the *Bernese GNSS Software version 5.2* (Dach *et al.* 2015) has been used for data calculation.

Within the frames of the Thesis, to ensure data control and homogeneity, it was decided to re-compute GNSS station positions of both networks for the period from 2012 to 2014 applying the latest version of the software; in this way obtaining the time series for 4 years (2012–2015) by *Bernese version 5.2*.

CODE (IGS before) precise orbits, Earth orientation and clock products with CODE final ionosphere product were used for GNSS data processing (CODE data – available at: <ftp://ftp.unibe.ch/aiub/CODE>; IGS data – available at: <ftp://igscb.jpl.nasa.gov/igscb/product>). The dry global mapping function (DRY_GMF) as the *a priori* troposphere model was used; a cut-off elevation angle of 3 degrees was selected (satellite observations below 3 degrees are excluded). The positions for all stations are corrected for solid Earth tide effect (Haritonova 2012a; 2012b; 2012c; 2013; 2015; Haritonova and Balodis 2012) according to IERS Conventions 2010 (Petit and Luzum 2010), as well as the ocean tide loading (FES2004 ocean tide model was selected) using online provider by H.-G. Scherneck (available at: <http://holt.oso.chalmers.se/loading>).

It should be noted that only GPS observations were used until 2015, starting with the first day of that year the combined processing of GPS and GLONASS has been applied.

Table 3.1 summarizes all steps performed to obtain station velocities and RMS values from GNSS observations for both solutions (Haritonova *et al.* 2016).

Table 3.1

Flow chart of GNSS data processing

Steps	Institution	Additional description	ECC cumulative weekly solution (2008–2014)	GGI daily solution (2012–2015)
Data processing	GGI	Software	<i>Bernese GPS Software version 5.0</i>	<i>Bernese GNSS Software version 5.2</i>
		Data sets	IGS and CODE databases	CODE database
		Observations (RINEX files)	GPS	GPS and GLONASS (since 1st day of 2015)
		Fiducial stations	5–7 EPN (A and B-class)/IGS stations	9 EPN (A-class)/IGS stations
Station coordinates and transformations	ECC/ GGI	–	Daily solutions in IGS05/08: composed to weekly SINEX solutions and submitted to ECC for further combination into a single weekly EUPOS [®] solution	Daily solutions in IGB08: ITRF2008-to-ETRF2000 one-step transformation using 14 transformation parameters according to Boucher and Altamimi (2011)
Time series analysis and trend derivation	ECC/ GGI	–	–	Corrections for offsets, outlier elimination
Station velocities and RMS values	ECC/ GGI	–	Horizontal velocities are expressed in the ETRF2000 frame, and velocities for Up component – in the ITRF2008	

Using Differential GNSS (relative) processing strategy, together with Precise Point Positioning (PPP) approach applied for initial coordinate determination, the site coordinates were computed in IGS05/08 frames, i.e in IGS08 since GPS week 1632 – introduction of the new IGS08 frame (Rebischung 2011), for mentioned 7-year period. The reference stations used are from EPN in the surroundings of Latvia. Most frequently 5–7 reference stations were selected from the following set: BPDF, BOGO, BOR1, BYDG, CNIV, JOEN, JOZE, KURE, MDVJ, METS, POLV, PULK, REDZ, RIGA, SPT0, SUUR, SUR4, SWKI, TOIL, TORA, TOR2, VAAS, VIS0, VLNS, WROC. The reason of such miscellaneous reference station selection in various days is the data acceptance by the *Bernese GPS Software v 5.0* depending

on the quality of proper station data in proper day, as well as an insufficient number of EPN easternmost reference stations for the territory of Latvia.

The obtained daily solutions of Latvian GNSS station positions were composed to weekly SINEX solutions and were submitted to ECC for further combination into a single weekly EUPOS[®] solution. For an example, Figure 3.4 shows LUNI station position time series in North, East and Up components from the EUPOS[®] cumulative solution.

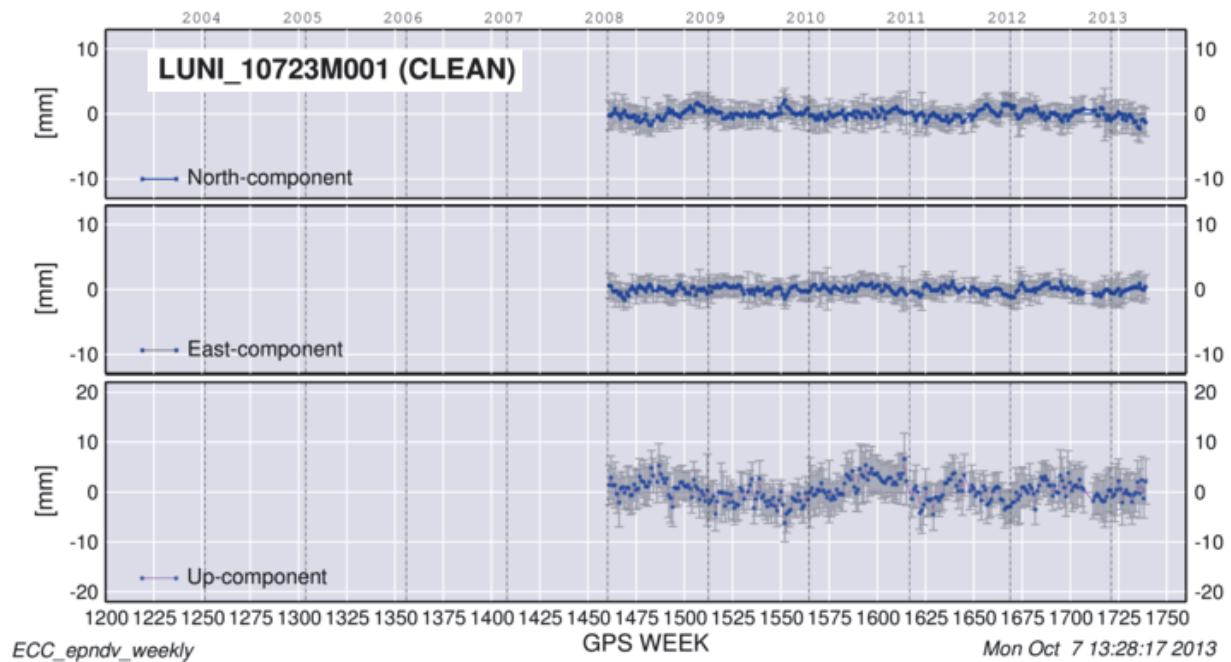


Figure 3.4. North, East and Up components of LUNI station position from the EUPOS[®] cumulative weekly solution

For computation of Latvian GNSS station positions by means of the *Bernese version 5.2*, the DGNSS (relative) processing strategy has been also implemented using 9 fiducial stations with the fixed coordinates and velocities in reference frame IGB08 (see Table 3.2) through all 4-year period processing sessions (station coordinates and velocities are available at EPN home page: [link to site information](#)).

The selected stations are the following: BOR1 (Poland), GLSV (Ukraine), JOEN (Finland), LAMA (Poland), MAR6 (Sweden), ONSA (Sweden), PULK (Russia), RIGA (Latvia), VLNS (Lithuania). As can be seen from Figure 3.5, different monumentation types and antenna mounts are used. The station locations are shown in Figure 3.6.



BOR1



GLSV



JOEN



LAMA



MAR6



ONSA



PULK



RIGA



VLNS

Figure 3.5. Fiducial stations from EPN/IGS networks: BOR1, GLSV, JOEN, LAMA, MAR6, ONSA, PULK, RIGA, VLNS

These stations belong to the EPN network as A-class stations (with the exception of GLSV site in 2015) (Kenyeres 2009). According to Bruyninx *et al.* (2013), only A-class stations are suitable as fiducial stations for the densification of the ETRS89.

Table 3.2

Positions and velocities of the fiducial GNSS stations in IGB08 at the epoch 001/2005

Station name	Position (m)			Velocity (m/yr)		
	X	Y	Z	V _X	V _Y	V _Z
BOR1 12205M002	3738358.45365	1148173.70965	5021815.77309	-0.01729	0.01564	0.00884
GLSV 12356M001	3512888.95355	2068979.88146	4888903.20075	-0.01992	0.01421	0.00821
JOEN 10512M001	2564139.08700	1486149.77000	5628951.44900	-0.01800	0.01320	0.00880
LAMA 12209M001	3524522.92500	1329693.62700	5129846.35700	-0.01830	0.01480	0.00820
MAR6 10405M002	2998189.41399	931451.77673	5533398.68146	-0.01338	0.01435	0.01355
ONSA 10402M004	3370658.54161	711877.13835	5349786.95244	-0.01416	0.01449	0.01034
PULK 12305M001	2778606.80700	1625494.66900	5487810.97000	-0.01900	0.01350	0.00850
RIGA 12302M002	3183899.19239	1421478.48916	5322810.79661	-0.01761	0.01432	0.00875
VLNS 10801M001	3343600.61700	1580417.73900	5179337.29300	-0.01920	0.01420	0.00790

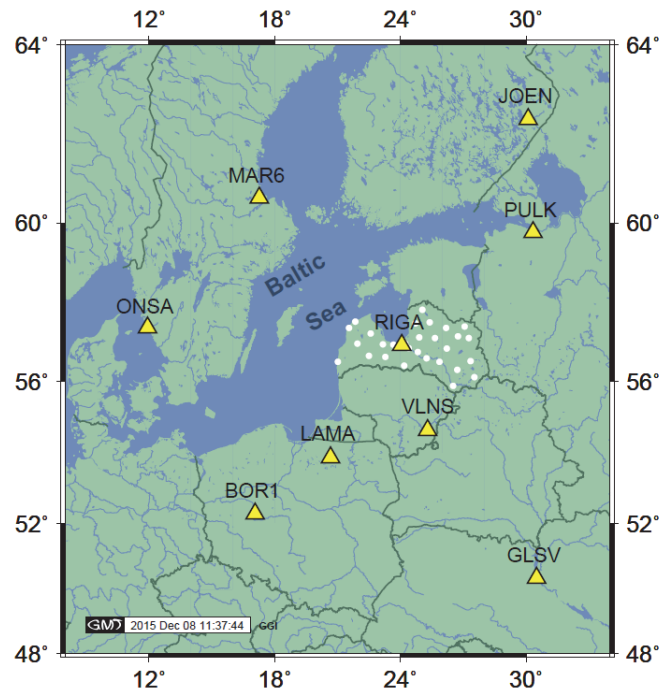


Figure 3.6. Latvian GNSS stations (white dots) and fiducial stations (yellow triangles) from EPN/IGS networks: BOR1, GLSV, JOEN, LAMA, MAR6, ONSA, PULK, RIGA, VLNS

3.4. Results and discussion

3.4.1. Velocity fields

The final velocity components derived from the ECC minimum constrained cumulative solution till GPS week 1830 (31st January 2015) are given in Table 3.3. The horizontal velocities are expressed in the ETRF2000 frame, and the velocities for Up component – in the ITRF2008. RMS values for each component are given as well. The velocity fields are depicted in Figures 3.7 and 3.8. Figure 3.7 shows the station vertical movements, and Figure 3.8 represents the horizontal movements. Additionally, the velocities from the deformation model NKG_RF03vel are shown with light vectors in these Figures; the velocity values are given in the Table 3.3.

The obtained results have displayed a positive tendency of the vertical movements in the western and central parts of Latvia – the station heights are increasing, and negative velocities are observed in the eastern part. The station vertical velocities are ranging from -2.32 to $+1.49$ mm/yr. As can be seen in Figure 3.7, there are velocities, which stand out against the background of the velocity field. Such outstanding values could be caused by the site-specific effects. The velocity range can be considerably reduced by eliminating these outliers.

Table 3.3

Latvian GNSS station velocities in North, East and Up components with RMS values from the ECC minimum constrained cumulative solution till GPS week 1830, released at 4th April 2015 by the EPN RF coordinator, and velocities from the deformation model NKG_RF03vel: values in bold – maximum and minimum values, underlined values – excluded values from the final data range

Network	GNSS station name	Station velocities according to the ECC cumulative weekly solution, mm/yr						Station velocities according to the deformation model NKG_RF03vel, mm/yr		
		ETRF2000			ITRF2008			North comp.	East comp.	Up comp.
		North comp.	RMS (North)	East comp.	RMS (East)	Up comp.	RMS (Up)			
LatPos	ALUK	-0.12	0.08	-0.17	0.06	<u>-1.88</u>	0.44	-0.57	0.07	0.73
	BALV	-0.81	0.03	0.29	0.02	0.40	0.16	-0.52	0.03	0.54
	BAUS	-0.33	0.01	-0.09	0.02	0.02	0.15	-0.46	-0.02	0.49
	DAGD	-0.45	0.06	-0.05	0.04	-0.23	0.35	-0.37	-0.10	0.04
	DAU1	-0.40	0.04	-0.16	0.04	0.05	0.29	-0.34	-0.12	0.04
	DOB1	-0.30	0.04	-0.10	0.05	0.63	0.29	-0.52	0.02	0.73
	IRBE	-0.49	0.05	-0.28	0.06	1.48	0.30	-0.73	0.15	1.72
	JEK1	-0.65	0.04	-0.34	0.04	-0.12	0.28	-0.45	-0.03	0.37
	KUL1	-1.02	0.07	-0.24	0.07	0.97	0.45	-0.62	0.07	1.18
	LIMB	-0.52	0.02	0.38	0.02	0.93	0.15	-0.64	0.12	1.14
	LIPJ	-0.41	0.04	-0.16	0.05	1.44	0.28	-0.54	-0.01	0.99
	LODE	0.10	0.04	-0.98	0.03	1.27	0.28	-0.56	0.06	0.74
	LVRD	-0.60	0.07	-0.06	0.07	1.49	0.42	-0.51	0.01	0.62
	MADO	-0.66	0.02	-0.15	0.02	-0.23	0.15	-0.50	0.01	0.51
	MAZS	-2.38	0.06	0.11	0.06	0.08	0.37	-0.69	0.17	1.37
	OJAR	-0.88	0.04	-1.14	0.04	0.07	0.30	-0.56	0.05	0.81
	PLSM	-0.82	0.07	0.29	0.06	0.38	0.36	-0.59	0.08	0.83
	PREI	-0.28	0.05	-0.55	0.04	-0.27	0.28	-0.40	-0.07	0.19
	REZ1	-0.51	0.04	-0.41	0.03	<u>-1.12</u>	0.25	-0.43	-0.05	0.24
	SIGU	-0.50	0.02	0.02	0.02	0.18	0.15	-0.58	0.07	0.85
SLD1	-0.43	0.04	-0.21	0.05	0.20	0.29	-0.54	0.02	0.86	
TALS	-0.63	0.02	-0.10	0.02	1.15	0.14	-0.65	0.10	1.29	
TKMS	-0.20	0.15	-0.18	0.16	0.79	0.93	-0.59	0.07	0.97	
VAL1	-0.74	0.05	-0.23	0.04	0.16	0.29	-0.63	0.11	1.04	
EUPOS®- Riga	KREI	-0.42	0.02	-0.09	0.02	0.00	0.15	-0.58	0.06	0.88
	LUNI	-0.63	0.02	0.17	0.02	0.28	0.15	-0.56	0.05	0.82
	SALP	-0.65	0.06	-0.29	0.07	<u>-2.32</u>	0.42	-0.54	0.03	0.73
	VAIV	-0.38	0.07	0.31	0.07	-0.56	0.43	-0.57	0.06	0.89
	VANG	-0.24	0.02	0.13	0.02	-0.09	0.15	-0.56	0.06	0.83
IGS/ EPN	RIGA	-0.43	0.01	-0.18	0.01	0.86	0.04	-0.56	0.05	0.83

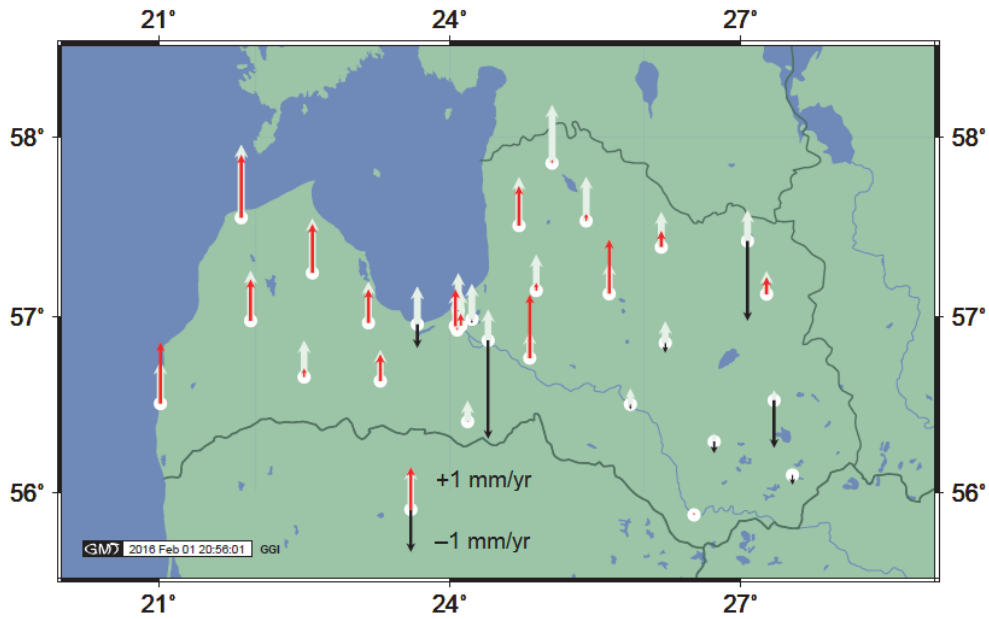


Figure 3.7. Latvian GNSS station cumulative vertical movements from EUPOS[®] observation set (till GPS week 1830) and vertical velocities from the model NKG_RF03vel

After outstanding data elimination, the resulting range of vertical velocities from ECC cumulative weekly solution for the territory of Latvia equals to 2.05 mm/yr, which makes from -0.56 to $+1.49$ mm/yr. It should be noted that the minimum velocity belongs to the station VAIV, which is located in the central part of Latvia. According to the model NKG_RF03vel, the vertical velocities of Latvian GNSS stations have a positive sign; the velocity range runs up to 1.68 mm/yr, with the minimum $+0.04$ mm/yr and the maximum $+1.72$ mm/yr.

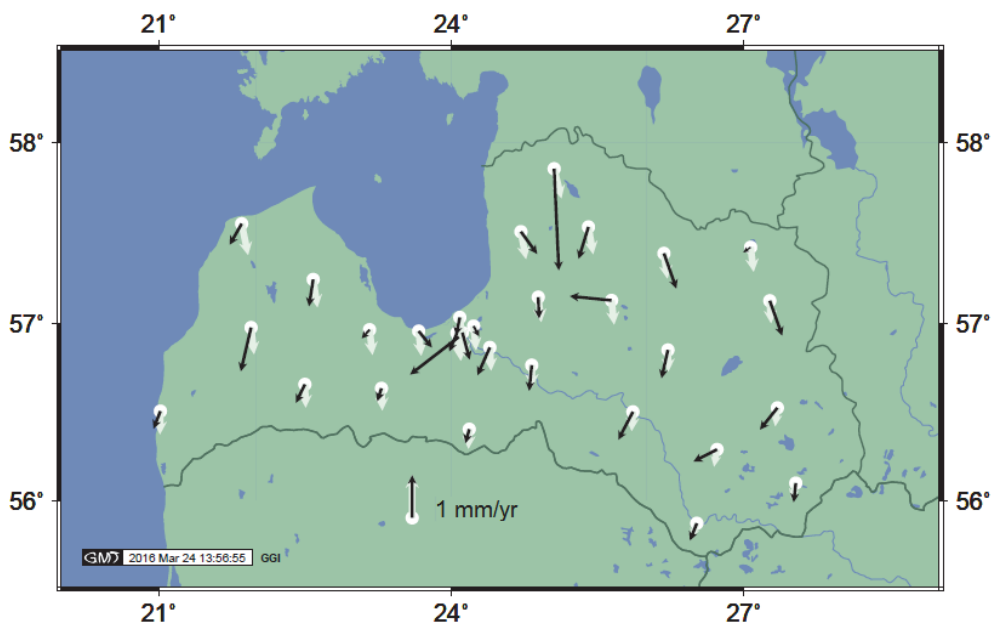


Figure 3.8. Latvian GNSS station cumulative horizontal movements from EUPOS[®] observation set (till GPS week 1830) and horizontal velocities from the model NKG_RF03vel

As to horizontal movements, the velocity field is also not homogeneous, showing the outstanding movements for some stations. Nevertheless, the site velocities are mostly oriented to the south and fail to exceed 1 mm/yr. In this case, one can observe relatively good correlation to the velocity field from the deformation model NKG_RF03vel.

Table 3.4

Latvian GNSS station velocities (mm/yr) in North, East and Up components with RMS values (mm) from daily solution for the period from 2012 to 2015: values in bold – maximum and minimum values, underlined values – excluded values from the final data range (see Appendix A to find station velocities and RMS values for each year separately)

Network	GNSS station name	Station velocities according to the daily solution obtained for the period from 2012 to 2015, mm/yr						
		ETRF2000				ITRF2008		
		North comp.	RMS (North)	East comp.	RMS (East)	Up comp.	Up comp.	RMS (Up)
LatPos	ALUK	0.01	0.05	-0.11	0.05	-0.22	0.76	0.17
	BALV	-0.11	0.04	0.03	0.07	-0.11	0.85	0.14
	BAUS	-0.26	0.04	0.29	0.05	-0.04	0.91	0.13
	DAGD	-0.15	0.05	-0.02	0.04	-0.22	0.73	0.15
	DAU1	-0.11	0.05	-0.18	0.05	-0.22	0.73	0.15
	DOB1	0.00	0.05	-0.11	0.05	0.01	0.97	0.13
	IRBE	-0.07	0.05	-0.15	0.05	0.91	1.89	0.19
	JEK1	-0.22	0.05	-0.11	0.04	0.02	0.97	0.16
	KUL1	-0.18	0.06	-0.02	0.05	0.22	1.19	0.15
	LIMB	-0.15	0.05	0.07	0.05	0.51	1.49	0.16
	LIPJ	-0.18	0.05	-0.15	0.05	0.33	1.29	0.16
	LODE	-0.26	0.05	-0.44	0.05	0.03	1.00	0.14
	LVRD	-0.07	0.06	-0.11	0.05	0.22	1.19	0.17
	MADO	-0.33	0.05	-0.37	0.05	0.04	1.00	0.15
	MAZS	-1.75	0.22	-0.01	0.14	0.33	1.31	0.21
	OJAR	-0.33	0.06	-0.47	0.08	0.40	1.37	0.17
	PLSM	-0.29	0.07	0.15	0.06	0.22	1.19	0.15
	PREI	-0.07	0.05	-0.18	0.09	-0.15	0.80	0.15
	REZ1	-0.18	0.07	-0.15	0.04	-0.18	0.77	0.16
	SIGU	-0.11	0.06	0.03	0.06	0.11	1.08	0.16
SLD1	-0.18	0.06	-0.07	0.09	0.00	0.97	0.13	
TALS	-0.15	0.05	-0.11	0.06	0.40	1.37	0.15	
TKMS	-0.07	0.05	0.04	0.04	0.18	1.15	0.11	
VAL1	-0.15	0.05	-0.22	0.05	0.26	1.24	0.14	
EUPOS®-Riga	KREI	-0.04	0.04	0.15	0.07	-0.01	0.96	0.15
	LUNI	-0.22	0.05	-0.15	0.06	0.07	1.03	0.13
	SALP	-0.29	0.12	-0.22	0.11	<u>-0.88</u>	<u>0.09</u>	0.18
	VAIV	-0.07	0.05	0.07	0.06	-0.11	0.85	0.15
	VANG	-0.15	0.05	0.15	0.08	0.18	1.15	0.15
IGS/EPN	RIGA	-0.99	0.06	-0.07	0.07	0.37	1.34	0.17

As mentioned above, the Latvian GNSS station observations were re-processed using the *Bernese version 5.2* with the aim to obtain more consistent results for the period of 4 years (2012–2015) (Balodis *et al.* 2016). The results are summarized in Table 3.4. The station velocities for Up component are given both in the ETRF2000 and ITRF2008 frame. The station velocities and residual position RMS values for each year separately are given in Appendix A, where the velocity components are expressed in ETRF2000 frame. The formula used for RMS error (in this case RMS of arithmetic mean) calculation is

$$S_{\bar{x}} = \sqrt{\frac{\sum_{i=1}^n (x_i - \bar{x})^2}{n(n-1)}}, \quad (3.1)$$

where x_i is station residual position (detrended), and \bar{x} – the arithmetic mean of positions.

The residual position time series of each GNSS station are shown in Appendix B. More evident outliers, usually occurred during the winter time (Kenyeres and Bruyninx 2009), and single extremes, which are out of the diapason of ± 15 mm in Up component, were eliminated from the time series.

The station vertical velocities obtained from the daily solution are shown in Figure 3.9. In the same manner as above the vertical velocities from the model NKG_RF03vel are shown as well. The differences between two data sets are depicted in Figure 3.10.

As can be seen, the vertical velocities have a positive sign, and only one station (SALP) has an outstanding velocity. After its elimination, the resulting range of vertical velocities comes up to 1.16 mm/yr, which is less compared to the range from ECC cumulative weekly solution and uplift range according to the model NKG_RF03vel.

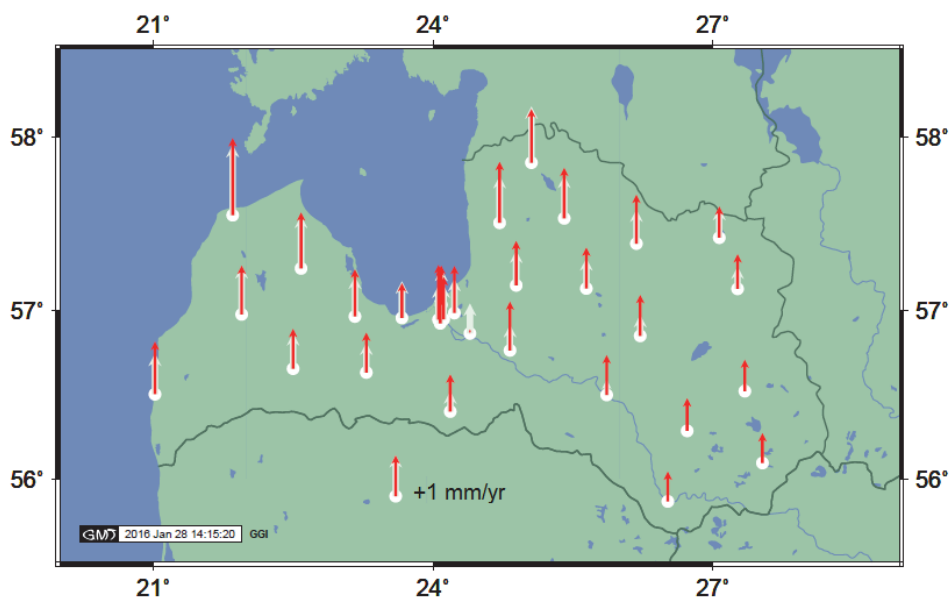


Figure 3.9. Latvian GNSS station vertical movements obtained from the daily solution (2012–2015), and vertical velocities – from the model NKG_RF03vel

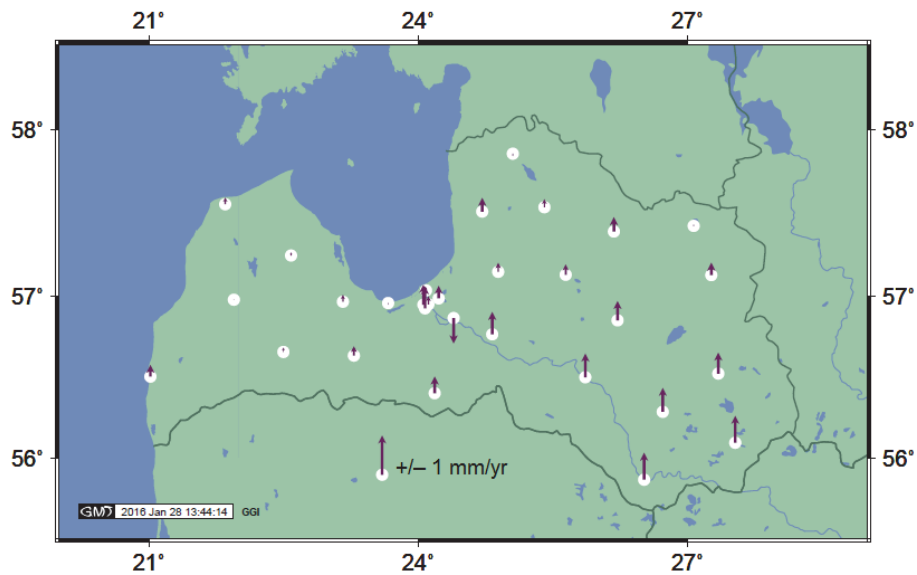


Figure 3.10. Differences between vertical velocities obtained from the daily solution (2012–2015) and from the model NKG_RF03vel

In Figure 3.10, one can observe that the movements of western GNSS stations correspond to the data of NKG_RF03vel. The highest velocity differences in Up component between the obtained results and the values from the model NKG_RF03vel are more pronounced in the case of the stations located in south-eastern part of Latvia; however, these differences are less than 1 mm/yr.

Figure 3.11 represents the station vertical velocities expressed in the frame ETRF2000, where in contradistinction to the results expressed in ITRF2008 both positive and negative values can be observed for the territory of Latvia. This is a good example of the selected reference frame influence on the resulting velocity field.

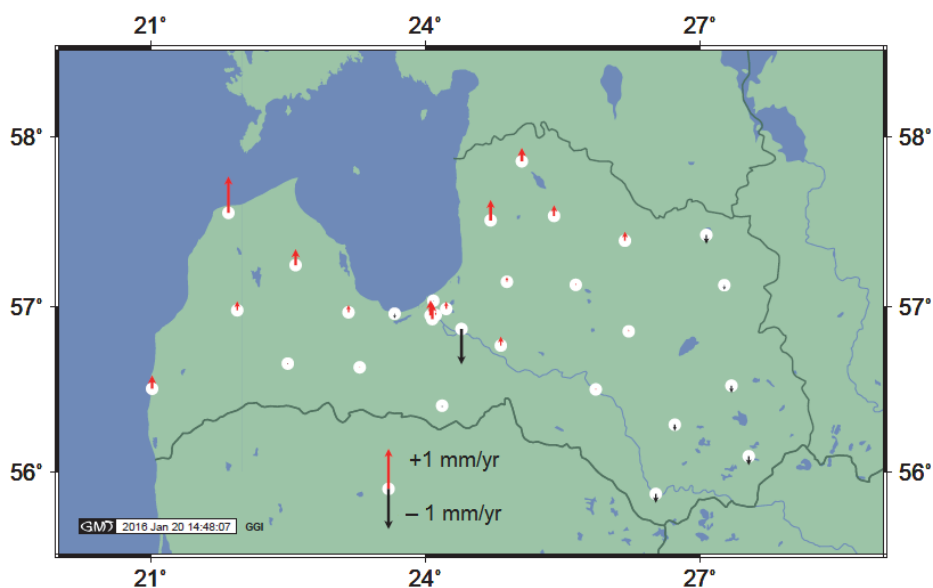


Figure 3.11. Latvian GNSS station vertical velocities obtained from the daily solution (2012–2015) and expressed in ETRF2000

The station horizontal movements obtained from the daily solution are shown in Figure 3.12. The magnitude of velocities for a larger number of stations comes to a few tenths of a millimetre. These velocities are less pronounced in comparison with the horizontal movements from the EUPOS[®] observation set. Nevertheless, one can observe that their orientation mostly corresponds to the orientation of horizontal movements according to the model NKG_RF03vel.

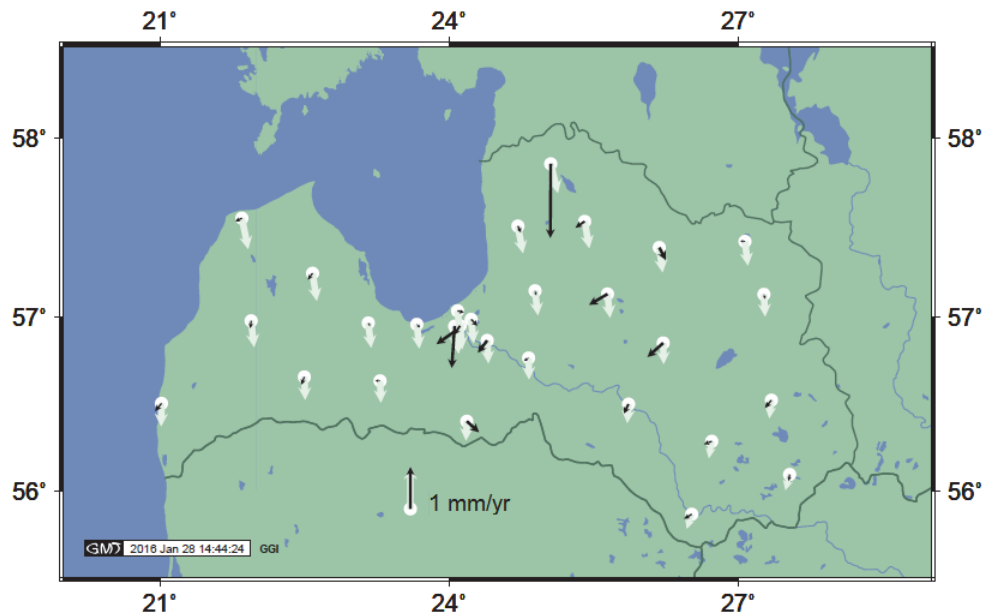


Figure 3.12. Latvian GNSS station horizontal movements obtained from the daily solution (2012–2015) and horizontal velocities from the model NKG_RF03vel

Figure 3.13 is shown to give an overview of annual horizontal movements at the GNSS stations. It is seen that one-year velocities greatly exceed 4-year cumulative velocities shown in Figure 3.12. As well as their orientation is different from year to year. There are a lot of influencing factors (Haritonova *et al.* 2013c); some of them are given in the next Section. Here should be noted that the non-tidal loading effect could have an impact, however it must be eliminated partially or totally by the method of double-differences within the network solution. According to Nordman *et al.* (2015), the Baltic Sea loading is well detectable in GNSS time series, and it is most prominent in the East component.

This is the fact why it is relevant to use long observation time series, according to the practice – not less than 3.5–4.5 year long observations.

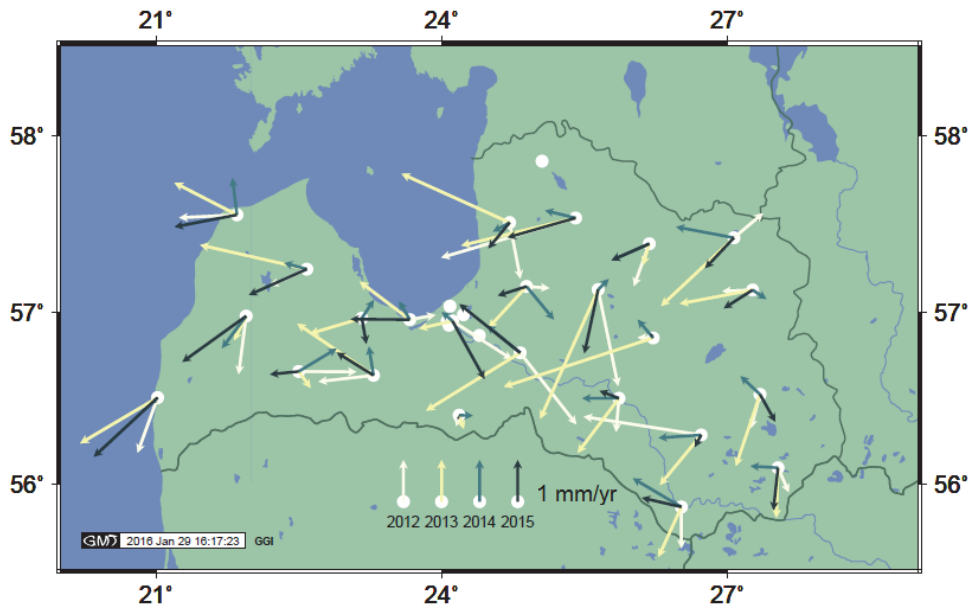


Figure 3.13. Latvian GNSS station annual horizontal movements obtained from the daily solution (2012–2015)

3.4.2. GNSS time series and site-specific effects

The horizontal and vertical velocity fields of the daily solution given in previous Section have been obtained after elimination of some effects in the station position time series. As has been mentioned above, more evident outliers, usually occurred during the winter time, and single (one-day) extremes, which are out of the diapason of ± 15 mm in Up component, were excluded.

Additionally, the time series were aligned from shifts occurred due to GNSS antenna change and introduction of GLONASS observations in 2015. Figure 3.14 shows the influence of antenna change in the year 2014 at the LODE station. Whereas, Figure 3.15 represents shift due to introduction of GLONASS observations.

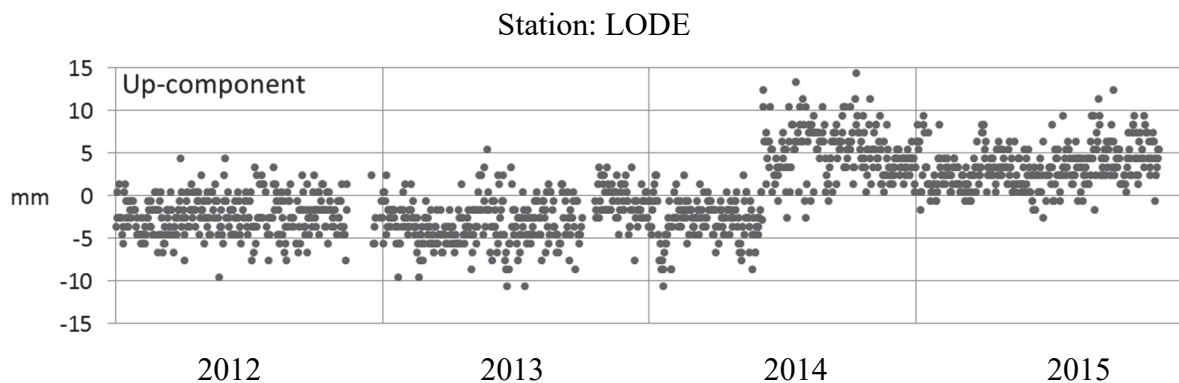


Figure 3.14. Station LODE time series in Up component with shift due to GNSS antenna change in 2014

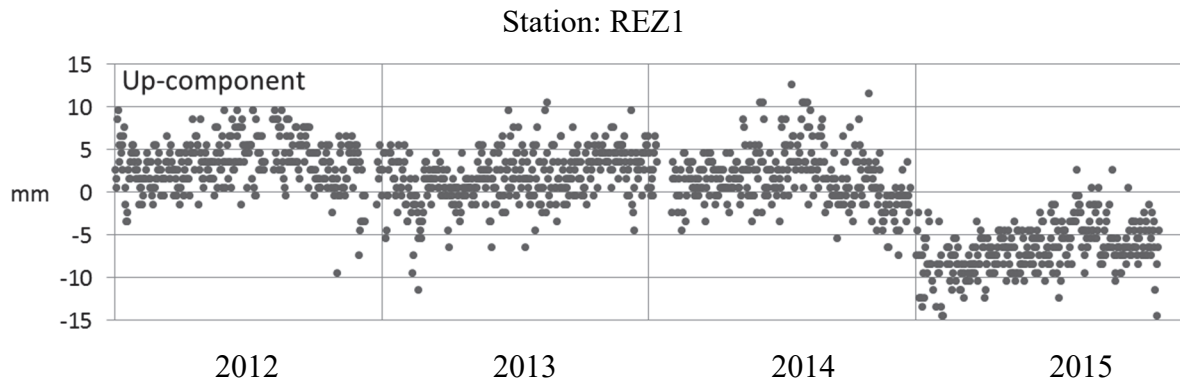


Figure 3.15. Station REZ1 time series in Up component with shift due to introduction of GLONASS observations in 2015

Not all effects have been excluded from the GNSS time series. For example, the annual variations, which have no strong impact on the resulting trend, have not been eliminated. The annual changes have been identified in the time series of few stations. More pronounced variations are observable at the following stations: PREI (East component), REZ1 (North component), SALP (all components) (see Figure 3.16) and SLD1 (East component). The point is that this annual variations are not typical for all components of stations, with one exception in the case of station SALP. The main reason of such behaviour could be local effects, for example, seasonal deformations of construction where antenna has been fixed, ground deformations and others.

One more factor distorting the trend of time series – the lack of observations, as shown in Figure 3.17 for RIGA station being used as a fiducial station in data processing.

The station MAZS should be mentioned as well. The antenna installation of this station differs from others; the antenna has been fixed on 8 m long post (see Appendix B), which is not appropriate base for geodynamic studies. Variations in the time series are shown in Figure 3.18.

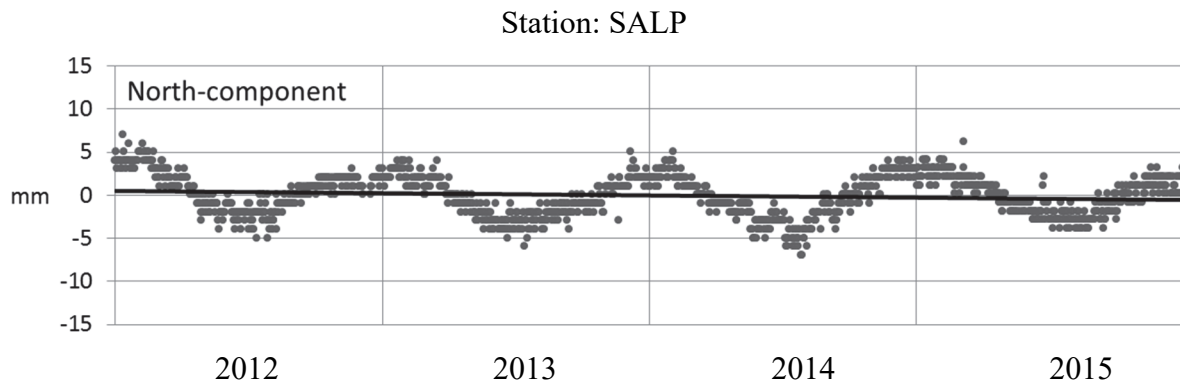


Figure 3.16. Station SALP time series in North component affected by annual variations

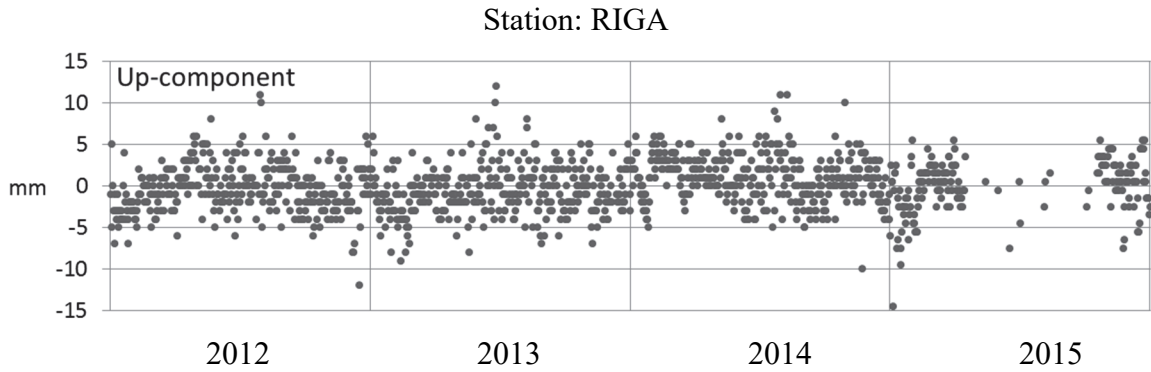


Figure 3.17. Station RIGA time series in Up component with missing data in 2015

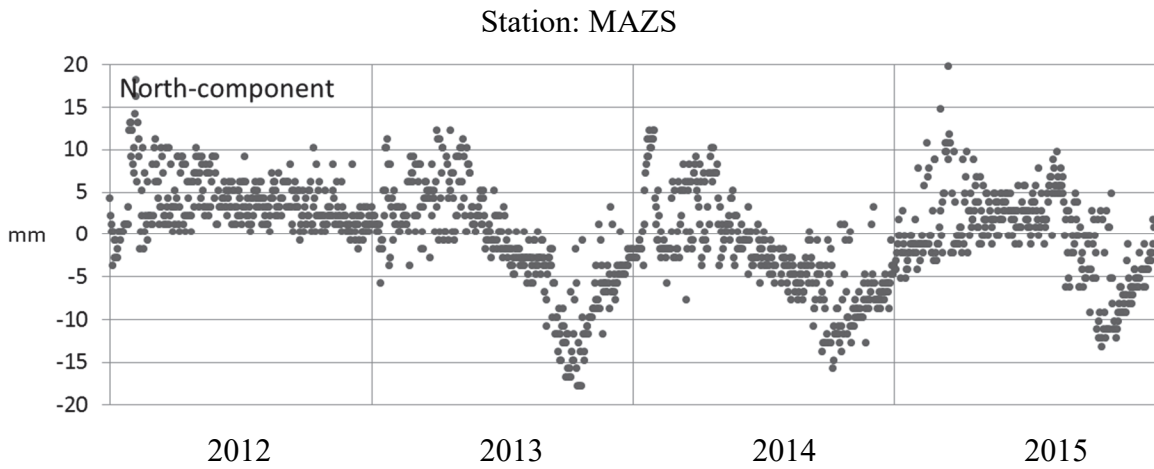


Figure 3.18. Station MAZS time series in North component

The results of the daily solution testify that the station IRBE has the highest (after MAZS station) RMS value for Up component's time series (see Table 3.4 and Appendix A for details). This should be noted because the observations of this station are often used for processing among other Baltic countries. IRBE station time series are shown in Figure 3.19.

The time series of each site from the daily solution, as well as the station information and coordinates are summarized in the catalogue, which is enclosed in Appendix B.

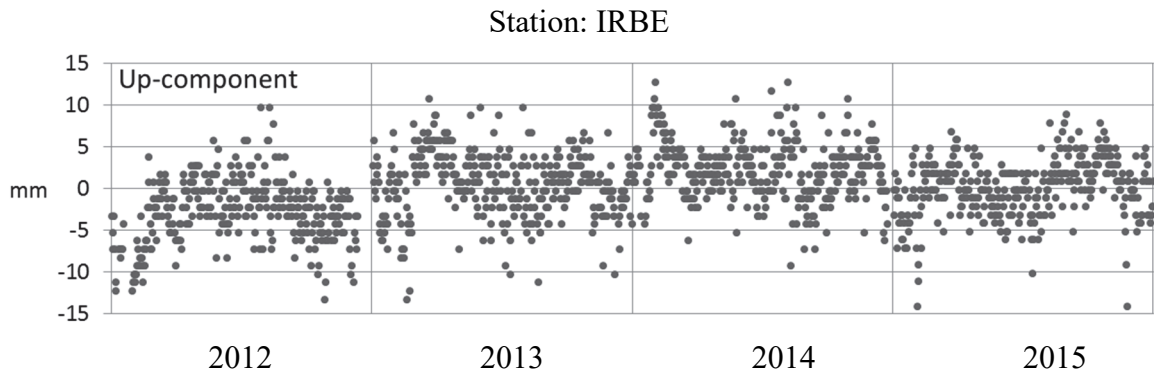


Figure 3.19. Station IRBE time series in Up component

3.5. Conclusions

EUPOS[®]-Riga and LatPos station displacements obtained from the continuous GNSS observations have been summarized for the period of 8 years, i.e., from 2008 to 2015. Two data sets are presented: ECC cumulative weekly solution (2008–2014) and GGI daily solution (2012–2015); for the last the data were re-processed using the *Bernese version 5.2*.

The results of ECC cumulative weekly solution have shown a positive tendency of the vertical movements in the western and central parts of Latvia, and a negative one – in the eastern part. The resulting range of vertical velocities from weekly solution for the territory of Latvia equals to 2.05 mm/yr; i.e., from –0.56 to +1.49 mm/yr.

In the case of daily solution the vertical velocities have a positive sign for all stations. The resulting range equals to 1.16 mm/yr: from +0.73 to +1.89 mm/yr, which is less compared to the range from ECC cumulative weekly solution. Besides, the vertical velocity field from the daily solution is more homogeneous.

The station horizontal displacements have similar orientation for both solutions; the velocities are mostly oriented to the south, but vectors have different magnitudes, however, the values do not exceed 1 mm/yr.

The rate of the present deformations due to the ongoing relaxation of the Earth in response to the past ice mass loss equals to ~10 mm/yr in the vertical direction in the northern Scandinavia (Kierulf *et al.* 2014). In the horizontal direction the rates are smaller: about 0–2 mm/yr (Milne *et al.* 2001).

The obtained GNSS time series have proved the existence of the Fennoscandian rebound effect in the territory of Latvia; however, it is relatively small. The comparison of obtained results with the data from the deformation model NKG_RF03vel has been made. According to the model, the vertical velocities of Latvian GNSS stations have a positive sign; the velocity range is 1.68 mm/yr, with the minimum +0.04 mm/yr and the maximum +1.72 mm/yr.

According to the daily solution, the vertical velocities of western GNSS stations correlate to the data of NKG_RF03vel. The highest velocity differences in the vertical component between the obtained results and values from the model are more pronounced in the case of the stations located in south-eastern part of Latvia; however, these differences are less than 1 mm/yr.

The station horizontal velocities from the weekly solution have comparatively adequate correlation to the velocity field from the deformation model NKG_RF03vel.

4. SEA LEVEL VARIATIONS AT THE LATVIAN COASTAL HYDROLOGICAL STATIONS

4.1. Introduction

Latvia benefits from 500 km long coastline of the Baltic Sea. The west coast of Latvia is washed by the open sea up to the north (Cape Kolka) meeting the waters of the Gulf of Riga there. The Gulf of Riga is a shallow semi-enclosed basin separated by Estonia's Saaremaa Island and connected to the Baltic Sea via two major canals towards north and west.

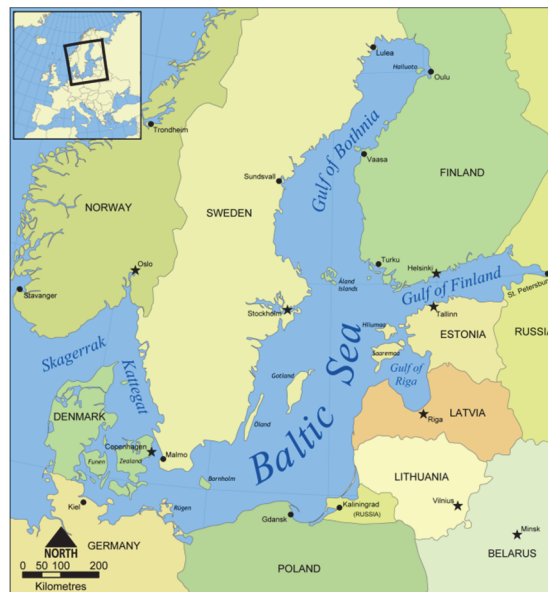


Figure 4.1. Map of the Baltic Sea (Einstein 2006)

As the Baltic Sea is a permanently stratified system, a key physical feature is the deep-water circulation and its implications on the overall dynamics. There are still a lot of gaps in understanding of the physics of Baltic Sea deep-water dynamics. This subject was discussed by several authors earlier, but has been seriously considered only in a few more recent studies (Elken and Matthäus 2008; Matthäus 2006; Meier 2006). The main problems involve different inflows and stagnation periods, water exchange between basins, diapycnal mixing, eddies and entrainment (Omstedt *et al.* 2014). Figure 4.2 displays the scheme of the large-scale internal water cycle in the Baltic Sea.

The Baltic Sea mass variation contains a rich spectrum of different oscillation phenomena (Ruotsalainen *et al.* 2015). The wind-driven free oscillation patterns on the surface of the Baltic Sea are complicated by the shape of the gulfs and islands (Lisitzin 1959; Wübbler and Krauss 1979).

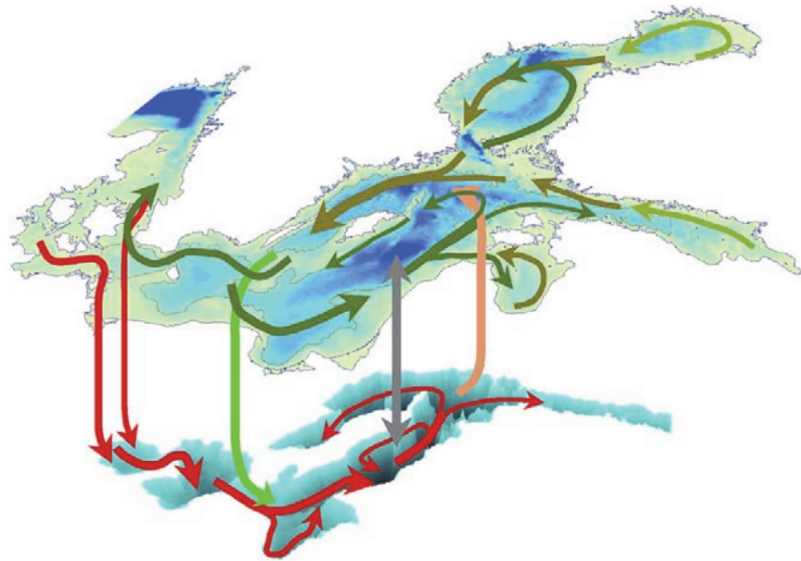


Figure 4.2. Scheme of the large-scale internal water cycle in the Baltic Sea shown as two-layer system: green and red arrows show the surface and bottom layer circulations, the light green and beige arrows show entrainment, and the grey arrow shows diffusion (Elken and Matthäus 2008)

According to Ekman (2009), the general picture of the sea level variations in the Baltic Sea can be summarized in the three following items:

- 1) short-term sea level variations (on the time scale of days) – to a limited extent caused by air pressure variations producing an inverted barometer effect;
- 2) short-term sea level variations (on the time scale of days) – to a larger extent caused by winds redistributing water within the Baltic Sea; that mainly affects the northern, eastern and south-western shores of the Baltic;
- 3) long-term sea level variations (on the time scale of months and years) – caused by persistent winds redistributing water between the Atlantic Ocean (the North Sea) and the Baltic Sea; that affects the Baltic as a whole.

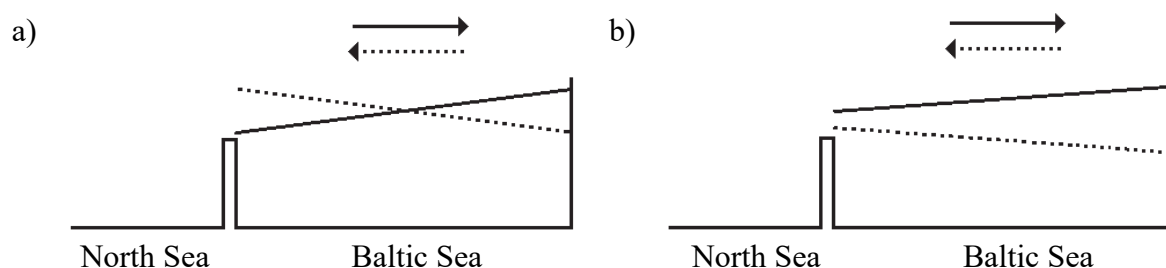


Figure 4.3. The short-term effect on the Baltic Sea level caused by a temporary wind (a) and the long-term effect caused by a persistent wind (b): continuous line – south-west wind and dashed line – north-east wind (Ekman 2009)

The short-term effect on the Baltic Sea level caused by a temporary wind is shown in Figure 4.3a and the long-term effect caused by a persistent wind is depicted in Figure 4.3b. It should be noted that the short-term variations are mainly internally driven variations, with maximum amplitudes in the far north and the far south, and a nodal line close to Stockholm in the middle. Thus short-term sea level variations are nearly eliminated at this site (Ekman 2009).

The tidal variation of the Baltic Sea varies in the order of centimeters only. However, the range of non-tidal variation is up to 2–3 m on the coasts of the Gulf of Bothnia and Gulf of Finland (Virtanen and Mäkinen 2003a).

Such geodynamic effect as the ocean tide loading is routinely removed from GNSS measurements according to the recommendations disclosed by IERS Conventions. At the same time there is also the effect of non-tidal ocean loading variation with its own impact on geodetic observations, especially near the coastline. For example, one meter layer of water in the whole of the Baltic Sea can cause vertical deformation near the Latvian coast which equals about –15 mm (Nordman *et al.* 2015).

This makes it important to explore variations occurring in the Baltic Sea. The objective of this study is to analyze the water level variations in the Baltic Sea at the Latvian coast using sea level gauge observations and identify tidal waves as well.

4.2. Data selection and processing

Hydrological observations in Latvia are carried out by the Latvian Environment, Geology and Meteorology Centre (LEGMC). Totally 9 coastal hydrological stations are maintained on the Latvian coast providing continuous observations.

For this study the observations from 7 sea level stations have been used (Haritonova 2016). Data from two other stations (Roja and Skulte) are not used because there are great gaps in the observation series for desired 3-year period – from year 2013 to 2015. The locations of the selected stations are shown in Figure 4.4; five stations (Kolka, Mērsrags, Lielupes grīva, Daugavgrīva and Salacgrīva) are located on the coast of the Gulf of Riga, and two (Liepāja and Ventspils) – on the west coast of Latvia, washed by the open sea.

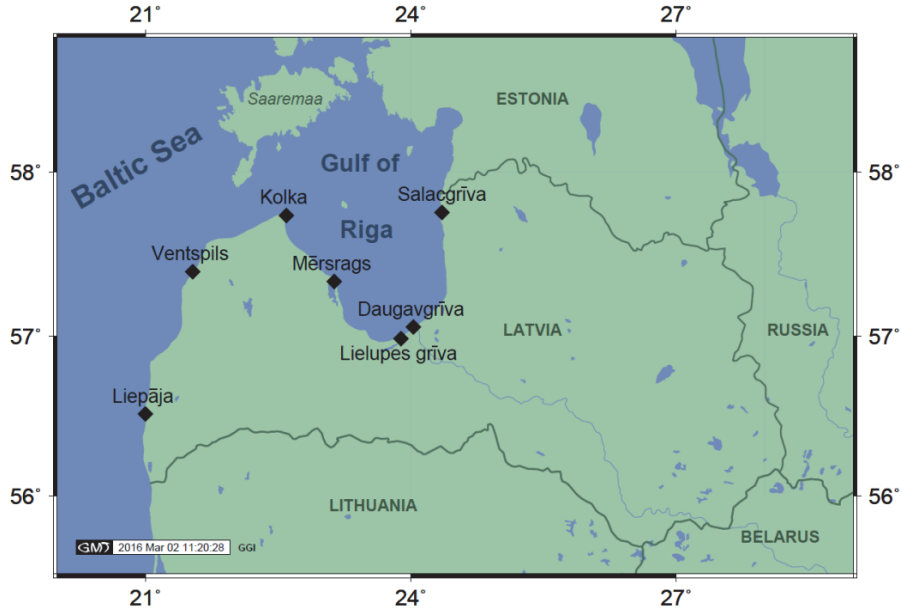


Figure 4.4. Latvian sea level stations: Liepāja, Ventspils, Kolka, Mērsrags, Lielupes grīva, Daugavgrīva and Salacgrīva

The sea level data used for this analysis are mean values of the last 15 minutes of an hour, in this way having 24 values for each day (LEGMC sea level observations are available at: <https://www.meteo.lv/en/hidrologija-datu-pieejamiba/?nid=912>). Of course, during 3-year period, there were some short gaps in the time series of each sea level station, mostly 1 to 3 hour long. To perform spectral analysis the data has been interpolated. In the case of long gaps, the data of a whole year has not been used as it can be seen in the next Section.

The Fourier transform with Parzen window $w(k)$ has been applied to perform spectral analysis. The sea level time series have been detrended separating non-harmonic influence.

The common formula for computation of the smoothed spectral density function is

$$\bar{R}_{xx}(l) = 2 \left[1 + 2 \sum_{k=1}^{L-1} r_{xx}(k) w(k) \cos \frac{\pi lk}{F} \right], l = 0, 1, \dots, F, \quad (4.1)$$

where L – window bandwidth,

$$r_{xx}(k) = \frac{c_{xx}(k)}{c_{xx}(0)} \quad (4.2)$$

is the sample autocorrelation function with the autocovariance function estimate

$$c_{xx}(k) = \frac{1}{n} \sum_{t=1}^{n-k} (x_t - \bar{x})(x_{t+k} - \bar{x}). \quad (4.3)$$

For more details refer to Jenkins and Watts (1968).

4.3. Results and discussion

The time series of sea level for the mentioned 3-year observation period are shown in Figure 4.5. The sea level data is given above the gauge zero.

As one can see from the Figure 4.5, the sea level ranging diapason is quite high; it runs up to 2 m during one year. One more obvious fact is that the time series have a distinct increase in the amplitude during the winter season; with increasing sea levels in early winter and decreasing sea levels in late winter.

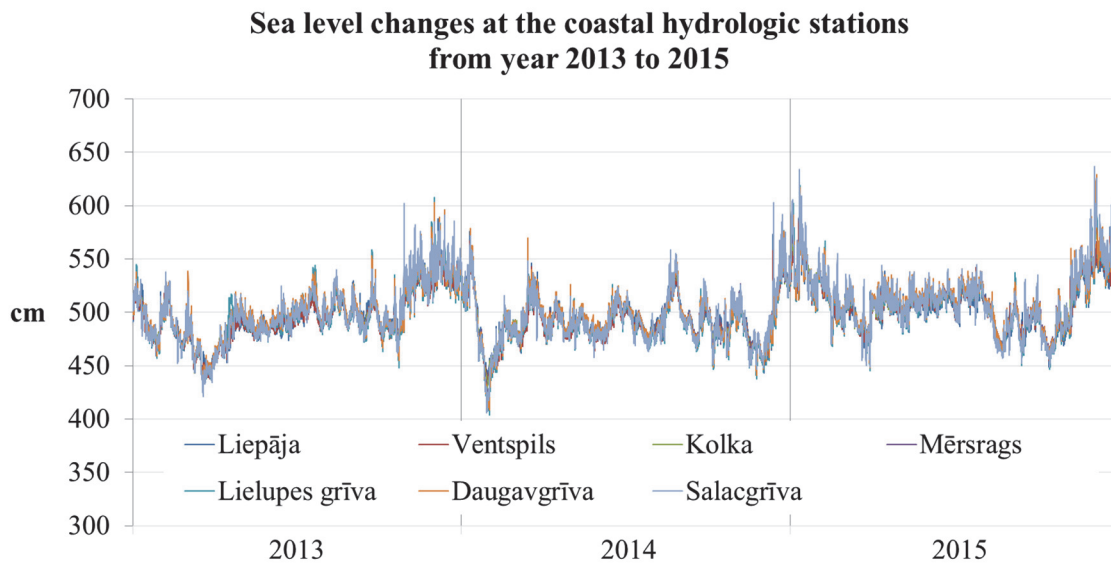


Figure 4.5. Sea level time series of the Latvian coastal hydrological stations Liepāja, Ventspils, Kolka, Mērsrags, Lielupes grīva, Daugavgrīva and Salacgrīva from year 2013 to 2015

This effect was pointed out by Ekman (1998). Comparing the sea level data with wind data from the Baltic entrance for the whole period 1825 – 1984, it was found that the main origin of the amplitude increase is a secular change in the winter wind conditions, with increasing south-westerly winds in early winter and decreasing south-westerlies in late winter (Ekman 2009).

More representative picture of the sea level dynamics at the Latvian coast is shown by Figure 4.6, where the differences between sea level maximum and minimum at appropriate station are given. The stations in a graph are in consecutive order starting with the station Liepāja and continuing along the coastline till the station Salacgrīva.

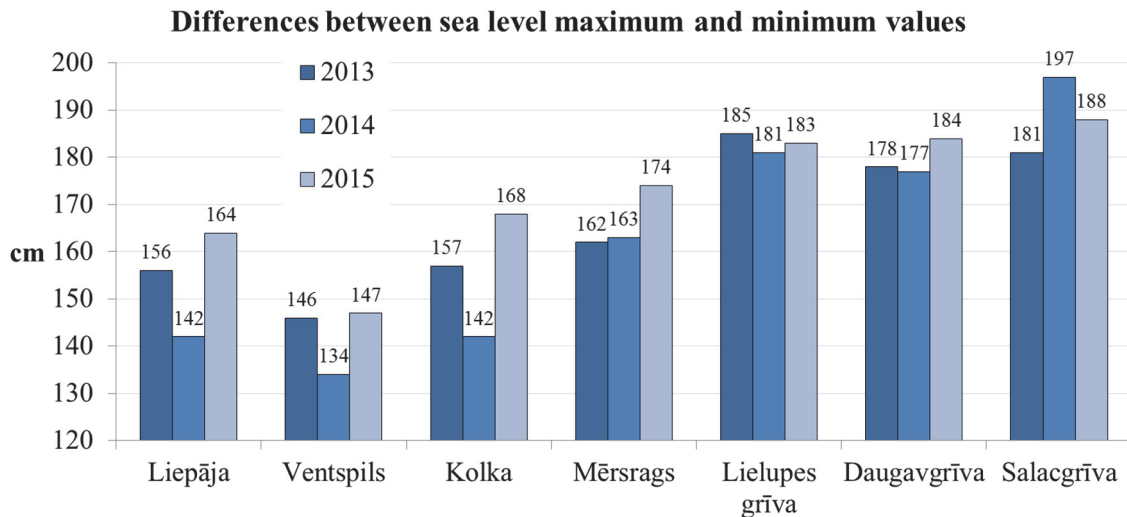


Figure 4.6. Differences between sea level maximum and minimum values at the 7 Latvian coastal hydrological stations given for 3 years

One can observe that the sea level differences are mostly increasing with every next station. The stations Liepāja, Ventspils and Kolka have the smallest sea level differences in the background of other station data for all three years. It can be explained by the fact that the stations have direct access to the open sea and their locations are close to the nodal line of sea level variations as in the case of Stockholm station. In spite of more strong impact of the open sea flows due to wind, the short-term variations are nearly eliminated, and the long-term sea level variations have mean values as described before and depicted in Figure 4.3.

Additionally, the differences between the sea level maximum and minimum at the stations Liepāja, Ventspils and Kolka have more pronounced annual changes in comparison with the data of other stations. The explanation of this could be the annual meteorological conditions of the Baltic Sea, whose changing is more observable in the open sea.

According to Wübbler and Krauss (1979), the Gulf of Riga is of considerable importance for the seiches of the Baltic Sea. The sea level variations in the interior areas of the gulfs behave like standing waves; this holds for the Gulf of Riga as well. It exhibits the highest amplitudes, which seems to be due to a co-oscillating mode of this basin.

The sea level stations Lielupes grīva, Daugavgrīva and Salacgrīva are more eastern stations of the Gulf of Riga. The sea level differences at these stations show the highest values that absolutely correspond to the previous statement.

The results obtained after spectral analysis are shown in Figures 4.7 and 4.8. The spectral density functions for the time series of the sea level at the Latvian coastal hydrological stations for each year are depicted there.

Totally, 4 main tidal waves (O_1 , K_1 , M_2 and S_2) have been identified in the spectrum of the sea-level changes. The magnitudes of tidal constituents are given in Table 4.1.

It can be observed that the magnitudes of the tidal oscillations obtained at the Gulf of Riga (Kolka, Mērsrags, Lielupes grīva, Daugavgrīva, Salacgrīva) are higher than those obtained at the west coast of Latvia (Liepāja and Ventspils). The similar results were published by Keruss and Sennikovs (1999), where the considerably longer sea level time series from 4 Latvian coastal hydrological stations were used. The explanation of this effect is the following: the changes in the sea level at the coast of the Baltic Sea are more dependent on meteorological forcing than at the coast of the Gulf of Riga; the spectral noise produced by it prevents from identifying of the true magnitudes of tidal oscillations.

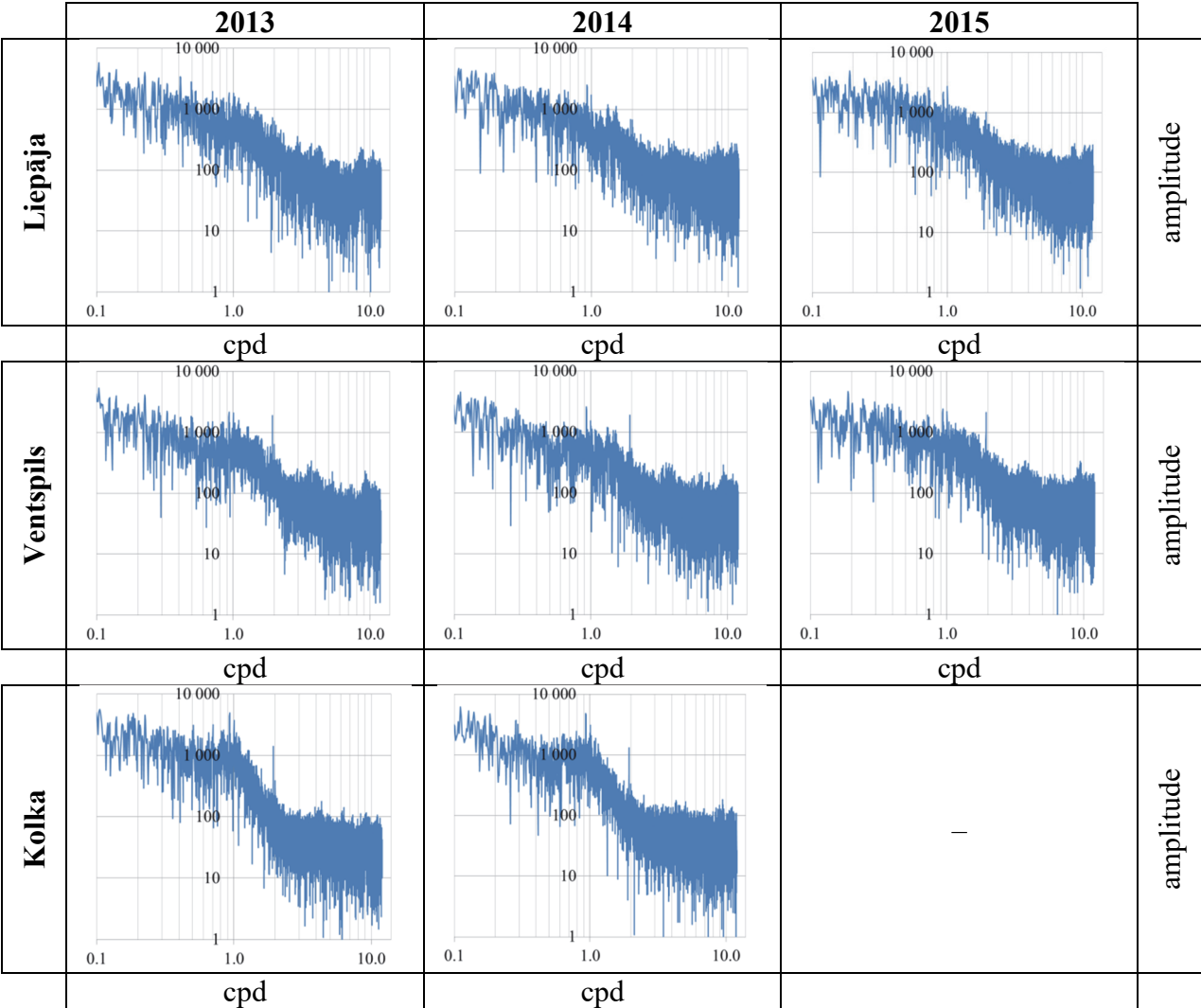


Figure 4.7. Spectral density functions for the time series of sea level at the Latvian coastal hydrological stations: Liepāja, Ventspils and Kolka

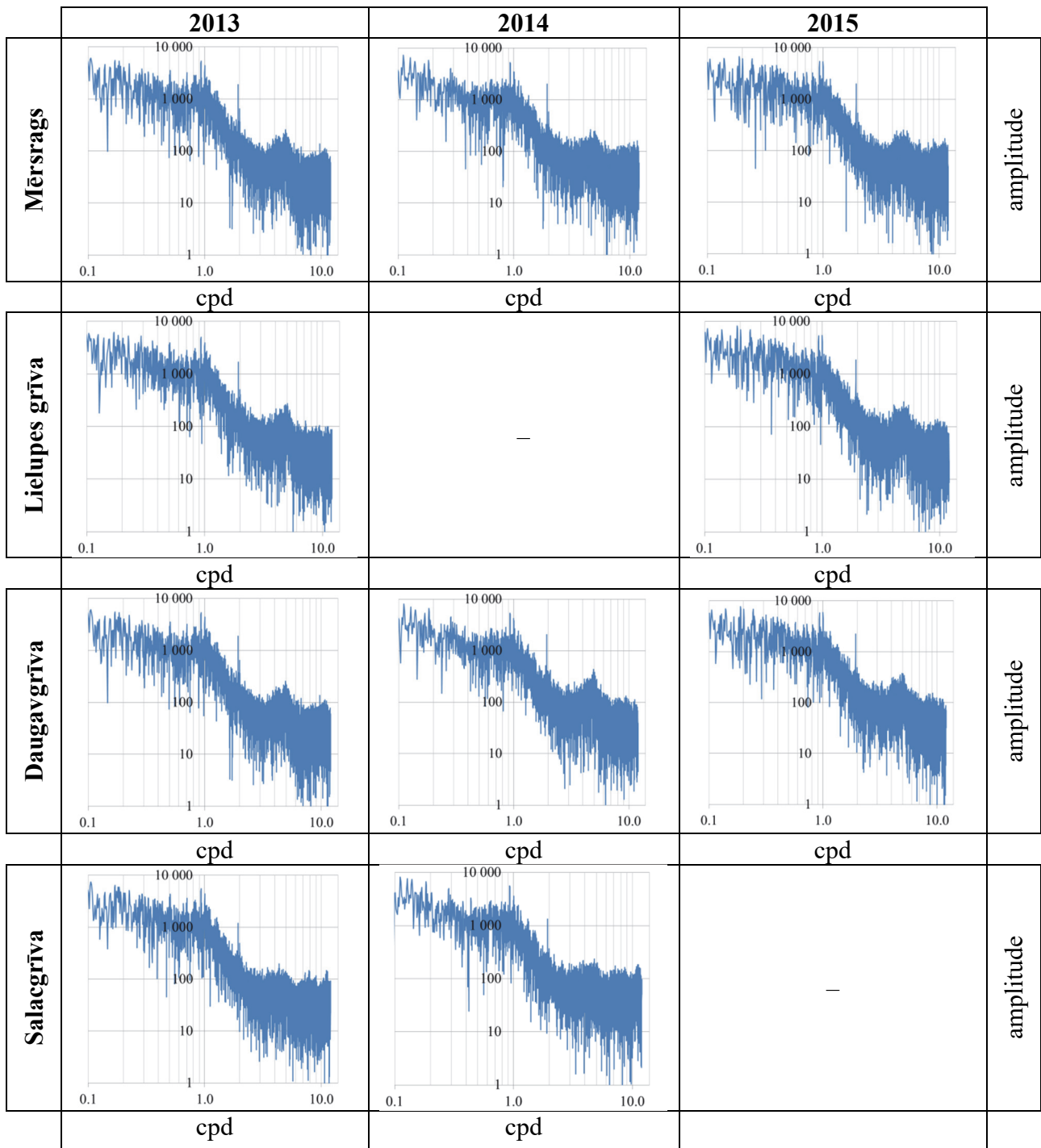


Figure 4.8. Spectral density functions for the time series of sea level at the Latvian coastal hydrological stations: Mērsrags, Lielupes grīva, Daugavgrīva, Salacgrīva

As can be seen from Table 4.1, the magnitudes of tidal constituents are not the same comparing values for each year. This also can be explained by the changing meteorological conditions of the Baltic Sea, which have affected the sea level time series.

Table 4.1

Magnitudes (cm) of main tidal constituents at the Latvian coastal hydrological stations:
frequency is given in cycles per day

Tidal constituent	O ₁			K ₁			M ₂			S ₂		
Frequency, cpd	0.930			1.002			1.932			2.000		
Years	2013	2014	2015	2013	2014	2015	2013	2014	2015	2013	2014	2015
Liepāja	0.52	0.69	0.61	0.51	0.48	0.75	0.20	0.19	0.28	0.18	0.19	0.18
Ventspils	0.60	0.72	0.67	0.58	0.42	0.61	0.53	0.53	0.59	0.18	0.15	0.14
Kolka	1.36	1.35	–	1.04	0.87	–	0.39	0.37	–	0.11	0.09	–
Mērsrags	1.50	1.47	1.53	1.22	0.96	1.49	0.53	0.56	0.55	0.18	0.16	0.15
Lielupes grīva	1.38	–	1.49	1.08	–	1.51	0.47	–	0.51	0.14	–	0.06
Daugavgrīva	1.50	1.49	1.63	1.22	1.18	1.66	0.53	0.57	0.62	0.18	0.11	0.11
Salacgrīva	1.55	1.58	–	1.23	1.01	–	0.33	0.38	–	0.14	0.10	–

Figure 4.9 represents the mean magnitudes of the tidal constituents obtained from the values given in the Table 4.1. The magnitude of diurnal constituent O₁ is the highest for all stations. Close to it is the magnitude of diurnal constituent K₁, except the two stations Salacgrīva and Kolka, which are more northern Latvian stations in the Gulf of Riga. It is noticeable that the magnitude of diurnal constituent K₁ is practically equal to the magnitude of semi-diurnal constituent M₂ at the station Ventspils. Comparing semi-diurnal constituents, the magnitude of M₂ is 3 to 5 times higher than the magnitude of S₂, but not in the case of station Liepāja, where these magnitudes are sub-equal.

Additionally, the spectral density functions in Figure 4.8 show explicit power at the frequency of 5 cpd. This frequency fails to correspond to the tidal frequency. The magnitude of this oscillation is not considerable; it makes up about 1 mm, however, it is worth noting that this is typical only for the stations Mērsrags, Lielupes grīva and Daugavgrīva. As these sea level stations are located relatively close together in the Gulf of Riga, the power could represent some local effect.

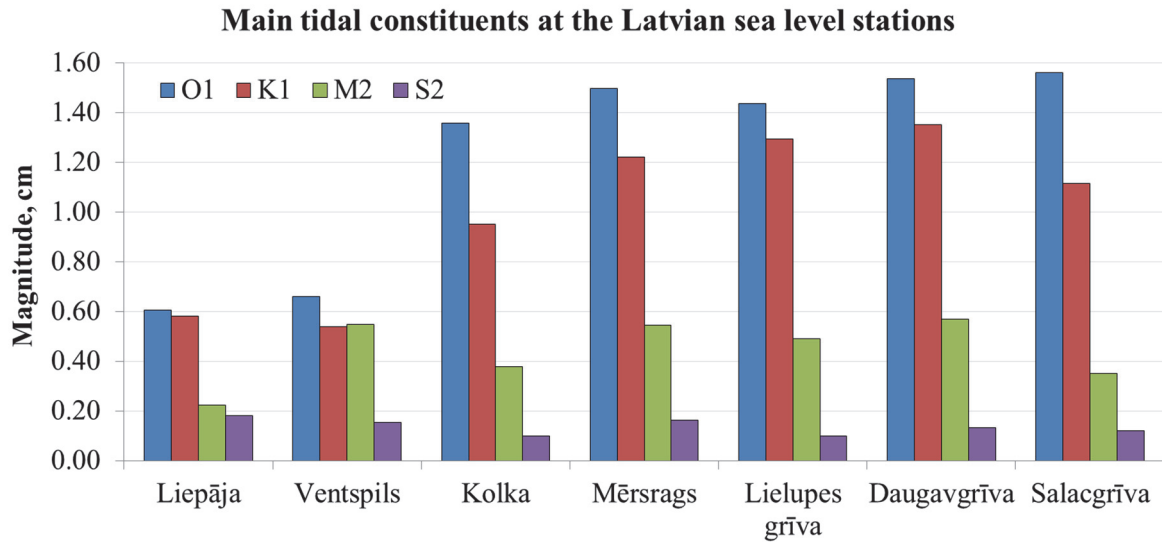


Figure 4.9. Magnitudes of main tidal constituents at the Latvian coastal hydrological stations

4.4. Conclusions

The sea level ranging diapason is quite high in the Gulf of Riga; during one year it ran up to 2 m at the Salacgrīva station. In the case of the stations located on the west coast of Latvia (Liepāja and Ventspils) and station Kolka this diapason is not so high, but the differences between the sea level maximum and minimum here have more pronounced annual changes in comparison with the other station data.

The spectral analysis of the sea level data from the Latvian coastal hydrological stations has proved the diurnal and semi-diurnal tide existence both in the Gulf of Riga and the Baltic Sea at the Latvian coast. Four main tidal waves (O₁, K₁, M₂ and S₂) have been identified. The magnitudes of the tidal oscillations in the Gulf of Riga are higher than in the open sea. Furthermore, the power at the frequency of 5 cpd has been detected for the stations in the Gulf of Riga, which could represent some local effect.

The spectral analysis of one year sea level data allows for the determination of 4 main tidal waves. To identify more tidal constituents it is necessary to use the long-term sea level observations.

5. DESIGN OF A NEW MULTI-PURPOSE OPTICAL TRACKING SYSTEM

Within the period from 2014 to 2015 the Institute of Geodesy and Geoinformatics of the University of Latvia in cooperation with the Institute of Physics of the University of Latvia were engaged in a joint project resulted in the development of the experimental instrument of a new multi-purpose optical tracking system (twin-optics SLR) intended for both positional and laser ranging observations of near-Earth objects.

The overview of the observation methods, description of the system design, and the findings of functionality tests of an astrometric subsystem are summarized in this Chapter.

5.1. Methods and their importance

5.1.1. CCD technology

The determination of the directions from the ground to satellites based on optical observations is one of the early methods of satellite geodesy leading to remarkable results. In addition, the optical tracking of satellites is of fundamental importance because it is the only technique in satellite geodesy that directly establishes the access to the inertial reference frame. All other methods like GNSS and SLR only indirectly provide a link to the frame through the equation of motion (Seeber 2003).

In the last decade of the 20th century, the fast development of electronic position sensors, in particular the Charge Coupled Device (CCD), initiated a revival of optical methods in astrometry and also satellite geodesy. The key factors, when compared with traditional photographic or even visual methods are:

- a) higher sensitivity, improved accuracy, shorter observation time,
- b) the image information is available in digital form,
- c) fully automatic data flow; no time consuming coordinate measurement necessary, and
- d) availability of new star catalogues with sufficient and accurate reference stars.

In geodetic astronomy many classical observation techniques have been supplanted by the new technology based on the use of CCD (Fosu 1998; Hirt 2001; Schildknecht 1994).

Satellites are fast moving objects and hence generate particular problems; however, wide experience and solutions of many concepts can be gained from astrometry and classical photographic satellite tracking.

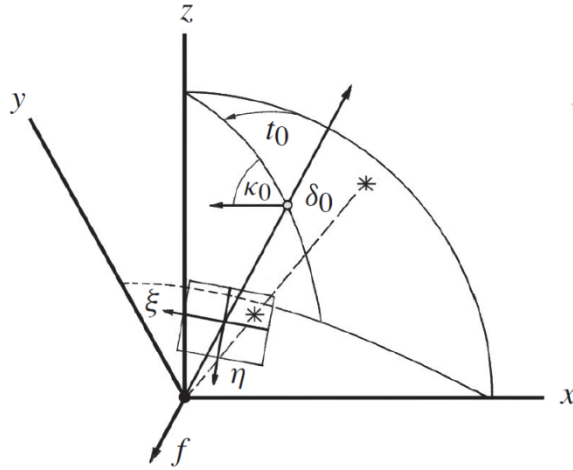


Figure 5.1. Perspective projection and camera orientation (Seeber 2003)

The basic objective is to determine the orientation of a camera with respect to the inertial frame. The camera may be either fixed to the ground (Earth based station) or to a space vehicle (satellite, rocket, and platform). In both cases the orientation angles (see Figure 5.1) have to be determined: declination δ_0 , right ascension α_0 (or hour angle t_0), and the swing angle κ_0 around the camera axis. The process widely follows the procedure that has been developed in the photographic technique. The main steps are depicted in Figure 5.2.

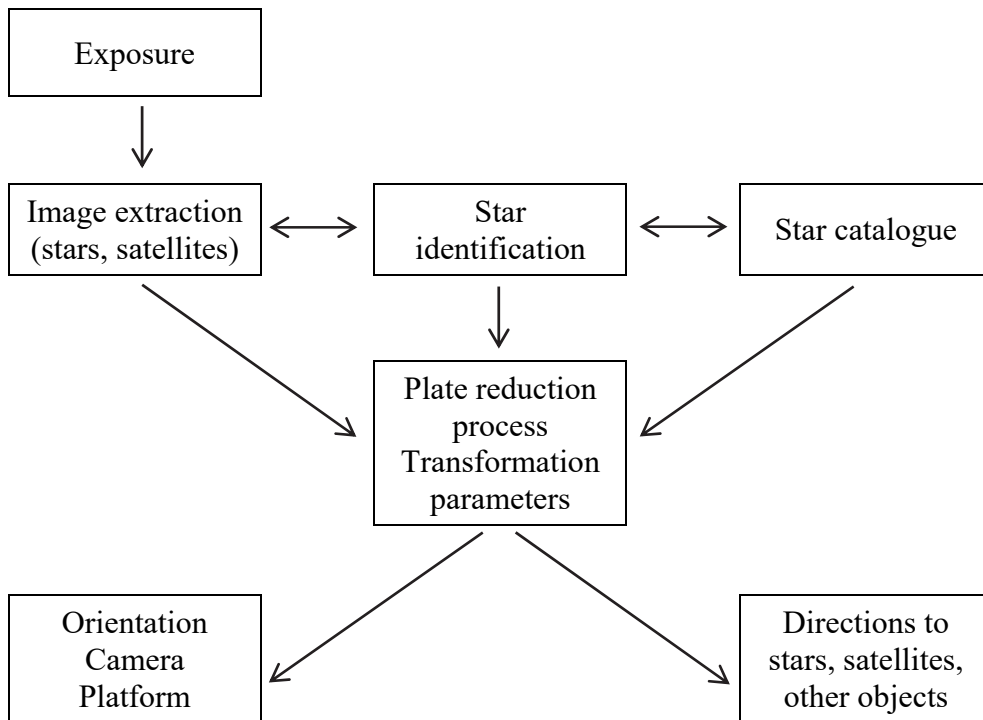


Figure 5.2. Process of CCD observations (Seeber 2003)

A CCD camera uses a CCD sensor instead of the photographic plate or film to store the image information. The CCD sensor makes use of the photoelectric effect in silicon to convert photons into charges. The sensor or chip consists of a certain number of lines and columns forming an array of pixels.

In order to obtain image coordinates for objects of interest the images of stars and satellites have to be recognized, and the coordinates of the image centers have to be determined. This is the process of image extraction. The images are considered to be a group of pixels with similar properties; they differ from the background through significantly higher grey values.

In the next step star images in the digital photogram have to be identified (Zariņš *et al.* 2014; Balodis *et al.* 2014) and related to the equatorial positions given by a star catalogue. Because of the small field of view and high sensitivity of CCD sensors, the star catalogues with a very high number of precise star positions, down to apparent magnitudes of 15m or fainter, are required.

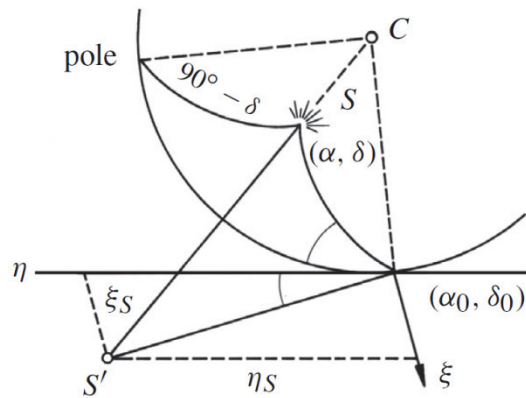


Figure 5.3. Tangential coordinates ζ, η (Seeber, 2003)

For the process of star identification the approximate region of the photogram is delineated in the star catalogue, and the equatorial star positions α_i, δ_i are converted to plane tangential coordinates ζ_i, η_i and the approximate camera orientation α_0, δ_0 . The two point ensembles x_i, y_i (measured coordinates in the image coordinate system) and ζ_i, η_i are matched against one another with a suitable algorithm using translation, rotation, and scale, until highest correlation is achieved. To start with, some arbitrary points from both ensembles are set to be identical. To accelerate the process, the search algorithm can be restricted to the brightest stars of the field.

Within the plate reduction process an adequate model for the relation between tangential star coordinates ζ, η and measured coordinates x, y has to be found. Once the parameters of this

model are identified, they can be used to transform the measured satellite coordinates x_s, y_s via the tangential coordinates ζ_s, η_s into equatorial satellite directions α_s, δ_s .

As a result, the orientation of the camera axis in inertial space and/or the directions from the camera position to space objects like satellites are obtained.

5.1.2. Laser ranging

In laser distance measurements to satellites, the time of the flight of a laser pulse (as it travels between a ground station and a satellite) is observed. A short laser pulse is generated in the ground station, and is transmitted through an optical system to the satellite (see Figure 5.4). A part of the outgoing laser pulse is used to start an electronic time interval counter. The target satellite has appropriate retroreflectors. The reflected pulse is received at the ground station, detected, amplified, analysed, and used to stop the electronic counter (Seeber 2003).

The two-way travel time of the signal (total signal propagation time Δt) is derived from the two readings of the user clock, and is scaled into the distance d , with the signal propagation velocity c . The basic observation equation is:

$$d = \frac{\Delta t}{2} c . \quad (5.1)$$

New fields of SLR application have been evolving with the increasing accuracy of the measuring systems. With an accuracy range of ± 1 cm or better, considerable contributions can be made to the establishment of reference frames, geodynamics, the determination of precise satellite orbits and the modelling of Earth's gravity field.

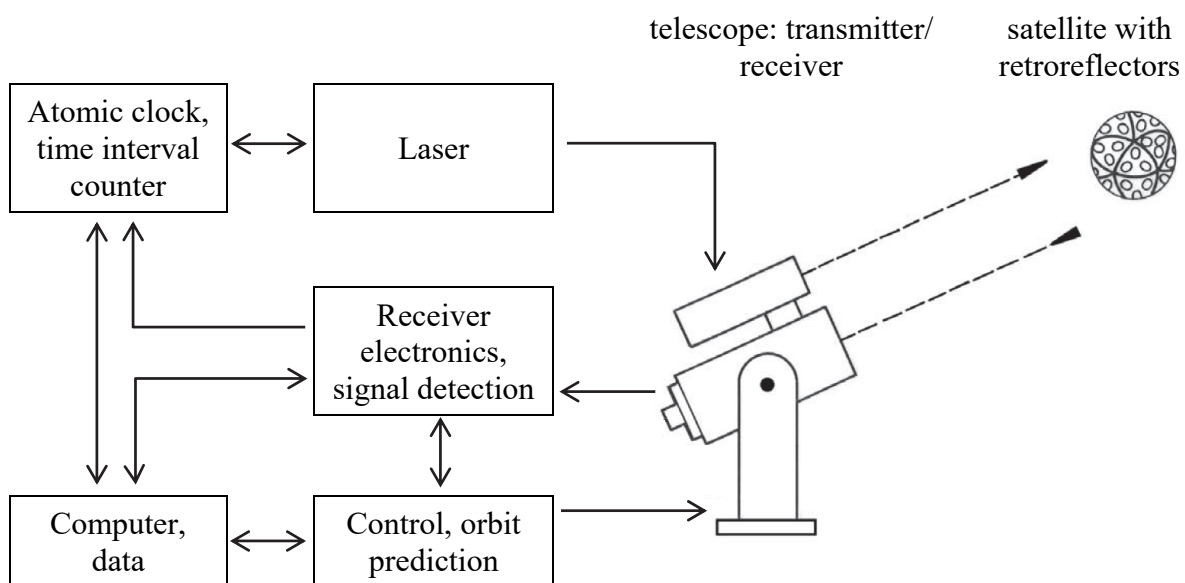


Figure 5.4. The principle of satellite laser ranging (Seeber 2003)

5.2. Design of the new instrument

The construction design of the instrument has been completed; all major components have been manufactured or purchased to be assembled together (see Figures 5.5 and 5.6). The principal functionality of control software has been already implemented; presently hardware control and inter-process communication tests and adjustments are being done (Balodis *et al.* 2016).



Figure 5.5. Installation of the instrument

As active mode observations, including daytime tracking, require precise pointing, an original optical scheme with three optical channels, i.e., one transmitter and two receivers, has been designed. The three dimensional scheme of optics is shown in Figure 5.7.

The one of the twin optical systems is fitted with a CCD and used for astrometric purposes; including mount pointing direction determination, object coordinate determination and object guiding. The other, fitted with a reflected light pulse detector, will be used for SLR pulse processing (Kaminskis *et al.* 2015; Haritonova *et al.* 2016).

The target technical features of the system are (Zarins *et al.* 2015):

- a) twin 41 cm optical systems on Alt-Alt mount, separate transmitted beam collimator;

- b) motors and control sensors for pointing and tracking of any orbital object with positioning accuracy within a few arcseconds;
- c) positional observation accuracy within a fraction of arcsecond for objects with optical magnitude up to 15m;
- d) SLR capability (depending on laser transmitter properties) up to geostationary orbit;
- e) option of simultaneous positional and SLR observations – usage of both optical systems in various combinations.

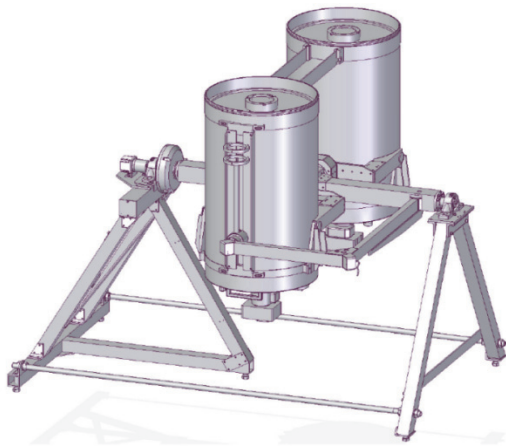


Figure 5.6. Design of the new multi-purpose optical tracking system

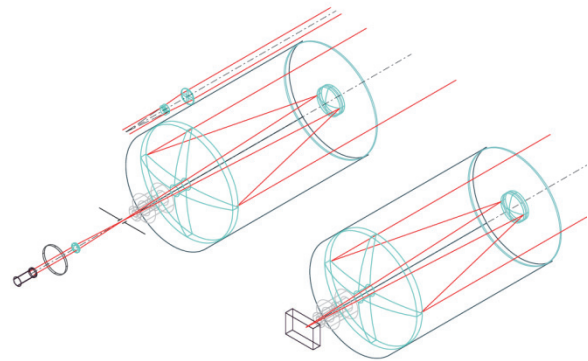


Figure 5.7. Three dimensional scheme of optics

An optical transmitter directs laser beam through the system with 4 beam turning mirrors (see Figure 5.8):

- a) the first two mirrors of laser path are equipped with actuators;
- b) each mirror reflects 99.5 % of laser beam light;
- c) laser beam turns at the mirrors with optimized performances at 532 nm wavelength;
- d) laser beam diameter is 6 mm;
- e) laser beam expander (10× expansion presently).

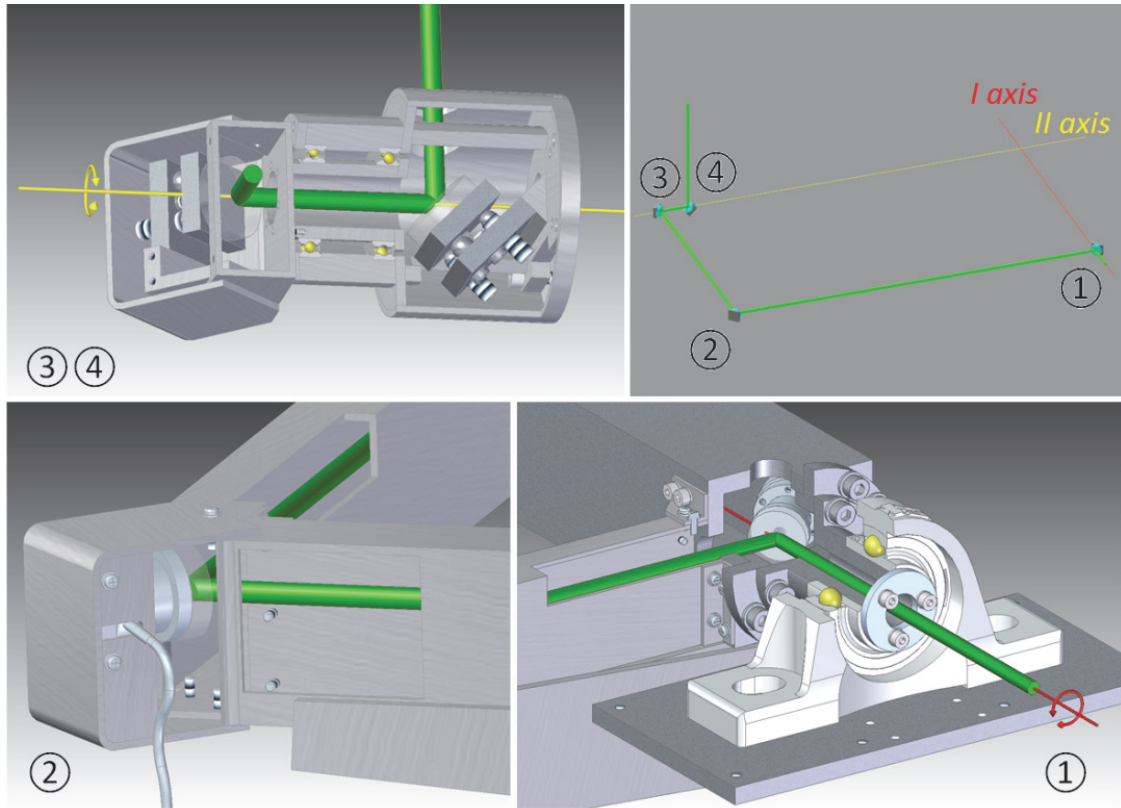


Figure 5.8. Design of separate optical units with laser path in beam turning mirrors assembly

5.2.1. Deformations of optical system's transmitting path

Deformation of the system first axis causes the turning of the first mirror. Figure 5.9b shows the calculated deformations of the first axis under the load of own weight and the weight of corresponding montage parts (≈ 1200 N) at an angle of 40° . For the compensation of this additional turning the computer controlled high-performance tripod design actuator associated with a mirror is likely to be used.

Deformations due to the load of the laser beam path (see Figure 5.9c) will be eliminated as well using actuator in the second unit of the path (see Figure 5.8). Each actuator ensures beam deflection up to 2.4 mrad (Haritonova *et al.* 2014c).

Taking into account the fact that the manufacturing possibilities of mechanical parts of complicated configuration and high precision are limited, the design of the system mount has to be maximally optimized to minimize deformations. All calculations of deformations have been performed applying *Solid Edge ST5*.

Besides, a software-implemented mount error model, which is described in Section 5.4.2, will be used to achieve the expected positioning accuracy.

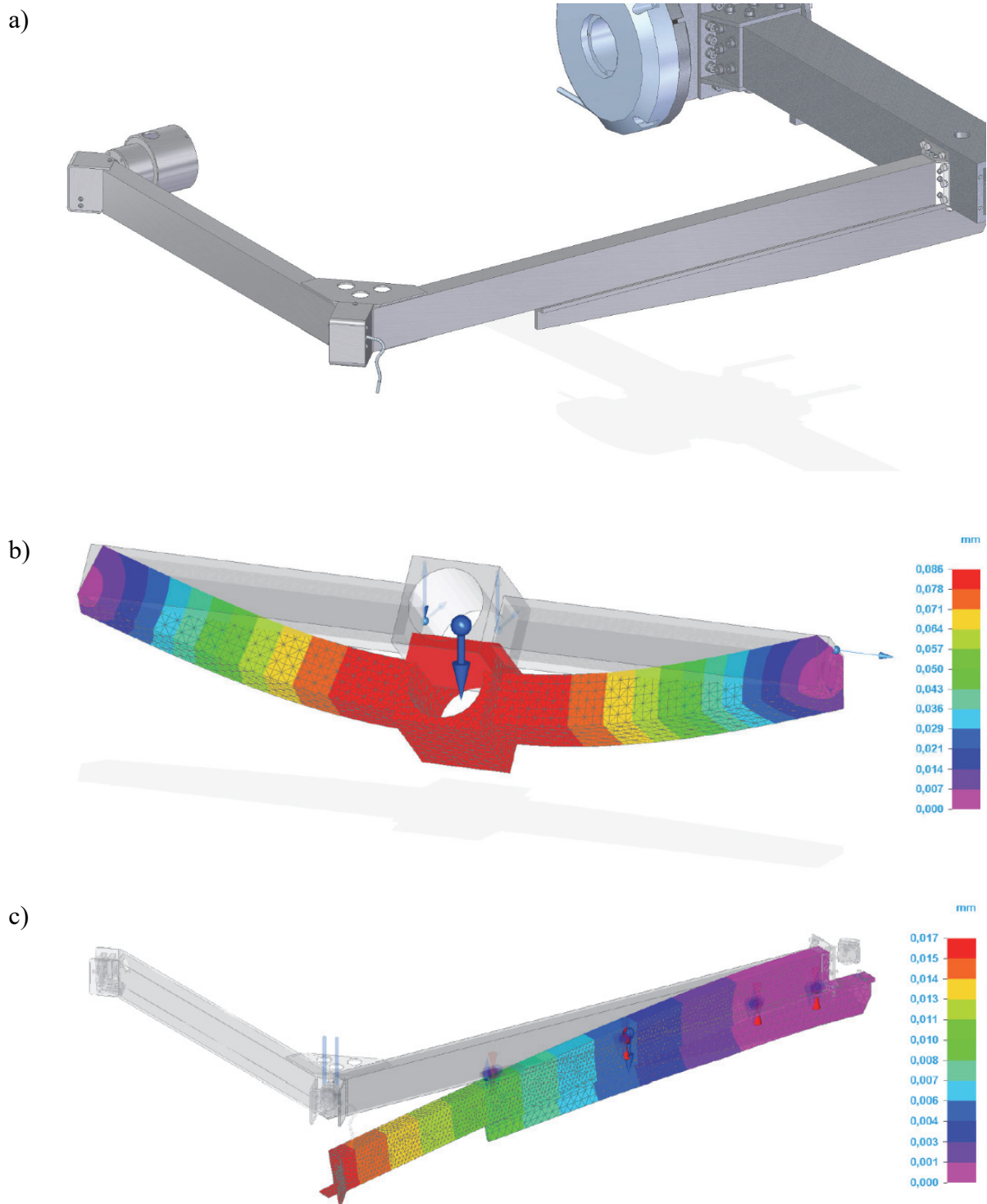


Figure 5.9. System transmitting path (a), calculated deformations of the system first axis (b) at an angle of 40° , and deformations of the laser beam path (c)

5.3. Control software main modules

The control software consists of 4 semi-autonomous main modules supporting the functionality of positioning, ephemeris, astrometry and SLR.

Figure 5.10 shows the scheme of the control software with main modules and their functions. The modules can reside on separate computers, joined in a local network; inter-process communication is asynchronous using Windows mailslot mechanism.

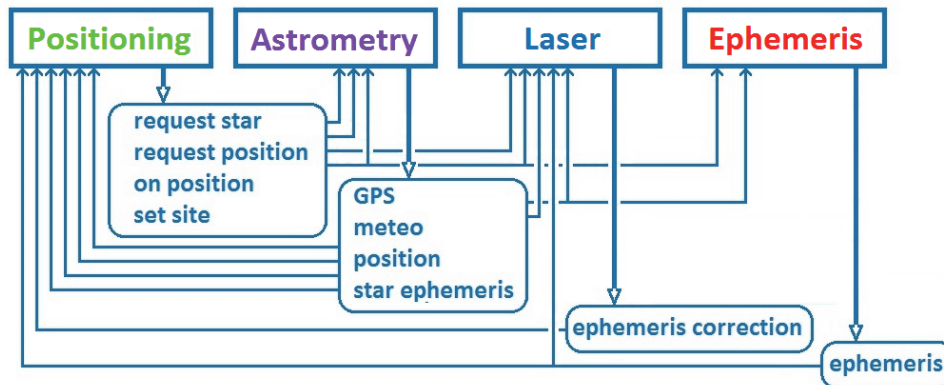


Figure 5.10. Scheme of the control software with main modules

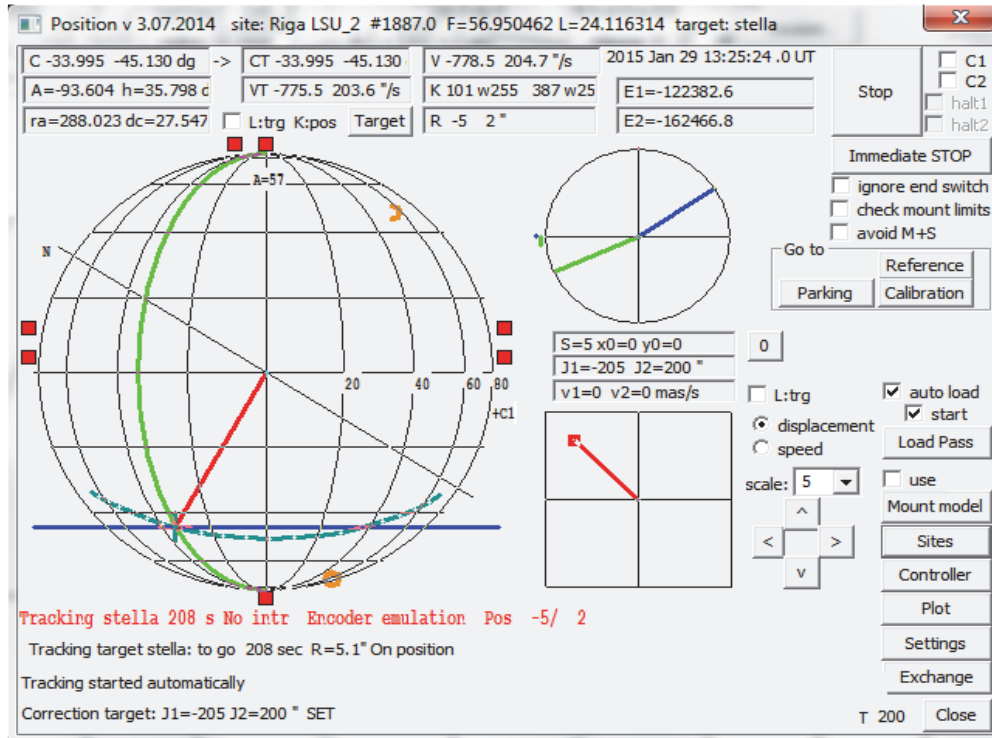


Figure 5.11. Interface of the positioning module

The positioning module (see Figure 5.11) is responsible for processing of encoder information, control of positioning motors and beam correction actuators, collecting and processing of mount error model measurements and implementation of the model. Prediction information is received from ephemeris or astrometry modules. The positioning module also visualizes the mount position; it contains manual mount control interface and instrument dome controls.

The astrometry module supports image acquisition and analysis, reference star selection and identification, astrometric processing of frame data (a subset of NOMAD star catalogue up to star magnitude 16m and NOVAS astrometry package are used), object recognition and test for presence in star or minor objects catalogues. Additionally, the focusing support and interfaces to GPS receiver and meteorstation are located here. Although a manual control is also optional, the astrometric processing is designed to be fully automatic. The interface of the astrometry module is shown in Figure 5.12.

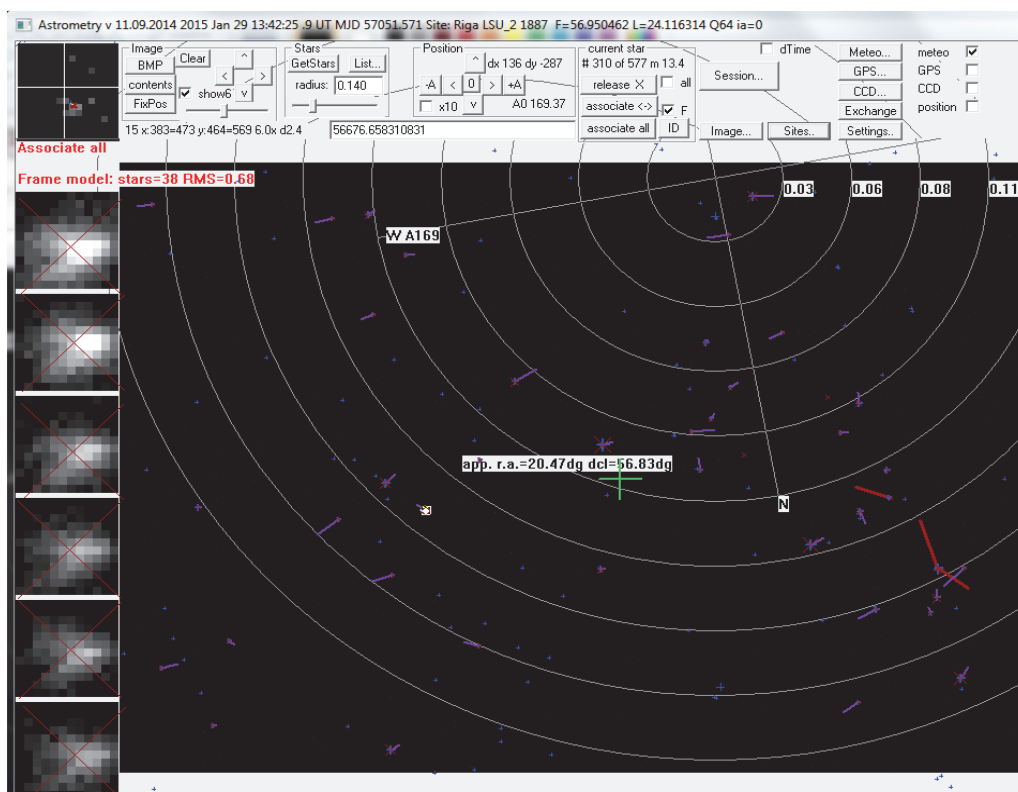


Figure 5.12. Interface of the astrometry module

The tasks of the ephemeris module, shown in Figure 5.13, are to enable satellite prediction data management, situation visualization and to provide current pass prediction to a positioning module. Sites, satellites and predictions databases are maintained here.

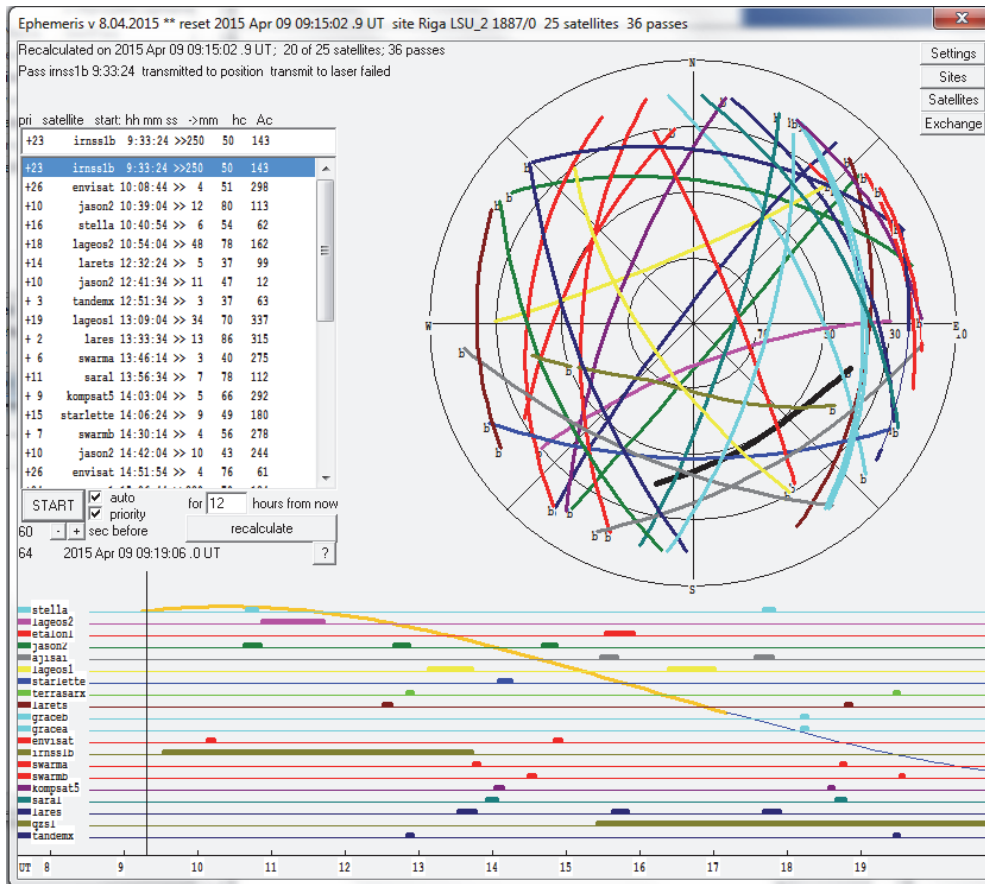


Figure 5.13. Interface of the ephemeris module

The hardware control is distributed between 3 control software modules. Ethernet, USB or RS232 communications are used depending on hardware specifics (see Figure 5.14).

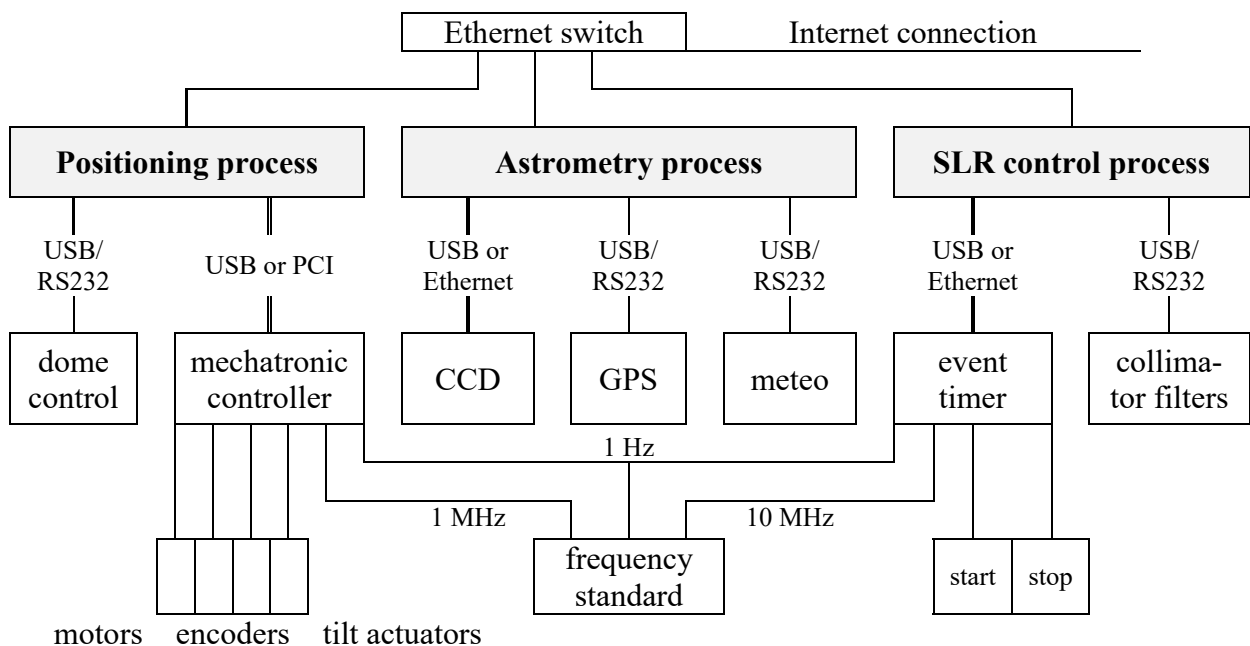


Figure 5.14. Scheme of the hardware control

Import of CPF prediction data from Internet is realized in a separate submodule. It regularly renovates the local CPF database for requested satellites (Haritonova *et al.* 2015b).

5.4. Field tests of astrometric subsystem

In late 2015 the device was brought out for the field tests of an astrometric subsystem. The main objectives of the field tests were the evaluation of performance capabilities and determination of parameters for optimal imaging and data processing.

Being a particularly demanding application, SLR requires high and technically precise accuracy for instrument positioning. Real-time astrometric position availability can be quite useful for positioning system testing and calibration. It would also enable the fast determination of instrument or object position for other purposes, in particular, for digital zenith camera's support (Abele *et al.* 2012; Zariņš *et al.* 2014; Balodis *et al.* 2015b).

This Section reflects the results of functional tests and deals with the adjustment of control software and hardware components for a multi-purpose optical tracking system (Zariņš *et al.* 2016).

5.4.1. Star image acquisition tests

Presently the device is equipped with a 8 Mpix CCD camera recognised for the following parameters:

- a) pixel size – 5.4 μ ;
- b) CCD dimensions – 18×13.5 mm;
- c) field of view – 0.27×0.2 dg;
- d) image scale – 0.29"/pixel.

Besides, full resolution, also 2×2, 3×3 and 9×9 pixel, binning modes are available.

Image reading and processing are much faster in binning mode, there is also some sensitivity gain. The camera lacks any direct hardware support for accurate image timing. If the accuracy in millisecond level is not essential (e.g., in the case of long exposures), the computer time of image acquisition request can be used, applying appropriate corrections for exposure delay and computer clock shift. The accuracy up to about 10 milliseconds can be ensured in this way, which is quite sufficient for most astrometric tasks. More accurate timing can be achieved by registering mechanical shutter “open/close” signal events using some timing reference (e.g., GPS receiver event timing mechanism).

As the location of used site does not have fine astroclimate (close to the sea, high humidity, haze, background lights due to proximity of a big city), the obtained image acquisition results probably are somewhat biased. Better results might be expected under more improved conditions. In particular, although theoretically Optical Tube Assembly (OTA) should provide near-diffraction resolution of better than 1", the smallest practically achieved size of star image was about 3". In these circumstances it has been found that the usage of full CCD resolution is not the best choice, and 2×2 pixel binning mode gives very similar accuracy, but is much faster, because of 4× smaller data amount to be read from CCD, stored in a file and processed, and besides gives some advantage in registered star magnitudes.

The imaging sensitivity, achieved during the tests, is summarized in Figure 5.15. The Figure represents the dependency of maximum star magnitude and number of stars in frame on exposure duration. As the CCD outcome is strongly dependent on a star's color, and many weaker stars have no visual or photographic magnitude estimates (the magnitude, representing the color, which is the closest to visual for the star, has been used in these cases), the maximum magnitude only approximately represents sensitivity. The minimum exposure for the camera is 0.12 seconds.

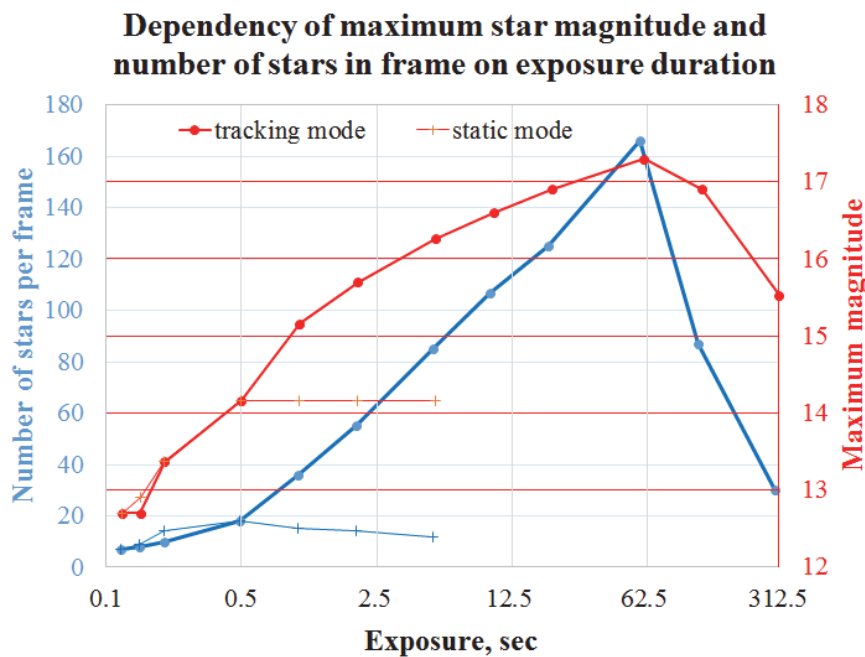


Figure 5.15. Number of star images on frame and biggest magnitude for both static and tracking imaging modes (a randomly selected sky area, close to zenith)

For static imaging (non-movable mount) of areas near celestial equator the exposures above 0.2 seconds perceptibly elongate images due to Earth rotation, undoing longer exposure gains – the number of star images does not increase any more. The images of mid-latitude areas are significantly elongated for exposures above 0.3 seconds, and in the case of exposures above 0.5 seconds the elongation is too big everywhere except polar areas. Therefore, the exposure duration about 0.2–0.3 seconds seems to be optimal for static imaging (see Figure 5.16).

The tracking accuracy of the device is limited by minimum displacement, corresponding to the step of a stepper motor, which in this case is about 0.5". On top of that, the control software is performing adjustments of tracking only when coordinate discrepancy increases above a configurable threshold. At angular encoder resolution of 0.37", it has been found that there is no benefit to set this threshold below 1". So, the tracking accuracy cannot be better than 1"–1.5", it occasionally experiences external perturbations, causing bigger bounces. Such tracking a bit, but not significantly, enlarges star images in comparison to short-exposure static mode.

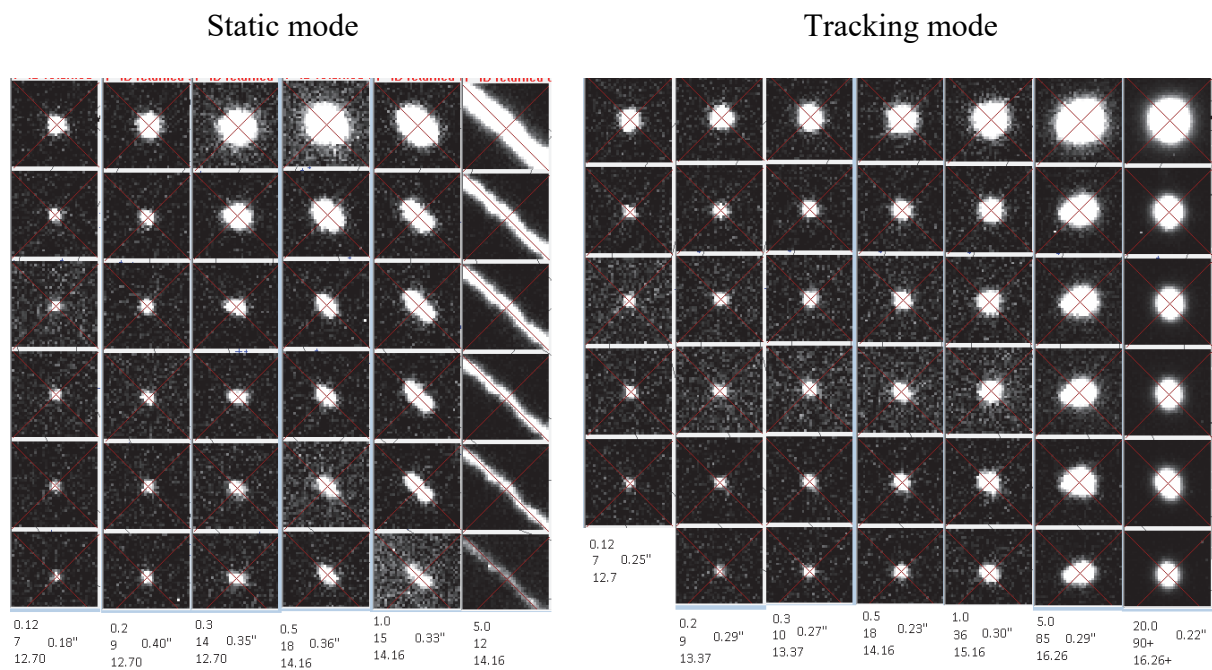


Figure 5.16. Star images at different exposures

The image acquisition tests in tracking mode indicate similar results to static imaging for short exposures, and steady increase in number of stars and maximum magnitude if the exposure has been increased up to about one minute. Further increase of exposure produces orioles around the brightest stars masking faint stars. Probably, better astroclimate and instrument location would eliminate much of this effect. The exposures over about 5 minutes

show the effect of field rotation, elongating star images in the periphery of frame. Without de-rotation equipment, a few minutes (or up to 10–20 minutes in the center of frame) seem to be the technical limit for the star field exposures by the device.

The maximum star magnitude in the results mentioned above refers to the star images with certainty recognized automatically. In our circumstances the best one refers to a slightly over 17m for one minute exposure, probably, it might be somewhat higher in good astroclimate. The closer inspection of images typically allows recognizing the signs of objects, which are fainter for about one magnitude.

In order to successfully perform the automatic star identification (software package described by Zariņš *et al.* (2014) was used), at least 5–6 star images should be present; bigger number of stars is desirable to increase the astrometric reduction accuracy. For used hardware layout, the frames obtained in a random sky area in static mode have provided the required minimum number of images in about 80% of cases. There could be two options, how it is possible to increase a success rate – either to take additional frames in adjacent areas, or to use tracking mode and longer exposure. Both show similar results and require some moving of the device. The choice probably should depend on priorities and limitations of the task.

5.4.2. Mount error model

Laser ranging capability is one of the principal design goals for the device. To perform laser ranging in automatic (“blind”) mode, the pointing accuracy must be better than the transmitted beam divergence (the other limiting component – field of view of reflected pulse detector; usually is bigger than divergence). As a sub-arcminute beam divergence is a common choice, it can be made a fraction of arcminute for ranging of far objects. Consequently, the pointing accuracy ideally should be within a few arcsecond range. It is difficult to ensure such accuracy by purely mechanical means; a very massive, accurately manufactured and expensive support structure to be needed. Instead, a mount error model, implemented in the control software, is applicable to introduce the necessary pointing corrections.

A problem is to find a simple mathematical model, effectively describing the physical deformations and misalignments of the mount. It is almost unfeasible to develop a reliable theoretical deformation model, including contributions of all physical components and their interactions. Therefore, the approximating models, based on position measurement data, are being used instead.

The simplest approach offers models based on power series or trigonometric series, or their combination. Also variations of cell- or zone- based models have been used (Zhaborovsky *et al.* 2012; Medvedsky and Pap 2008; Medvedsky and Suberlak 2002). The trigonometric models include some first members of Fourier series for both coordinate angles and some cross-products; additionally, the components of an analytical deformation model can be included (for example, as proposed in ILRS (2015)). Such models serve to reliably describe simple mount misalignments and rotation deformations. On the other hand, they have proved to be not so suitable in the event, when the character of deformations is complex. Power series models (kind of Turner transformation (Podobed and Nesterov 1975)) can be more reliable if complex deformations are dominating.

The device capabilities in question allow performing the acquisition of measurement data for a mount error model calculation in an automated process – to control the system a scenario file is provided, containing desired measurement positions. The set of positions is traversed at a rate of about one position per 10 seconds, taking one or several images in each position. Data processing can be performed either immediately after each frame, or when all frames are obtained. The processing results contain both position coordinates in instrument system (axes rotation angles C1 and C2 as acquired from angular encoders) and measured positions in topocentric system. The topocentric coordinates measured are transformed to instrument coordinates C1, C2, following the same procedure as for pointing targets. The mount error model then approximates the difference of measured and instrument coordinates.

Testing a number of combinations of model member functions, it has been found that more reliable results with least number of model parameters offer a model, consisting of power series. Inclusion of some trigonometric member functions (in particular, $\sin C1 \cdot \text{tg} C2$, $\cos C1 \cdot \text{tg} C2$) gave almost the same accuracy, but at bigger number of parameters. For the coordinate range, available for position measurements at the test site, no advantage has been found for trigonometric member functions. However, bigger coordinate range might present different situation.

Presently adopted structure of the model and the example set of calculated parameters are shown in Table 5.1.

Table 5.1

Member functions of mount error model and values for the coefficients (in arcseconds/rad)

Function	dC1	dC2
offset	267	-592
C2	-34	-419
C2 ²	-92	-250
C2 ³	-12	471
C1	-285	59
C1 ²	-101	620
C1 ³	160	-332
C1·C2	-1252	104
C1·C2 ²	19	-113
C1 ² ·C2	-402	744

Measurement data for this model has represented more than 100 positions mostly above $\approx 50^\circ$ elevation (lower elevations are not available because of observation site limitations; two frames have been taken at all positions). An example of distribution of measurement positions and corresponding approximation residuals are shown in Figure 5.17. A number of similar observation sets have been obtained. Apart from reflecting mechanical adjustments of the mount made between sessions, no significant variations of resulting mount error models have been found.

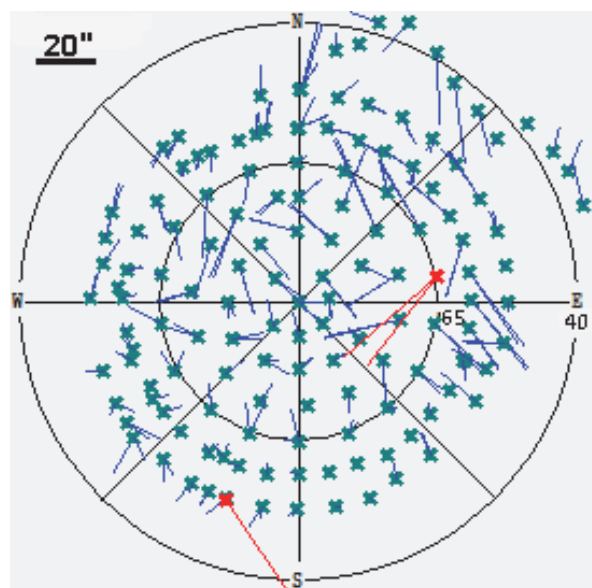


Figure 5.17. Measurement point positions of mount error model and approximation residuals (rejected measurements are marked red)

3-D representation of mount error model behavior (for each axis separately) is shown in Figures 5.18 and 5.19. Offset values represent the encoder zero-point marker position relative to the instrument coordinate system zero-points. For better representation of variability, they are removed from the graphs. The asymmetric character of the model graphs probably is the result of axes non-orthogonality with the value of 2 to 4 arcminutes. The considerable part of mount errors could account for the result of deformations caused by unbalancing of axes.

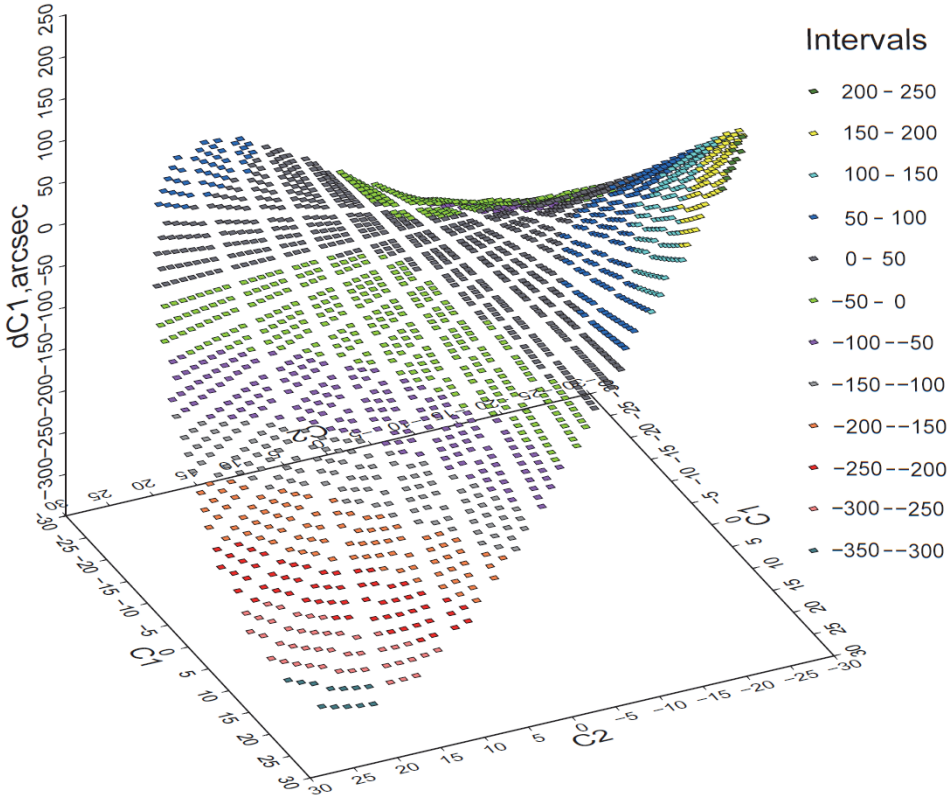


Figure 5.18. Mount error model: corrections of primary axis rotation (C1) as the functions of position

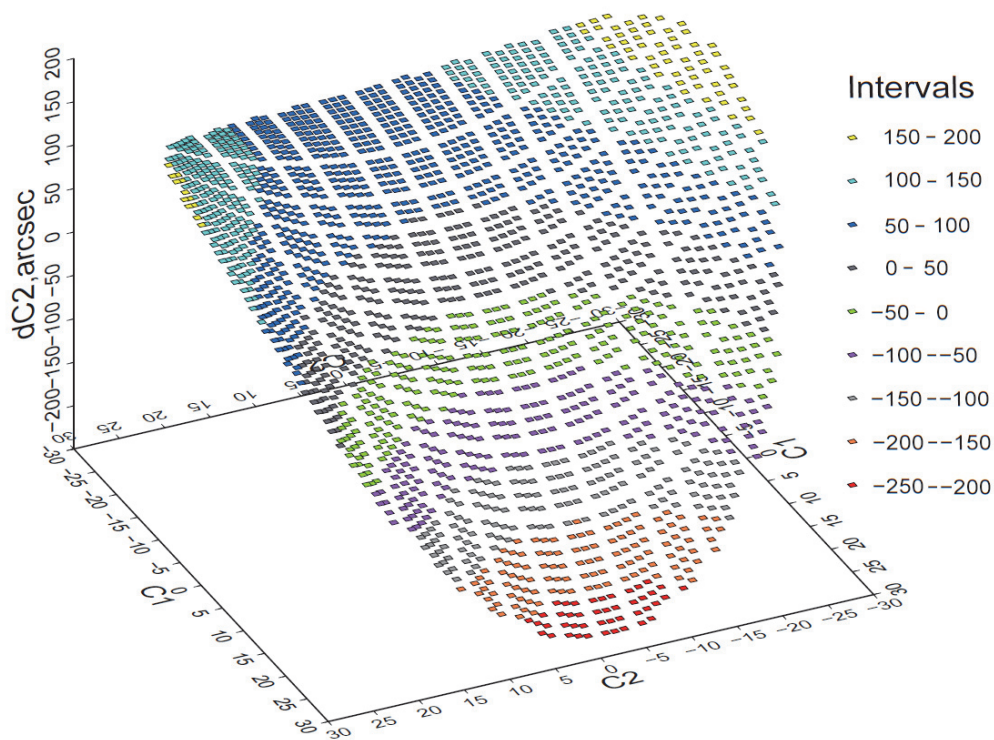


Figure 5.19. Mount error model: corrections of secondary axis rotation (C2) as the functions of position

Further experiments with different balancing properties are to be made to find out its effects. Correction members, proportional to the other axis value ($dC1 \sim C2$, $dC2 \sim C1$), depend, besides other effects, on the azimuth offset of the primary axis. Minimization of these member coefficients are used to improve primary axis's azimuth value, used in coordinate transformation from horizontal to instrument system.

RMS value of approximation residuals typically has shown a little below 10". The similar results have been obtained using data from several sets of observations; the difference between the respective model values has fallen within 10"–20". The model is definitely a simplification of the real situation, therefore a part of the approximation residual value reflects the inability of model to adhere to detailed structure of real mount errors, which represent the combined input from a number of sources: encoder irregularity (up to 2"–3"), positioning system residuals (~1"), astrometric position errors (estimated to be better than 1"), irregularities of axes shape and bearings (probably the dominating source). Potentially the effects of some non-elastic or temperature-inflicted deformations have been also present. It can be expected that the regular executing of mount error model measurements hereafter have to provide more insight into sources and character of mount positioning irregularities.

The application of the calculated mount error model has ensured the resulting positioning accuracy generally within 10"–20", which should already be adequate for a “blind” low-orbit satellite ranging. At that accuracy level some searching may be required for high-orbit satellites, if very small transmitted beam divergence is used. Hopefully, the further adjustment of mount mechanics and the improvement of mount error model structure are expected to eventually improve the positioning accuracy to 5"–10" or less.

5.5. Conclusions

The field tests of an astrometric subsystem of the near-Earth object tracking device have verified the imaging and positioning performance of the device in compliance with the expected designed features. The mount error model parameters have been efficiently calculated; the resulting positioning accuracy is proved to be already adequate for SLR purposes, at the same time, there is a potential for improvement through the adjustment of mechanical properties and error model structure. The magnitude limit for the astrometric position determination has been found to be about 17m having the option of some increase under good imaging conditions. A number of quality adjustments in control software have been induced due to real imaging and positioning environment. Some mechanical problems have been detected to be eliminated before the final installation of the instrument.

MAIN CONCLUSIONS

- 1) The formalized data on the Latvian GNSS station horizontal and vertical velocity fields as well as their position time series from the created catalogue (in Appendix B), have shown that:
 - a) the obtained velocities reveal the effect of the Fennoscandian rebound in the territory of Latvia, because in the case of both solutions – weekly (2008–2014) and daily (2012–2015) – the EUPOS[®]-Riga and LatPos station vertical velocity vectors have maximum values in the western part of Latvia and minimum values in the eastern part of Latvia; these ranges fail to exceed 2 mm/yr;
 - b) the field of vertical velocities from the daily solution is more homogeneous in comparison with the weekly solution, but disagrees with the deformation model NKG_RF03vel in the south-eastern part of Latvia; however, the discrepancy is only under 1 mm/yr;
 - c) the horizontal velocity vectors have similar orientation for both solutions; vectors are mostly oriented to the south – according to the deformation model NKG_RF03vel, but they have different values;
 - d) the annual coordinate changes appear in the case of some GNSS stations; the most distinguished ones belong to the stations PREI, REZ1, SALP and SLD1. The effect is assumed to be caused by building deformations where GNSS antenna has been mounted, or ground deformations.
- 2) The given description of the sea level variations at the Latvian coast supplements the earlier results concerning the dynamics of the Baltic Sea in this region and
 - a) shows that the sea level ranging diapason is quite high in the Gulf of Riga – it ran up to 2 m during one year at the Salacgrīva station. In the stations Liepāja, Ventspils and Kolka, the diapason is not so high, but the differences between the sea level maximum and minimum have more pronounced annual changes in comparison with the data of other stations;
 - b) approves the existence of the diurnal (O_1 , K_1) and semi-diurnal (M_2 , S_2) tides both in the Gulf of Riga and in the Baltic Sea at the Latvian coast;
 - c) reveals the existence of non-tidal frequency of 5 cycles per day at the stations of the Gulf of Riga, which could represent some local effect typical for this gulf.
- 3) The field tests of the designed new original and universal satellite laser ranging device have shown that the resulting positioning accuracy is already adequate for SLR

purposes; at the same time, there is a potential for improvement through the adjustment of mechanical properties and error model structure. The device offers an efficient innovative way to obtain the geodynamic data, and it can contribute to geodynamic studies not only in Latvia.

APPENDICES

Appendix A: Latvian GNSS station velocities (mm/yr) in North, East and Up components with residual position RMS values (mm) obtained for the daily solution for the period from 2012 to 2015:

A.1: Observations of the year 2012

A.2: Observations of the year 2013

A.3: Observations of the year 2014

A.4: Observations of the year 2015

Appendix B: Catalogue with information on Latvian GNSS station location and their position time series

Appendix A

Latvian GNSS station velocities (mm/yr) in North, East and Up components with residual position RMS values (mm) obtained for the daily solution for the period from 2012 to 2015

A.1: Observations of the year 2012

Network	GNSS station name	ETRF2000					
		North comp.	RMS (N)	East comp.	RMS (E)	Up comp.	RMS (Up)
LatPos	ALUK	0.59	0.06	0.70	0.06	-1.35	0.15
	BALV	-0.03	0.05	-0.73	0.06	0.15	0.14
	BAUS	-0.26	0.04	-0.07	0.05	0.66	0.13
	DAGD	-0.59	0.05	0.26	0.04	0.51	0.14
	DAU1	-0.99	0.04	0.00	0.05	0.81	0.13
	DOB1	-0.15	0.05	-1.32	0.06	1.35	0.12
	IRBE	-0.07	0.05	-1.39	0.05	1.54	0.21
	JEK1	-0.81	0.05	-0.07	0.04	0.81	0.15
	KUL1	-1.39	0.06	-0.18	0.05	1.79	0.14
	LIMB	-1.35	0.05	0.26	0.06	2.23	0.17
	LIPJ	-1.32	0.05	-0.48	0.05	2.12	0.15
	LODE	-2.31	0.06	0.48	0.05	0.33	0.13
	LVRD	-1.72	0.07	1.35	0.05	1.68	0.16
	MADO	0.01	0.04	-0.37	0.05	1.61	0.13
	MAZS	-2.64	0.17	-1.65	0.15	1.17	0.19
	OJAR	-1.50	0.08	-1.24	0.08	-0.44	0.17
	PLSM	-1.02	0.07	-0.37	0.06	2.82	0.15
	PREI	0.44	0.05	-2.82	0.09	-0.66	0.14
	REZ1	-0.81	0.09	-0.22	0.04	0.04	0.16
	SIGU	-0.04	0.07	0.55	0.07	3.29	0.15
SLD1	-0.01	0.06	1.39	0.09	1.06	0.12	
TALS	-0.40	0.06	-0.88	0.06	1.17	0.16	
TKMS	-	-	-	-	-	-	
VAL1	-0.95	0.06	-3.22	0.07	0.92	0.13	
EUPOS®-Riga	KREI	-0.62	0.04	1.94	0.06	-0.70	0.15
	LUNI	-0.92	0.06	1.43	0.06	1.32	0.13
	SALP	-2.31	0.12	-1.68	0.12	4.03	0.21
	VAIV	0.11	0.05	0.62	0.06	1.76	0.14
	VANG	-0.77	0.05	1.17	0.08	2.16	0.14
IGS/ EPN	RIGA	0.11	0.05	0.07	0.06	0.37	0.15
Average RMS values			0.06		0.06		0.15

A.2: Observations of the year 2013

Network	GNSS station name	ETRF2000					
		North comp.	RMS (N)	East comp.	RMS (E)	Up comp.	RMS (Up)
LatPos	ALUK	-1.64	0.05	-1.75	0.05	2.37	0.17
	BALV	-0.33	0.04	-1.75	0.07	5.58	0.14
	BAUS	-0.33	0.04	0.11	0.05	-0.99	0.13
	DAGD	-1.20	0.04	-0.04	0.04	2.63	0.15
	DAU1	-1.20	0.04	-0.55	0.05	1.64	0.16
	DOB1	1.24	0.05	-1.83	0.05	-1.75	0.13
	IRBE	0.77	0.05	-1.50	0.05	-1.13	0.20
	JEK1	-1.31	0.04	-0.99	0.04	4.78	0.16
	KUL1	-0.58	0.06	-0.29	0.04	-0.58	0.16
	LIMB	1.17	0.04	-2.59	0.05	3.14	0.16
	LIPJ	-1.10	0.04	-1.86	0.05	-4.12	0.16
	LODE	-3.10	0.05	-1.39	0.06	2.88	0.14
	LVRD	-1.39	0.05	-2.26	0.05	3.25	0.18
	MADO	-1.17	0.05	-3.58	0.05	1.83	0.15
	MAZS	-15.33	0.24	-0.11	0.16	1.31	0.24
	OJAR	-0.73	0.05	-4.56	0.08	0.00	0.17
	PLSM	-0.51	0.07	-0.15	0.06	3.94	0.14
	PREI	-1.20	0.05	-0.99	0.10	2.59	0.14
	REZ1	-1.72	0.07	-0.58	0.04	3.87	0.15
	SIGU	-0.99	0.06	-0.91	0.06	3.03	0.15
SLD1	-0.40	0.05	0.29	0.10	-2.19	0.13	
TALS	0.58	0.04	-2.56	0.06	-1.46	0.13	
TKMS	-0.37	0.07	-1.24	0.05	-0.95	0.15	
VAL1	-0.66	0.05	-2.74	0.05	3.91	0.14	
EUPOS®-Riga	KREI	0.44	0.04	-1.10	0.09	0.22	0.15
	LUNI	-0.18	0.05	-0.80	0.07	0.95	0.13
	SALP	-1.42	0.11	-3.43	0.12	-2.23	0.17
	VAIV	0.91	0.05	-1.20	0.07	-2.92	0.16
	VANG	-0.62	0.05	-3.18	0.09	-0.18	0.15
IGS/ EPN	RIGA	0.11	0.05	-0.29	0.08	1.28	0.15
Average RMS values			0.06		0.07		0.15

A.3: Observations of the year 2014

Network	GNSS station name	ETRF2000					
		North comp.	RMS (N)	East comp.	RMS (E)	Up comp.	RMS (Up)
LatPos	ALUK	0.26	0.05	-1.39	0.05	0.80	0.20
	BALV	-0.22	0.04	0.33	0.07	-1.28	0.16
	BAUS	-0.01	0.04	0.33	0.04	-0.18	0.14
	DAGD	0.04	0.05	-0.66	0.05	1.86	0.18
	DAU1	0.69	0.05	-1.17	0.05	-4.20	0.17
	DOB1	0.69	0.04	-0.11	0.04	-0.80	0.15
	IRBE	0.88	0.04	-0.11	0.05	-1.72	0.19
	JEK1	0.00	0.05	-0.88	0.05	-0.95	0.17
	KUL1	-0.77	0.06	-0.58	0.04	-1.83	0.16
	LIMB	-0.22	0.05	-0.40	0.05	3.65	0.17
	LIPJ	-0.15	0.05	-0.11	0.05	-0.66	0.17
	LODE	0.26	0.05	0.26	0.05	-0.44	0.15
	LVRD	0.66	0.05	-0.80	0.04	-1.02	0.17
	MADO	0.44	0.05	-0.37	0.05	-0.80	0.18
	MAZS	-13.54	0.21	-1.31	0.13	0.51	0.24
	OJAR	1.39	0.06	0.84	0.10	-1.64	0.16
	PLSM	-0.40	0.08	-0.91	0.05	0.51	0.18
	PREI	-0.07	0.05	-1.02	0.07	0.37	0.18
	REZ1	0.44	0.07	-0.47	0.04	-2.12	0.17
	SIGU	-0.80	0.06	0.66	0.05	0.37	0.16
SLD1	0.55	0.05	0.91	0.10	-2.34	0.14	
TALS	0.15	0.05	-0.55	0.06	-0.07	0.15	
TKMS	0.44	0.07	0.29	0.04	-0.37	0.14	
VAL1	0.18	0.04	-0.73	0.04	1.35	0.16	
EUPOS®-Riga	KREI	0.69	0.05	1.93	0.07	-1.02	0.16
	LUNI	0.22	0.05	-0.26	0.05	-1.02	0.13
	SALP	0.47	0.14	-2.08	0.11	-3.65	0.17
	VAIV	0.44	0.05	-0.26	0.06	-4.78	0.15
	VANG	0.66	0.05	1.93	0.07	-3.58	0.15
IGS/ EPN	RIGA	-0.11	0.05	1.75	0.06	-2.01	0.15
Average RMS values			0.06		0.06		0.17

A.4: Observations of the year 2015

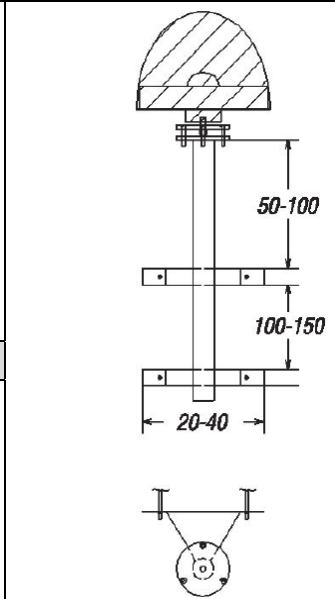
Network	GNSS station name	ETRF2000					
		North comp.	RMS (N)	East comp.	RMS (E)	Up comp.	RMS (Up)
LatPos	ALUK	-0.73	0.05	-0.69	0.05	1.20	0.15
	BALV	-0.44	0.04	-0.69	0.06	1.24	0.13
	BAUS	-0.11	0.05	-0.04	0.04	1.13	0.13
	DAGD	-1.02	0.05	-0.11	0.04	2.45	0.14
	DAU1	0.22	0.05	-0.95	0.04	1.28	0.14
	DOB1	0.55	0.04	-0.88	0.04	0.47	0.12
	IRBE	-0.29	0.04	-1.50	0.04	2.56	0.16
	JEK1	0.18	0.06	-0.47	0.04	2.19	0.16
	KUL1	-1.10	0.06	-1.53	0.05	0.15	0.15
	LIMB	-0.62	0.05	-0.51	0.05	2.04	0.13
	LIPJ	-1.42	0.05	-1.53	0.04	2.23	0.16
	LODE	-1.53	0.05	-0.33	0.04	2.92	0.13
	LVRD	1.17	0.05	-1.46	0.04	1.90	0.16
	MADO	0.11	0.05	-0.07	0.05	2.92	0.14
	MAZS	-7.23	0.25	1.64	0.12	2.34	0.18
	OJAR	0.07	0.05	-1.53	0.05	2.19	0.16
	PLSM	-0.40	0.06	-0.91	0.05	1.93	0.13
	PREI	-0.29	0.05	-0.15	0.09	2.04	0.15
	REZ1	-0.66	0.06	0.37	0.05	4.23	0.14
	SIGU	-0.22	0.05	-0.69	0.05	1.86	0.17
SLD1	-0.07	0.06	-0.69	0.08	1.64	0.13	
TALS	-0.62	0.05	-1.39	0.04	2.59	0.15	
TKMS	-0.62	0.06	0.11	0.05	0.66	0.13	
VAL1	-0.47	0.04	-1.64	0.04	1.93	0.14	
EUPOS®-Riga	KREI	-0.51	0.04	-1.39	0.06	5.91	0.14
	LUNI	-1.39	0.05	0.77	0.06	3.80	0.14
	SALP	-2.19	0.10	-0.29	0.10	6.75	0.17
	VAIV	0.01	0.05	-1.42	0.06	0.58	0.14
	VANG	-0.04	0.05	-1.35	0.07	4.09	0.14
IGS/ EPN	RIGA	-0.07	0.07	-0.33	0.08	1.75	0.21
Average RMS values			0.06		0.06		0.15

Appendix B

Catalogue with information on Latvian GNSS station location and their position time series

Station name: ALUK	Address: Lāčplēša iela 1, Alūksne		
Network: LatPos	Coordinates: X	Y	Z
<i>Reference frame: ETRF2000 at epoch 2015.5</i>			
	3065247.686	1566667.621	5351678.735

Monument	Antenna mounting
-----------------	-------------------------



(dimensions in cm)

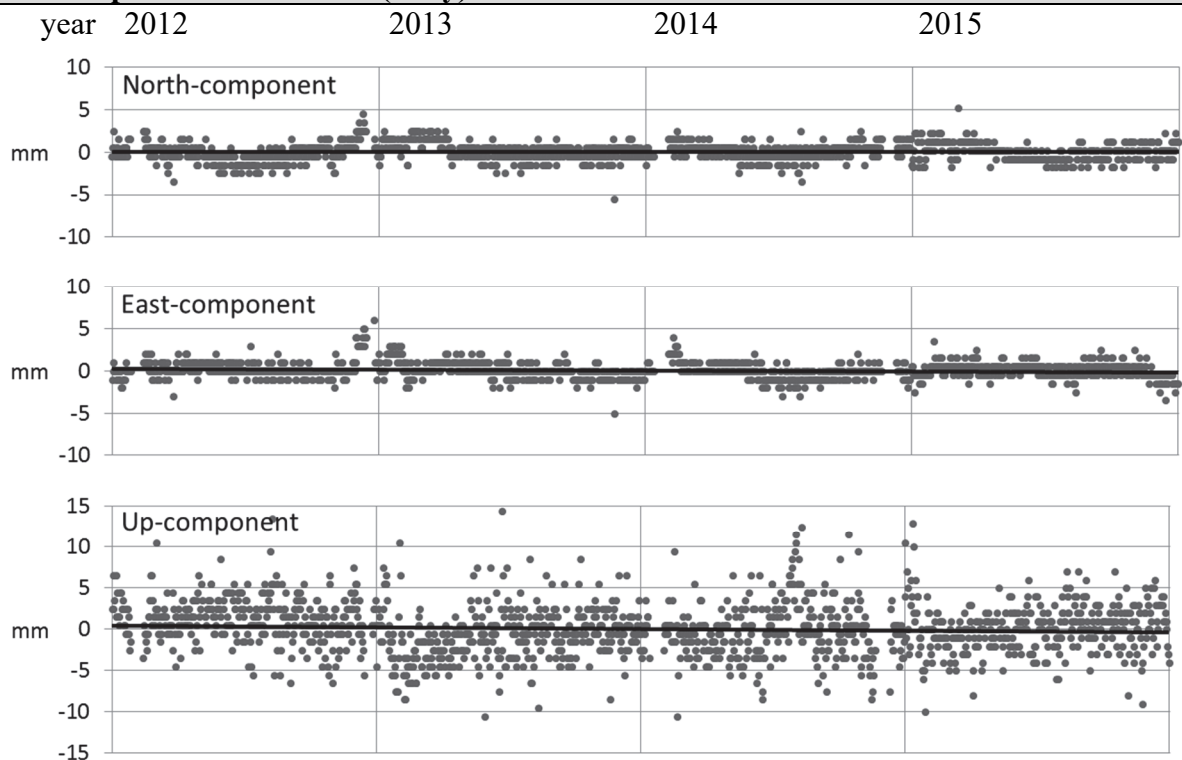
Site type: b1-005

Installation year: 2011

Location

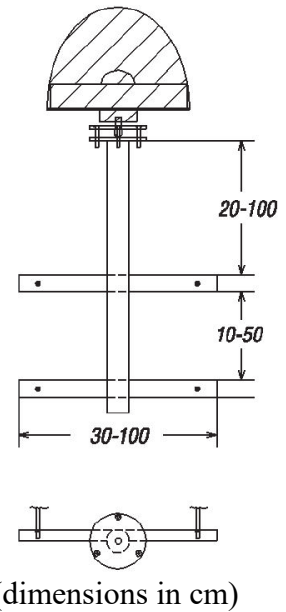


Residual position time series (daily)

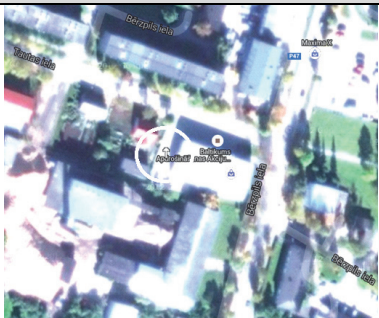


Station name: BALV	Address: Tautas iela 1, Balvi
Network: LatPos	Coordinates: X Y Z
<i>Reference frame: ETRF2000 at epoch 2015.5</i> 3084535.091 1589675.903 5333791.707	

Monument	Antenna mounting
-----------------	-------------------------

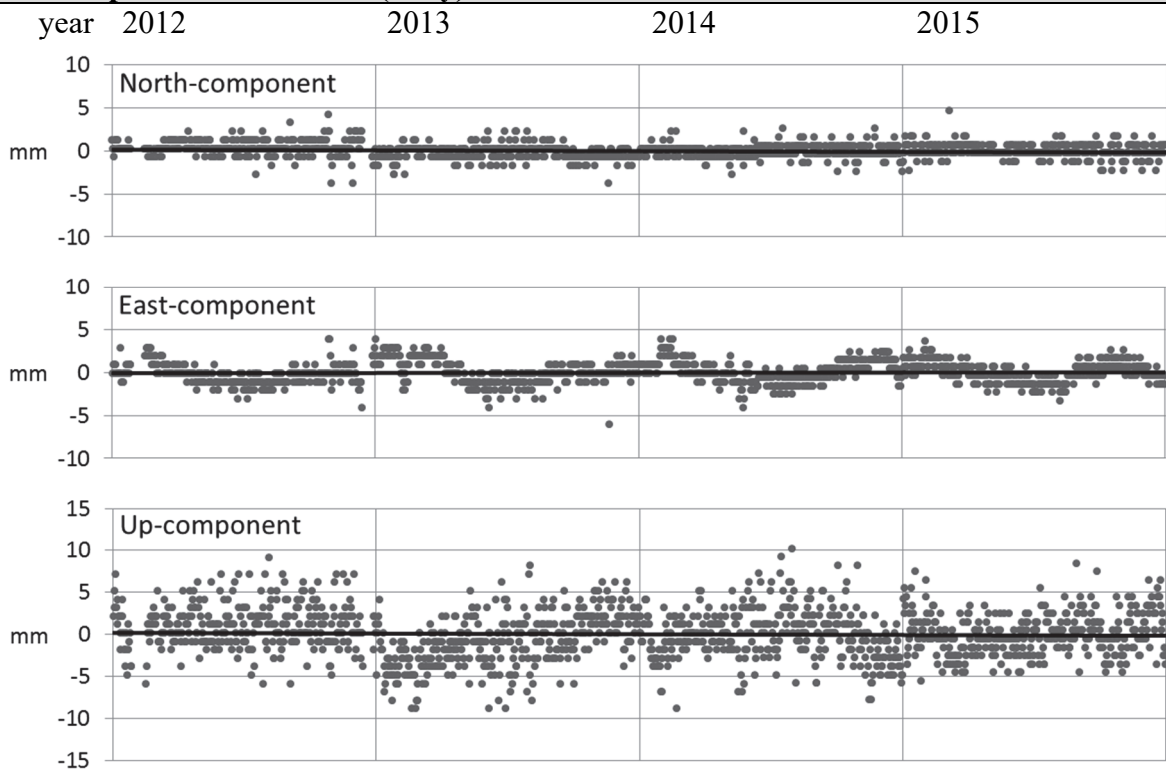


Location



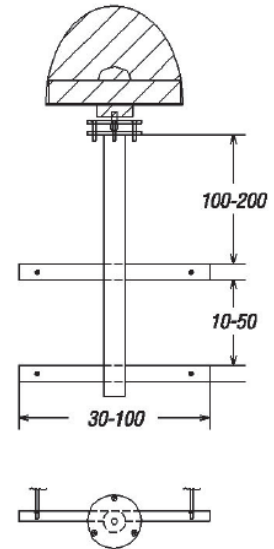
Site type: b1-007
Installation year: 2007

Residual position time series (daily)
--



Station name: BAUS	Address: Uzvaras iela 1, Bauska		
Network: LatPos	Coordinates: X	Y	Z
<i>Reference frame: ETRF2000 at epoch 2015.5</i>			
	3226815.008	1449250.139	5289639.361

Monument	Antenna mounting
-----------------	-------------------------



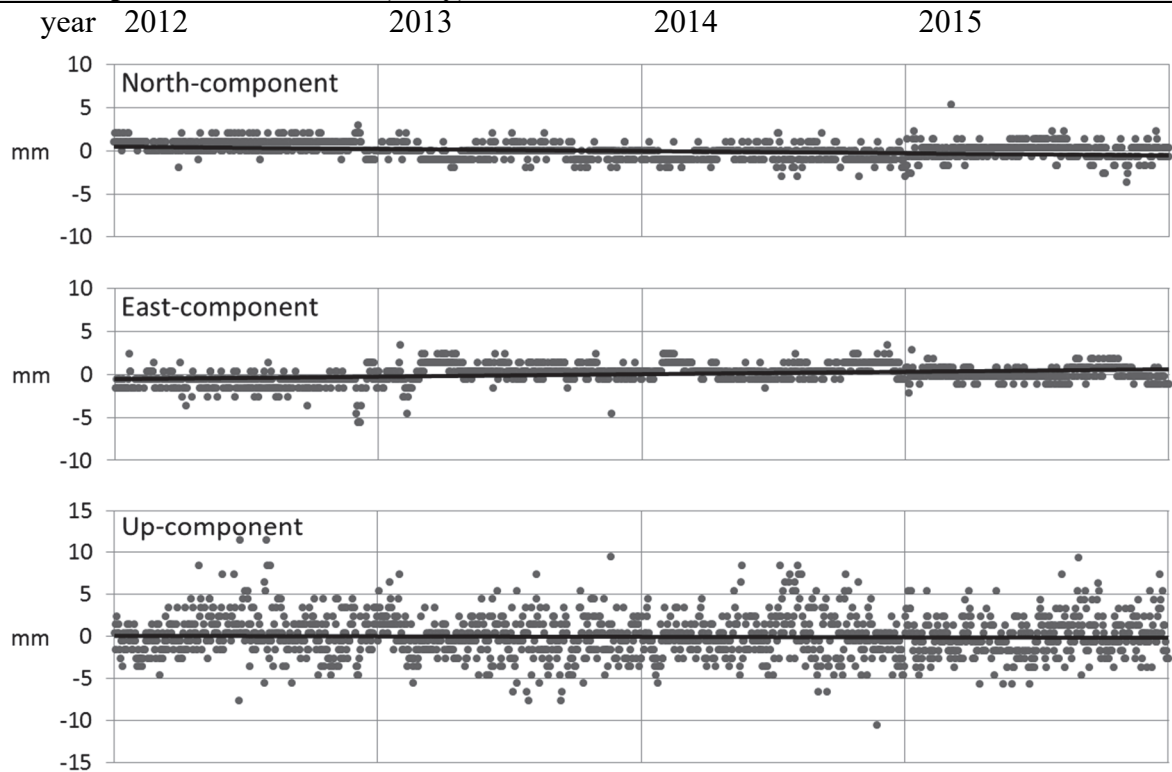
(dimensions in cm)

Site type: b1-006
Installation year: 2005

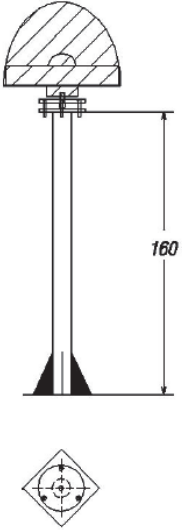
Location

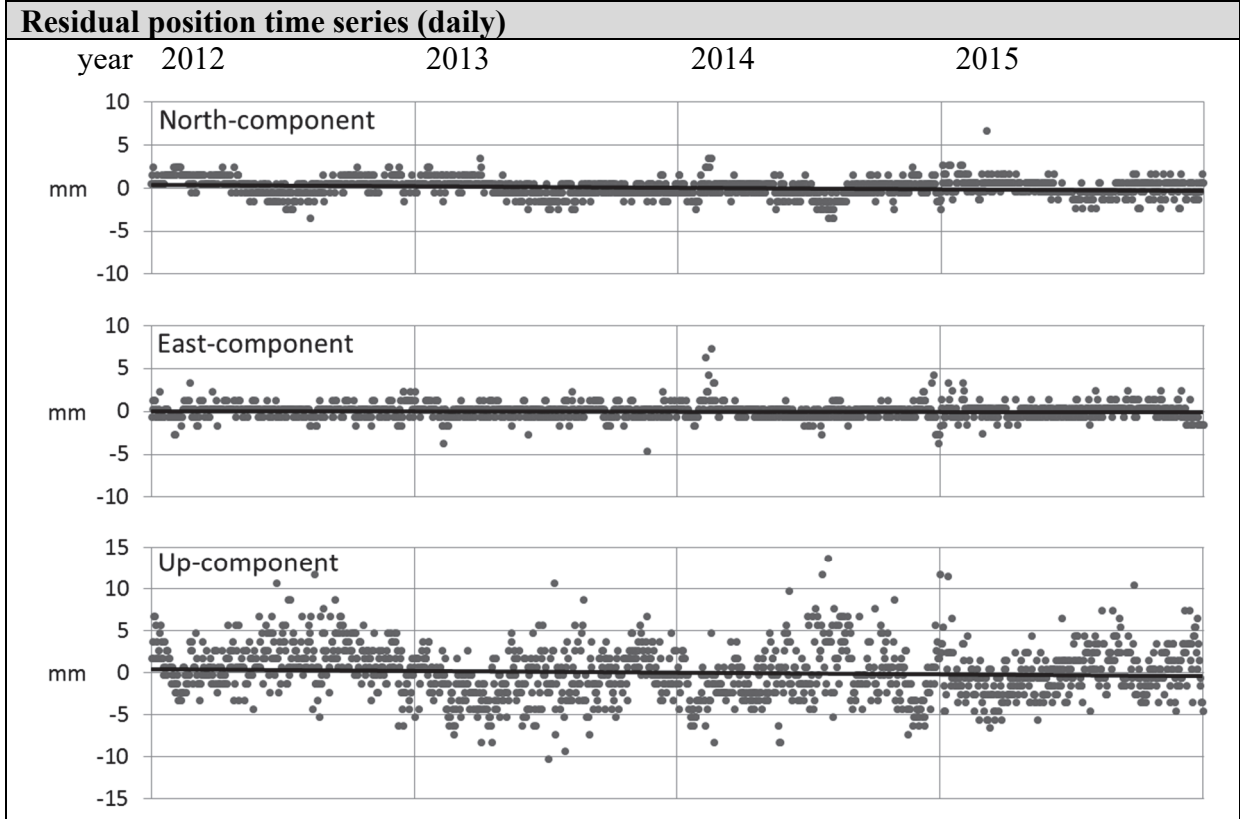


Residual position time series (daily)
--



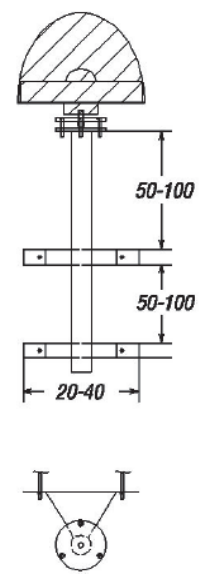
Station name: DAGD	Address: Mičurina iela 3a, Dagda		
Network: LatPos	Coordinates: X	Y	Z
<i>Reference frame: ETRF2000 at epoch 2015.5</i>			
	3162078.521	1648394.702	5270703.298

Monument	Antenna mounting
	 <p>(dimensions in cm)</p>
Location	
	<p>Site type: b1-002</p> <p>Installation year: 2011</p>

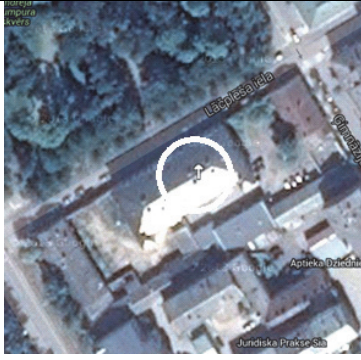


Station name: DAU1	Address: Lāčplēša iela 20, Daugavpils		
Network: LatPos	Coordinates: X	Y	Z
<i>Reference frame: ETRF2000 at epoch 2015.5</i> 3209600.864 1601536.379 5256389.471			

Monument	Antenna mounting
----------	------------------

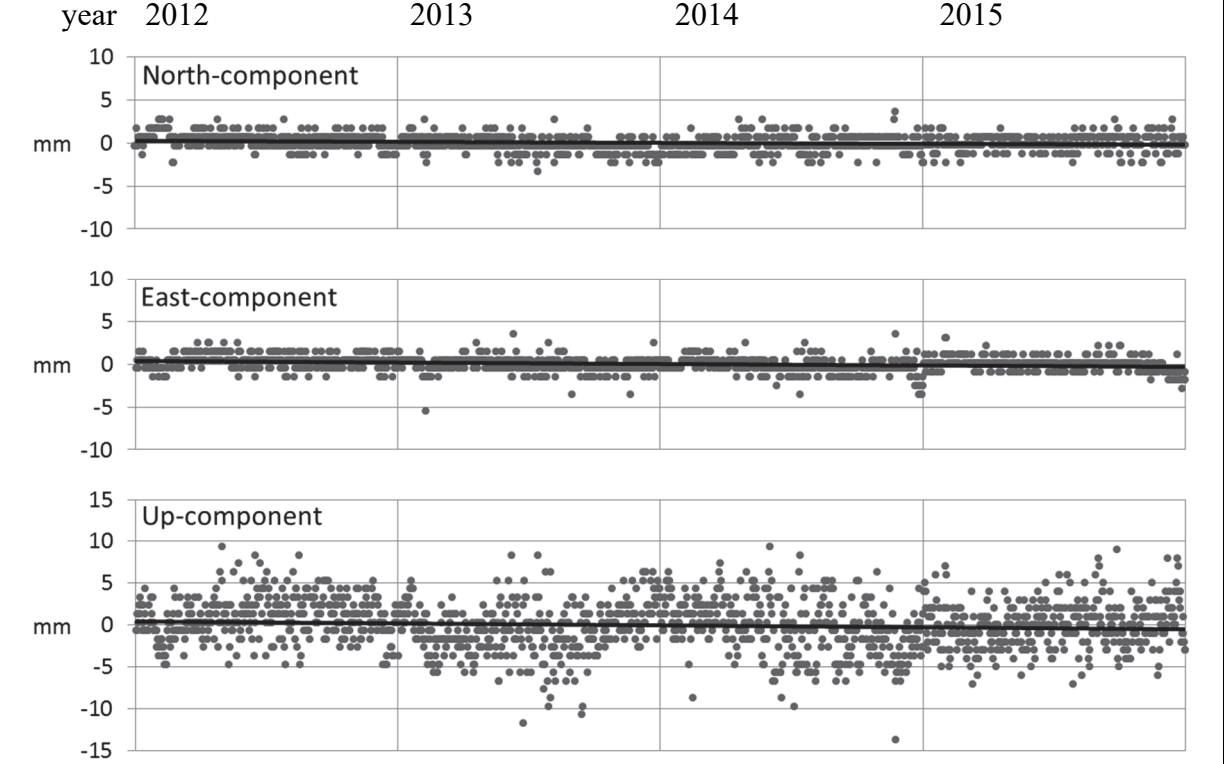


Location

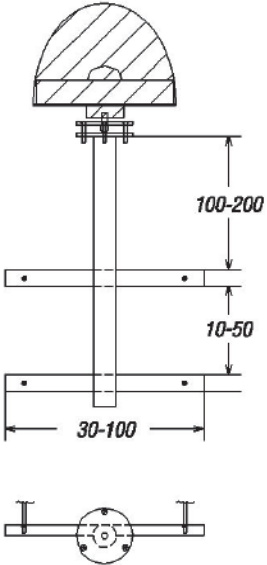


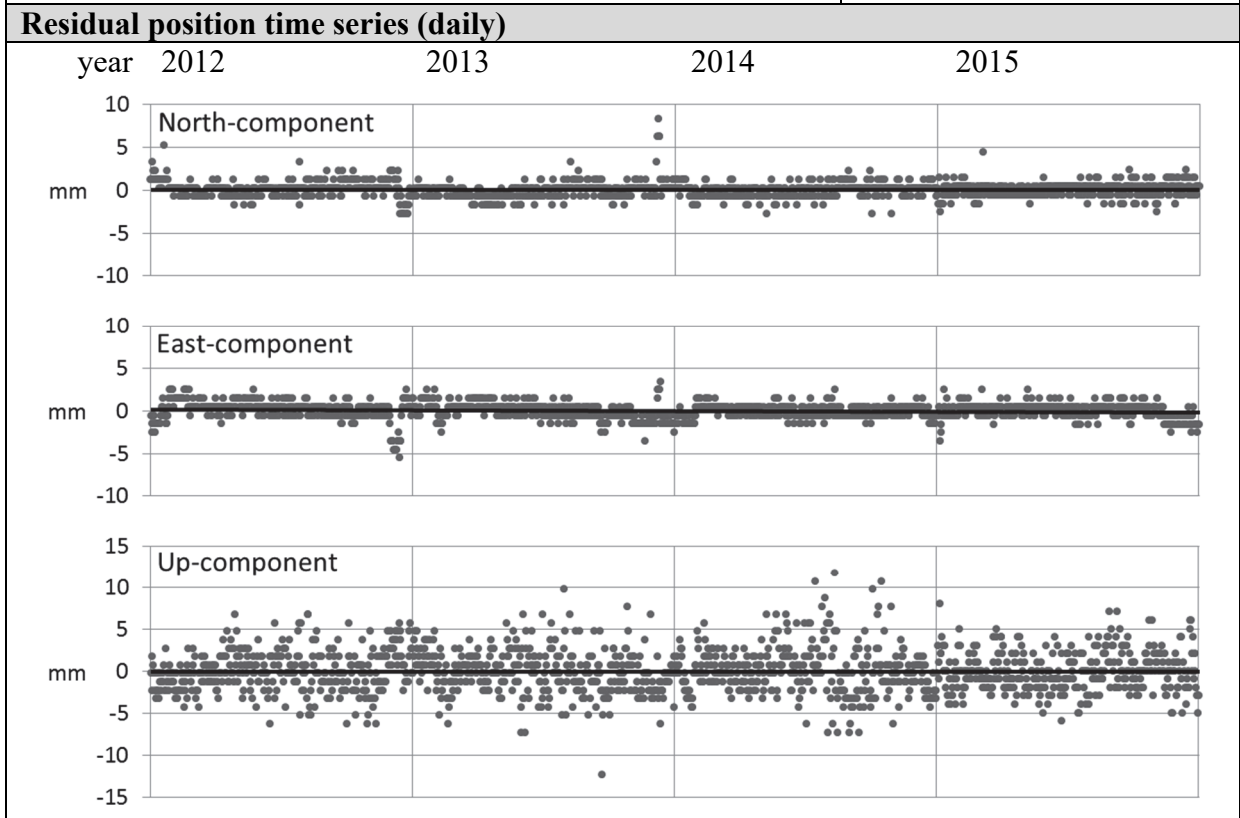
(dimensions in cm)
Site type: b1-003
Installation year: 2010

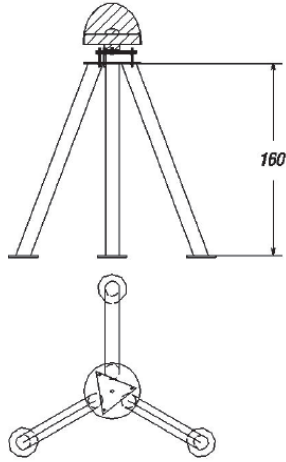
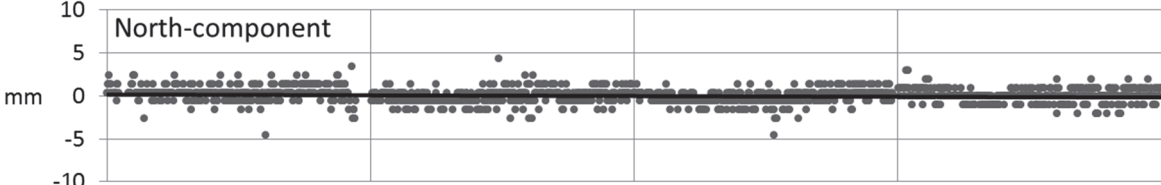
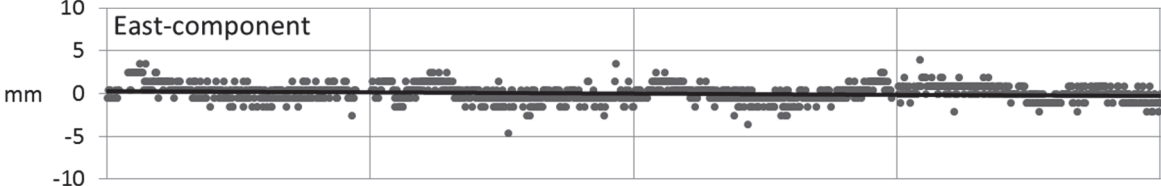
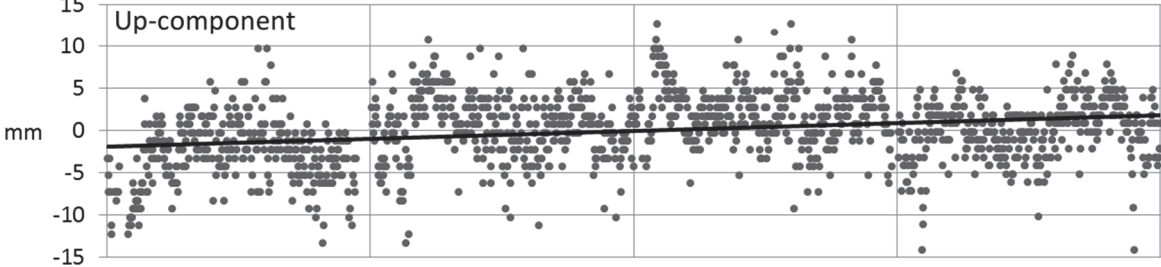
Residual position time series (daily)



Station name: DOB1	Address: Lauku iela 15, Dobele		
Network: LatPos	Coordinates: X	Y	Z
<i>Reference frame: ETRF2000 at epoch 2015.5</i>			
	3229567.834	1389764.093	5303835.629

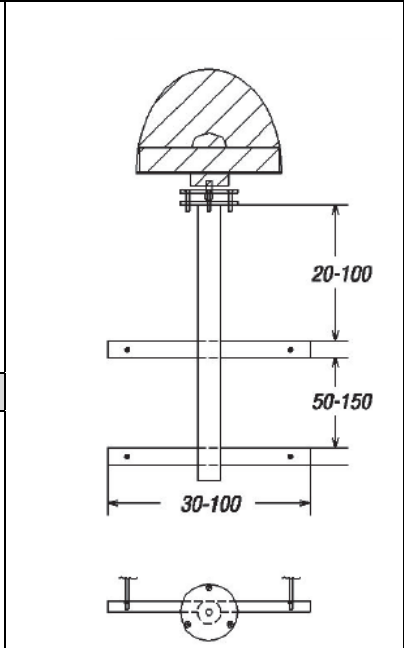
Monument	Antenna mounting
	 <p>(dimensions in cm)</p>
Location	
	<p>Site type: b1-006 Installation year: 2010</p>



Station name: IRBE	Address: Ventspils International Radio Astronomy Center, Irbene			
Network: LatPos	Coordinates: X Y Z			
<i>Reference frame: ETRF2000 at epoch 2015.5</i> 3183614.930 1276707.517 5359315.022				
Monument		Antenna mounting		
		 <p>(dimensions in cm)</p>		
Location		Site type: b1-010 Installation year: 1998		
				
Residual position time series (daily)				
year	2012	2013	2014	2015
mm				
mm				
mm				

Station name: JEK1	Address: Rīgas iela 199, Jēkabpils		
Network: LatPos	Coordinates: X	Y	Z
<i>Reference frame: ETRF2000 at epoch 2015.5</i> 3174732.726 1539143.656 5295773.121			

Monument	Antenna mounting
-----------------	-------------------------

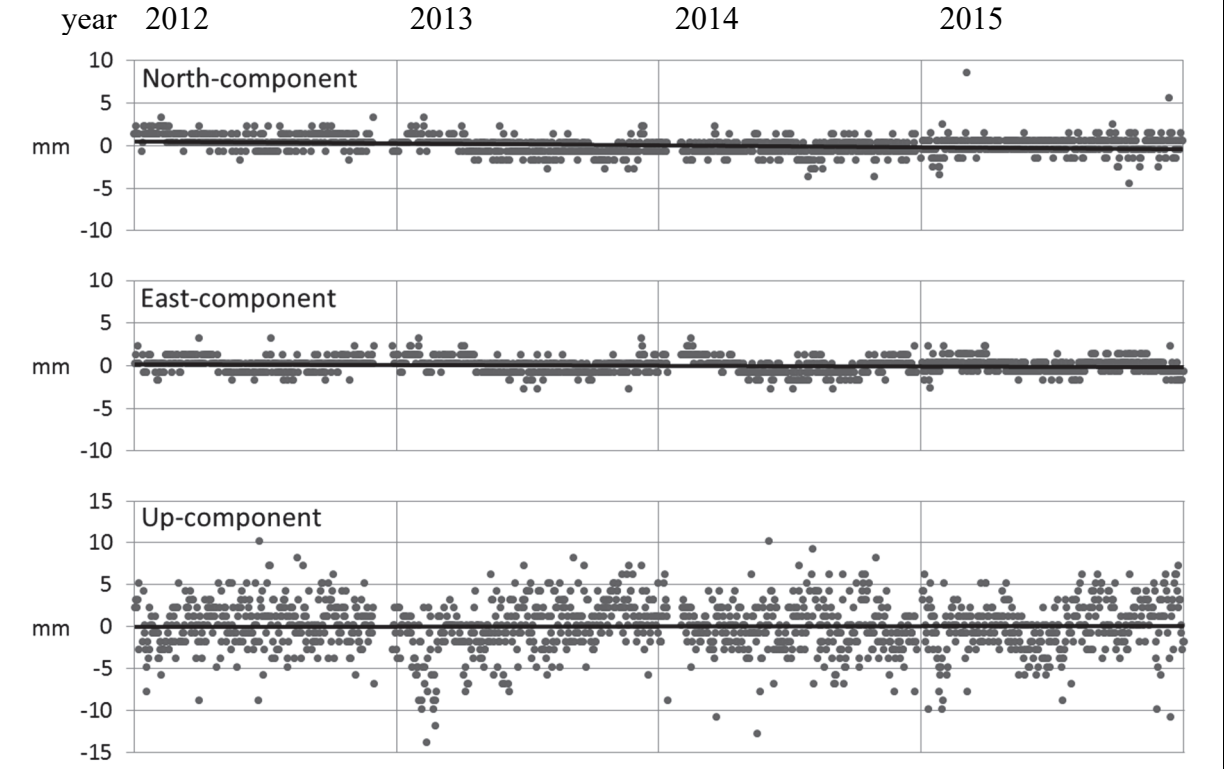


Location



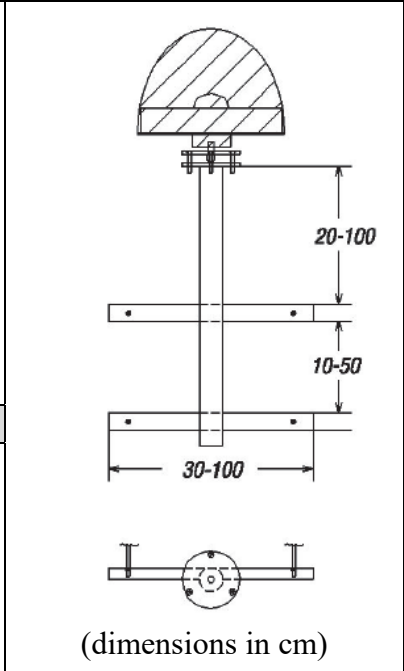
(dimensions in cm)
Site type: b1-008
Installation year: 2010

Residual position time series (daily)
--



Station name: KUL1	Address: Ventspils iela 101, Kuldīga		
Network: LatPos	Coordinates: X	Y	Z
<i>Reference frame: ETRF2000 at epoch 2015.5</i>			
	3231465.160	1302078.848	5324713.073

Monument	Antenna mounting
-----------------	-------------------------

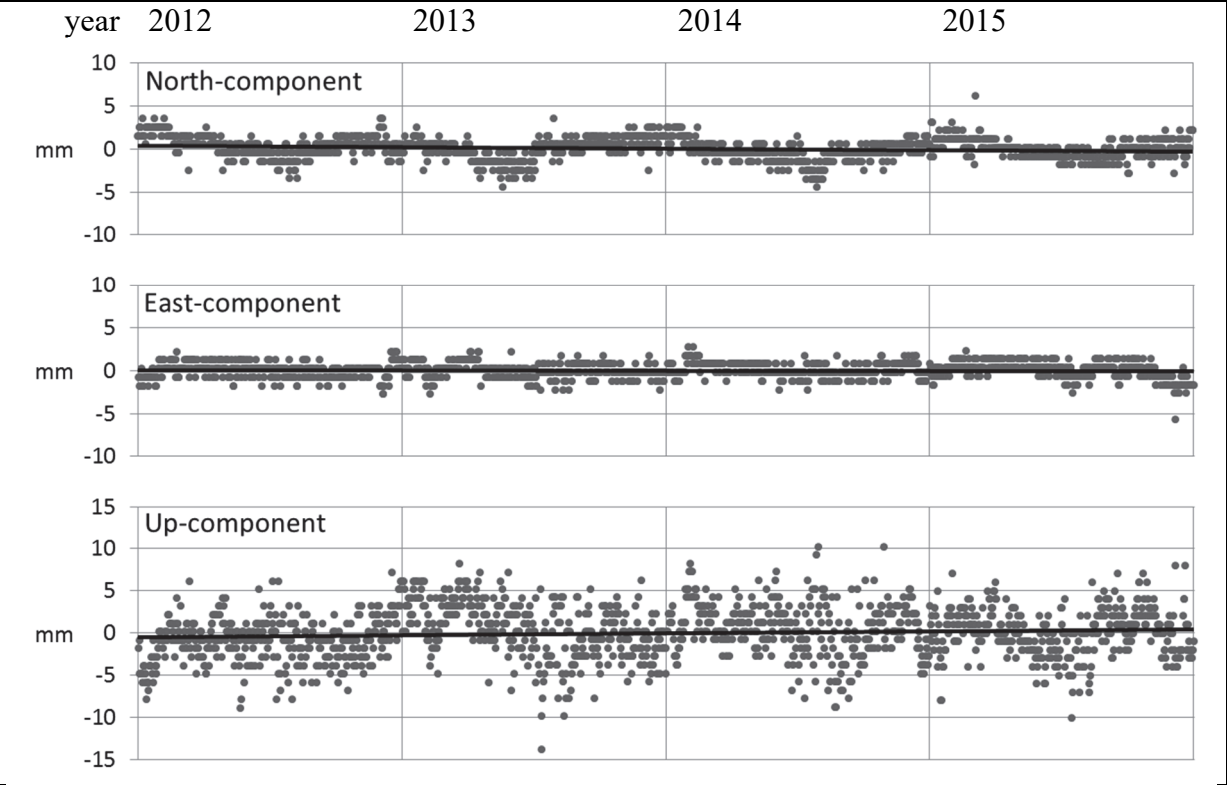


Location

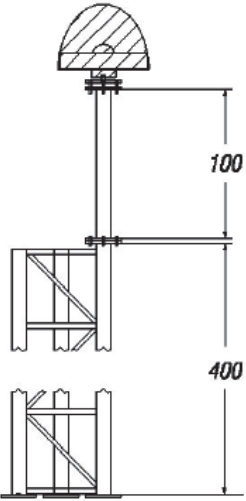


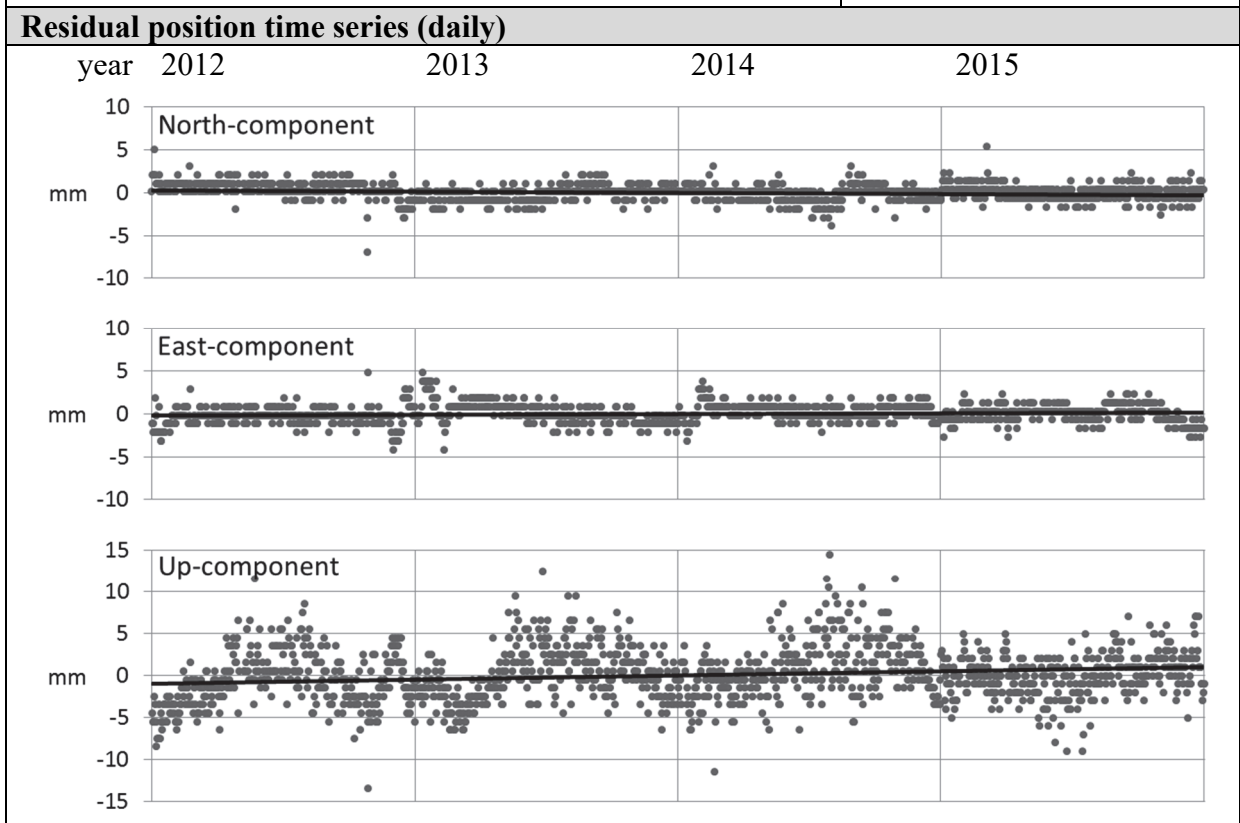
Site type: b1-007
Installation year: 2010

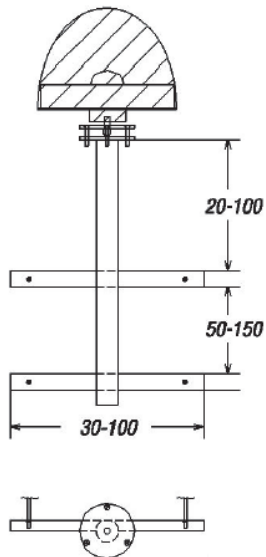
Residual position time series (daily)
--

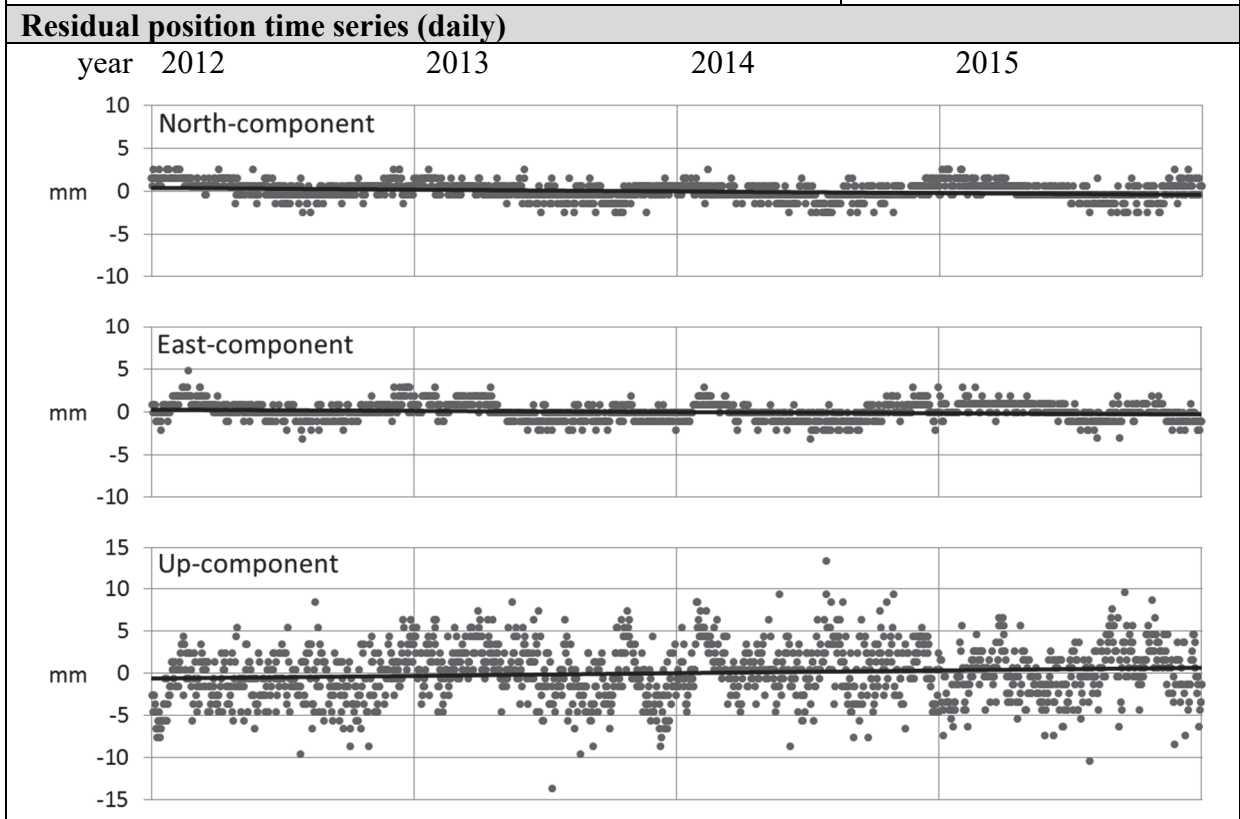


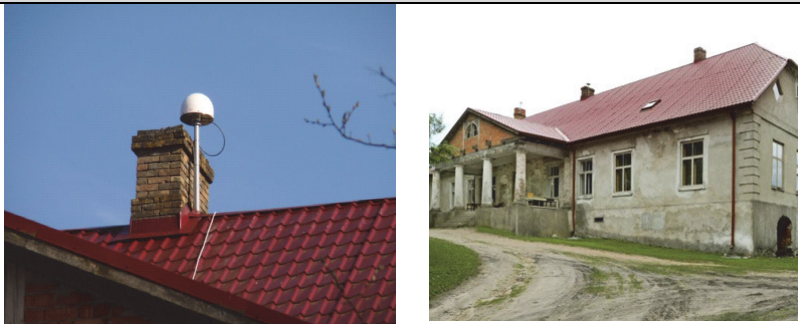
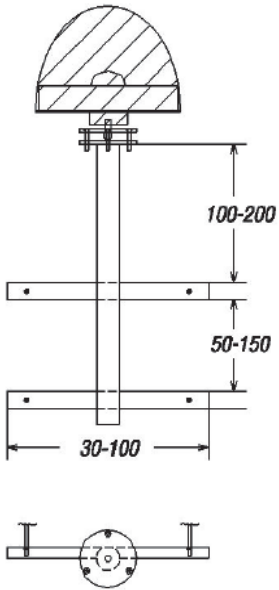
Station name: LIMB	Address: Rīgas iela 16, Limbaži		
Network: LatPos	Coordinates: X	Y	Z
<i>Reference frame: ETRF2000 at epoch 2015.5</i>			
	3119682.927	1435782.658	5356755.072

Monument		Antenna mounting
		 <p>(dimensions in cm)</p> <p>Site type: b1-013</p> <p>Installation year: 2007</p>
Location		
		

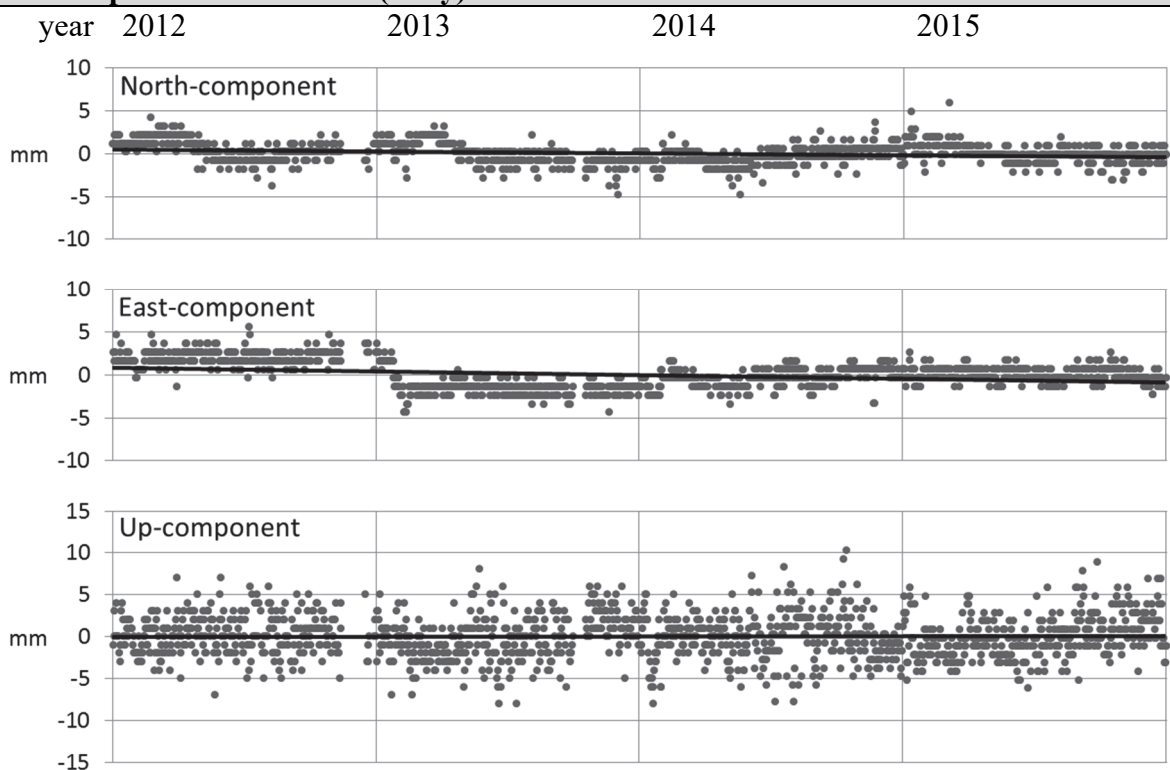


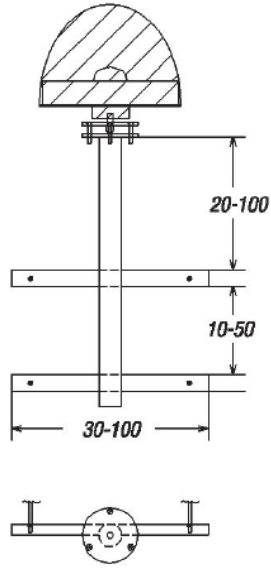
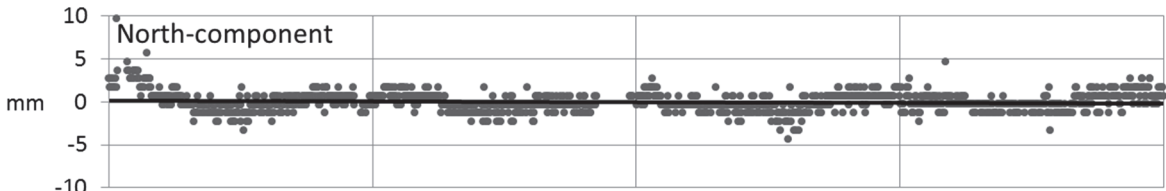
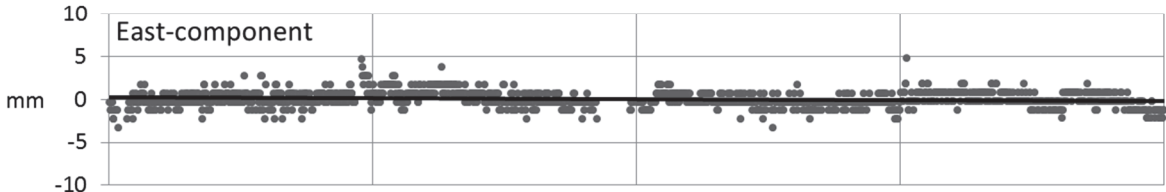
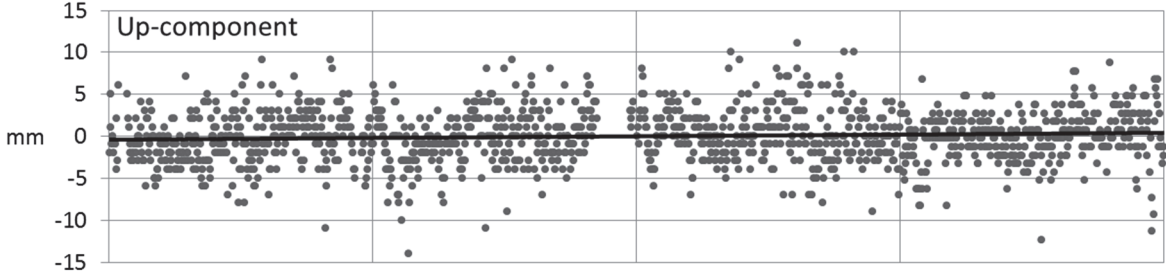
Station name: LIPJ	Address: Bāriņu iela 15, Liepāja		
Network: LatPos	Coordinates: X	Y	Z
<i>Reference frame: ETRF2000 at epoch 2015.5</i> 3293067.576 1265205.911 5295955.765			
Monument		Antenna mounting	
 		 <p>(dimensions in cm)</p>	
Location			
		Site type: b1-008 Installation year: 2010	



Station name: LODE	Address: Lodes muiža, Taurenas pagasts		
Network: LatPos	Coordinates: X	Y	Z
<i>Reference frame: ETRF2000 at epoch 2015.5</i>			
3128070.647 1501820.916 5333995.922			
Monument		Antenna mounting	
		 <p>(dimensions in cm)</p>	
Location		Site type: b1-009	
		Installation year: 2009	

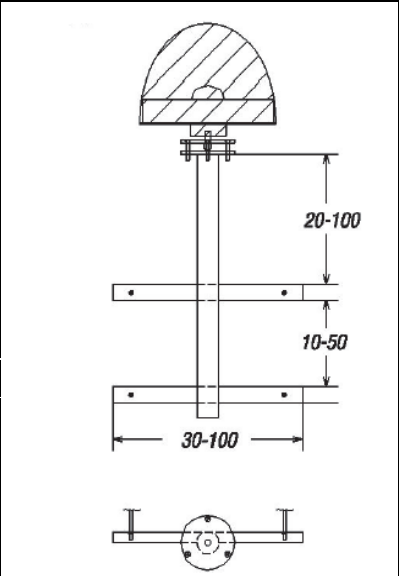
Residual position time series (daily)



Station name: LVRD	Address: Lielvārde military airfield, Rembates pagasts			
Network: LatPos	Coordinates: X Y Z			
<i>Reference frame: ETRF2000 at epoch 2015.5</i> 3179869.704 1471150.347 5311847.441				
Monument		Antenna mounting		
		 <p>(dimensions in cm)</p> <p>Site type: b1-007</p> <p>Installation year: 2011</p>		
Location				
				
Residual position time series (daily)				
year	2012	2013	2014	2015
mm				
mm				
mm				

Station name: MADO	Address: Tirgus iela 3, Madona		
Network: LatPos	Coordinates: X	Y	Z
<i>Reference frame: ETRF2000 at epoch 2015.5</i>			
	3136049.867	1544577.073	5317122.728

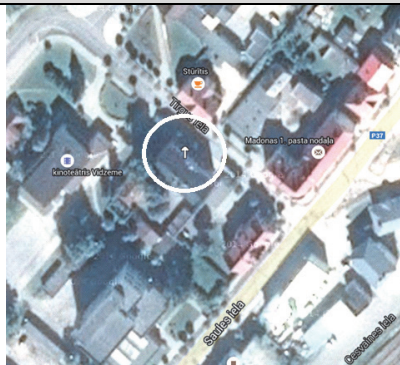
Monument	Antenna mounting
----------	------------------



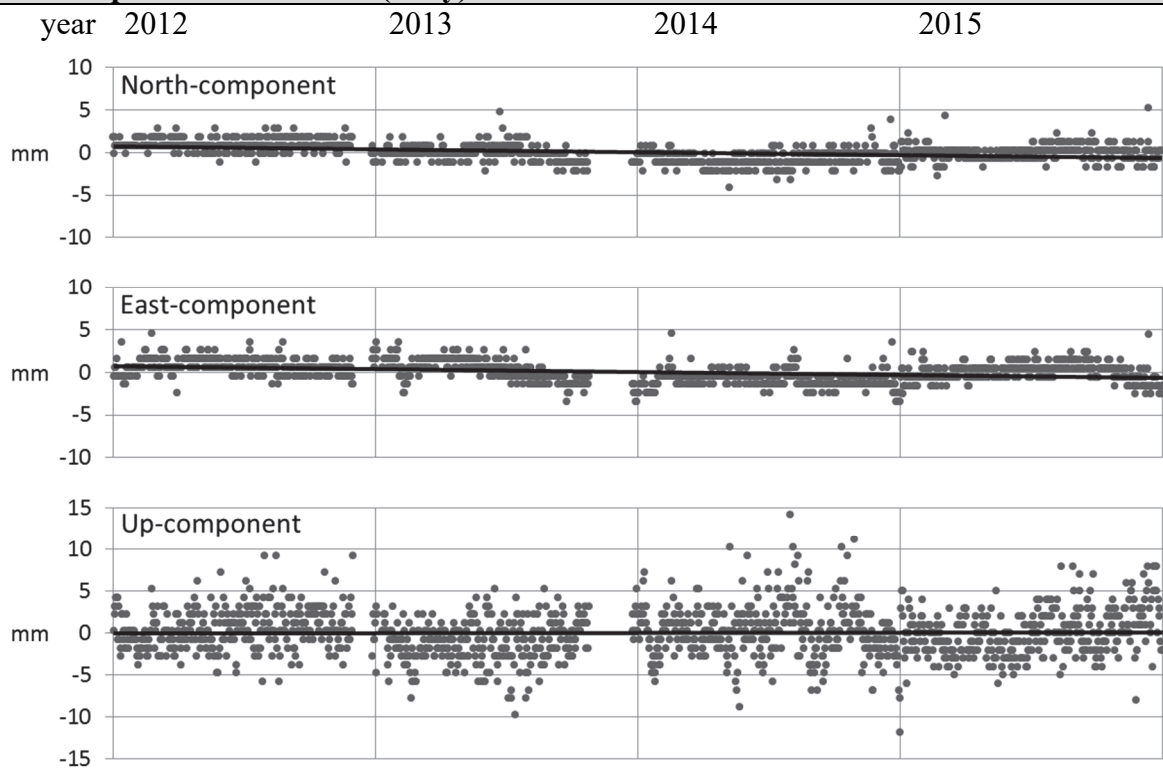
(dimensions in cm)

Site type: b1-007
Installation year: 2005

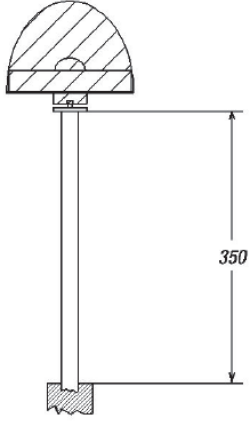
Location

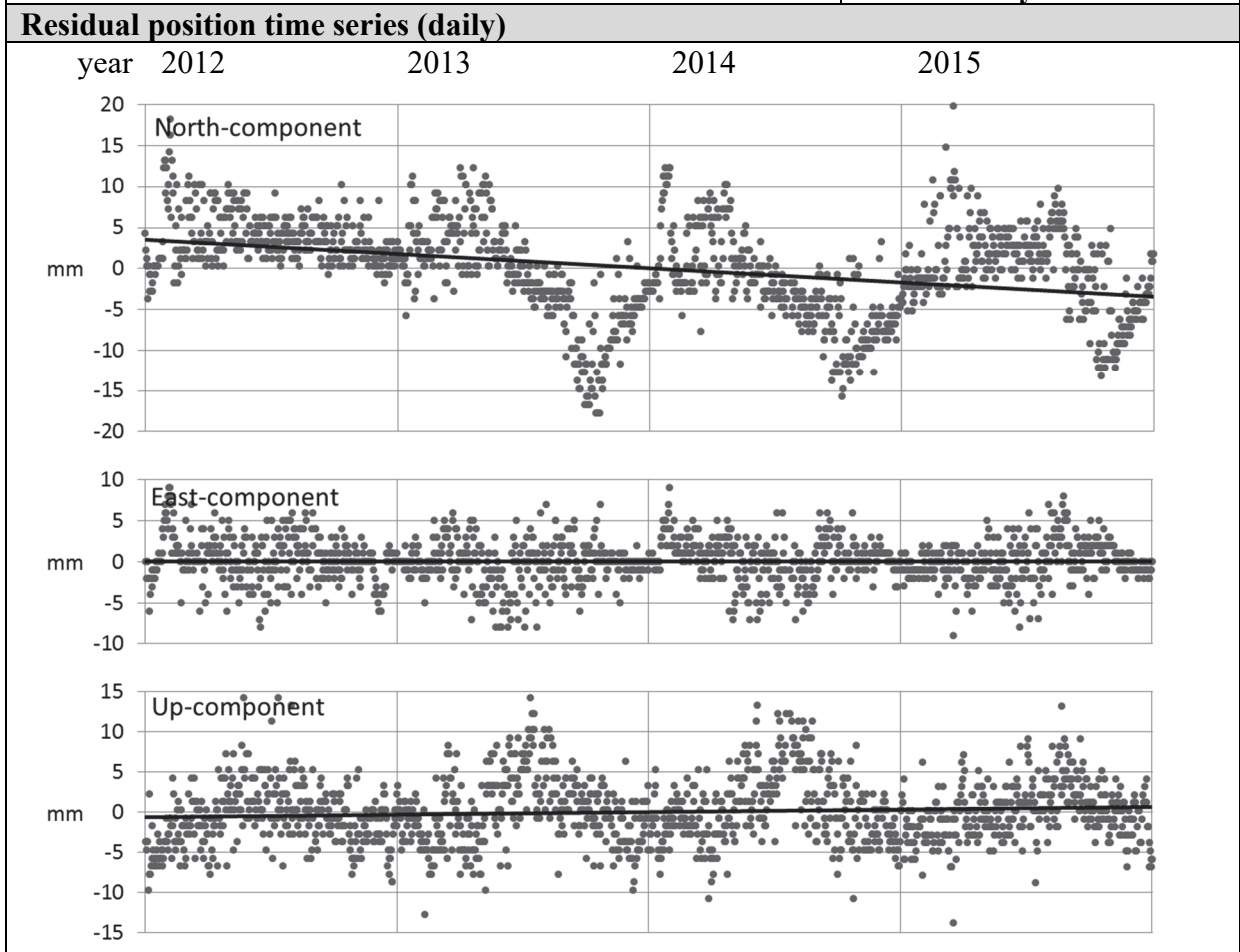


Residual position time series (daily)

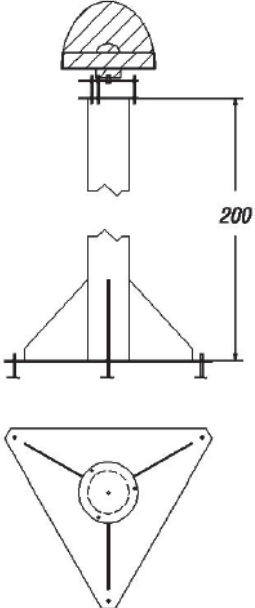


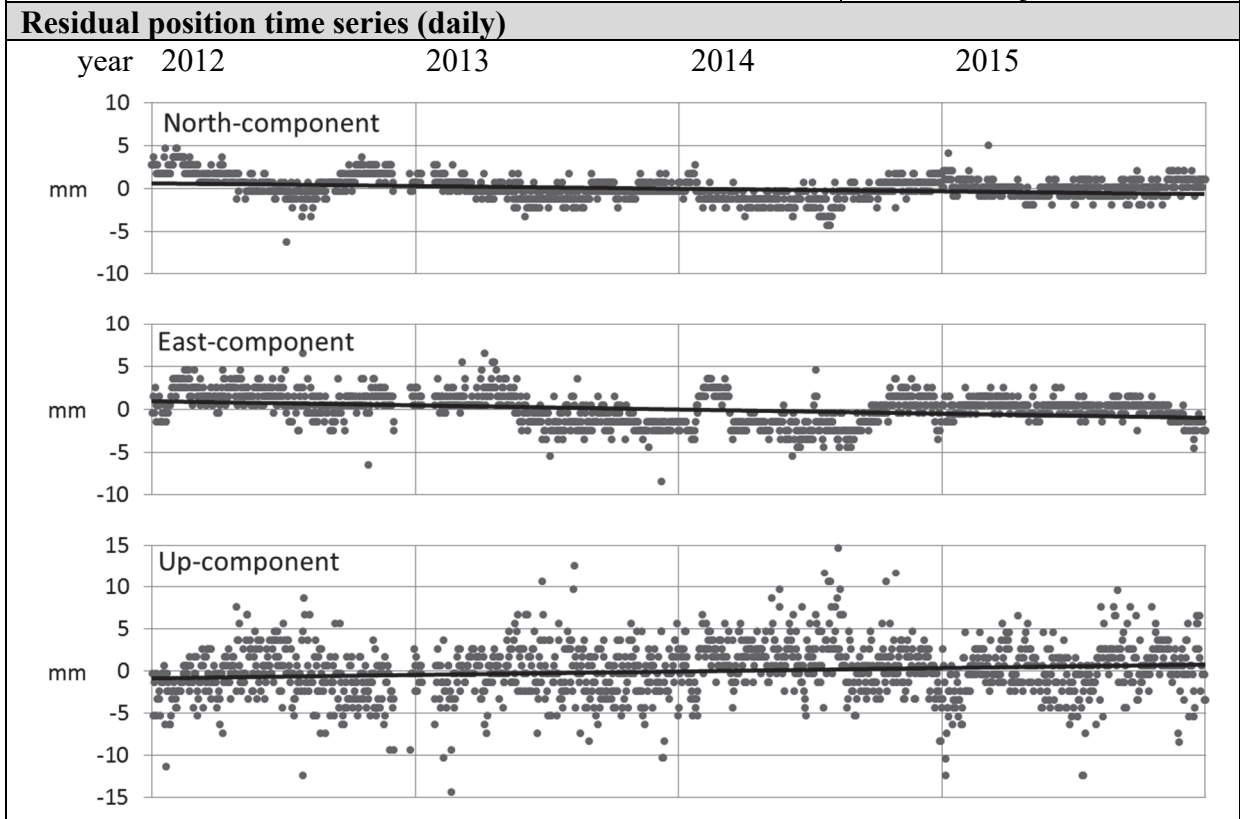
Station name: MAZS	Address: Rīgas iela 15, Mazsalaca		
Network: LatPos	Coordinates: X	Y	Z
<i>Reference frame: ETRF2000 at epoch 2015.5</i>			
	3081539.169	1440527.823	5377339.260

Monument	Antenna mounting
	
Location	
	
	(dimensions in cm)
	Site type: b1-012
	Installation year: 2010



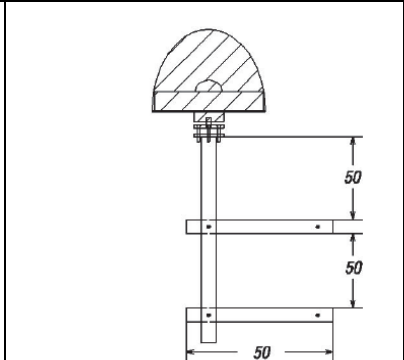
Station name: OJAR	Address: Ojāra Vācieša iela 43, Rīga		
Network: LatPos	Coordinates: X	Y	Z
<i>Reference frame: ETRF2000 at epoch 2015.5</i>			
	3185444.647	1423322.949	5321411.189

Monument	Antenna mounting
	 <p>(dimensions in cm)</p> <p>Site type: b1-001</p> <p>Installation year: 2001</p>
Location	
	



Station name: PLSM	Address: Culture House, Palsmane		
Network: LatPos	Coordinates: X	Y	Z
<i>Reference frame: ETRF2000 at epoch 2015.5</i> 3092007.964 1520314.525 5349551.206			

Monument	Antenna mounting
-----------------	-------------------------



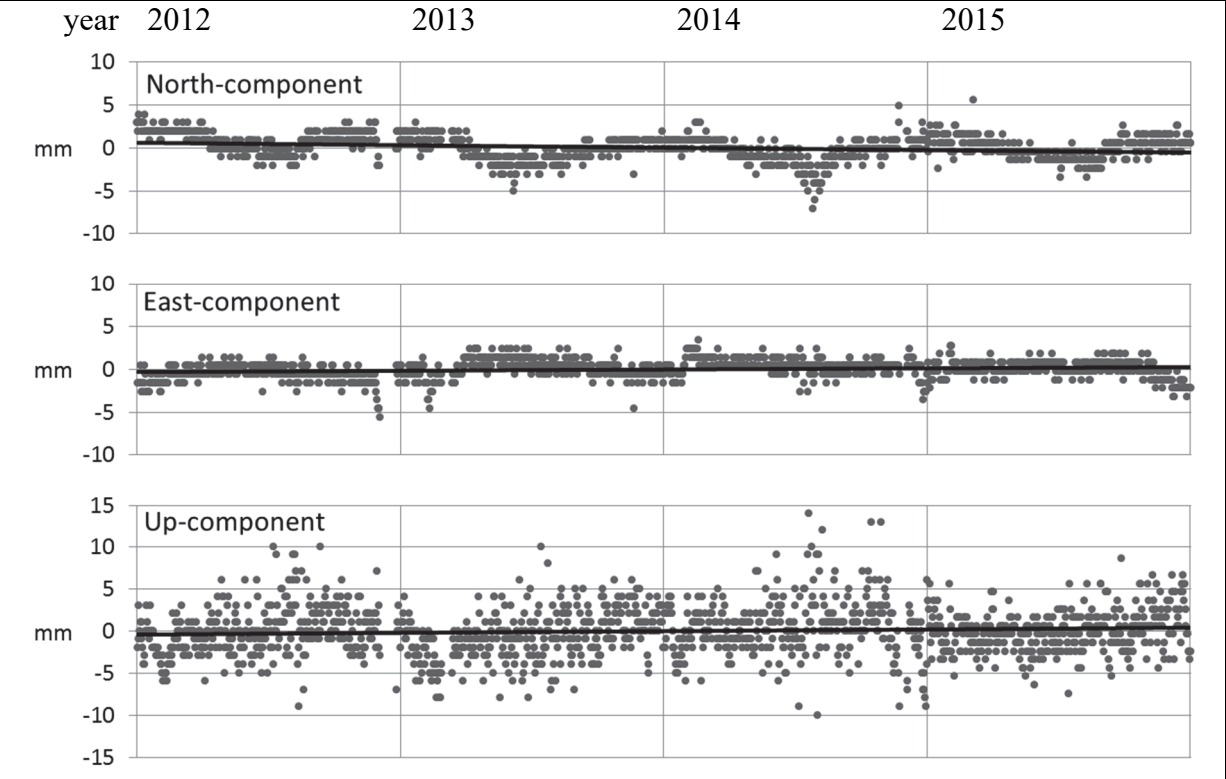
Location

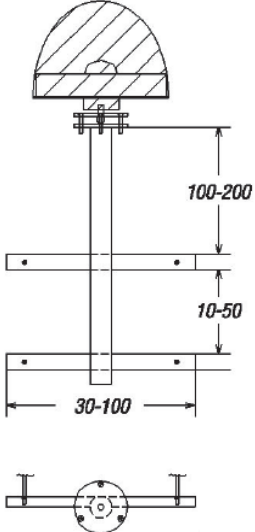
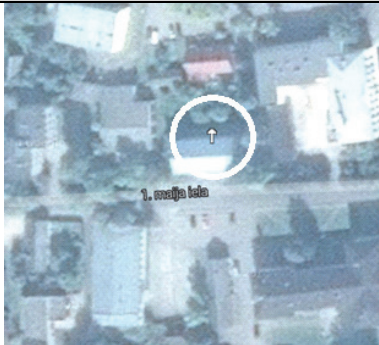
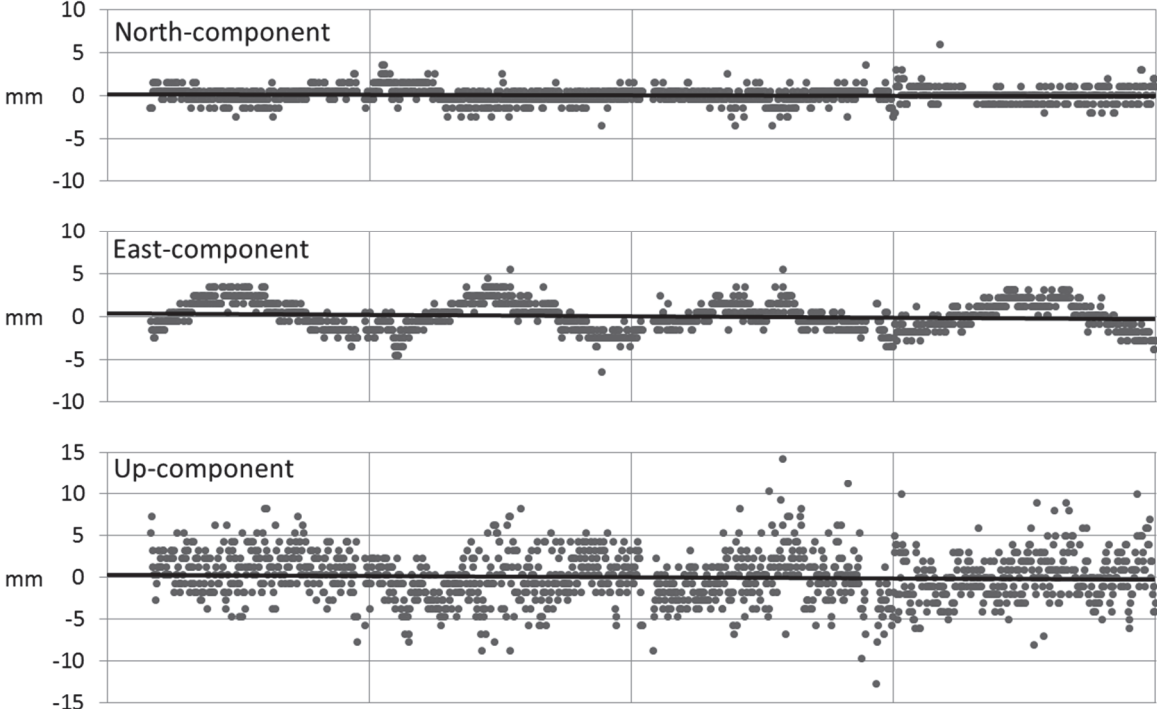


(dimensions in cm)

Site type: b1-011
Installation year: 2011

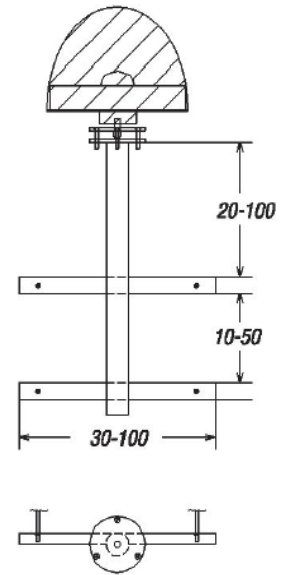
Residual position time series (daily)
--



Station name: PREI	Address: 1. maija iela 7, Preiļi			
Network: LatPos	Coordinates: X Y Z			
<i>Reference frame: ETRF2000 at epoch 2015.5</i> 3169094.116 1595616.248 5282560.853				
Monument		Antenna mounting		
		 <p>(dimensions in cm)</p>		
Location		Site type: b1-006		
		Installation year: 2006		
Residual position time series (daily)				
year	2012	2013	2014	2015
mm				

Station name: REZ1	Address: Atbrīvošanas aleja 155, Rēzekne		
Network: LatPos	Coordinates: X	Y	Z
<i>Reference frame: ETRF2000 at epoch 2015.5</i>			
	3132106.577	1619598.785	5297236.972

Monument	Antenna mounting
-----------------	-------------------------



(dimensions in cm)

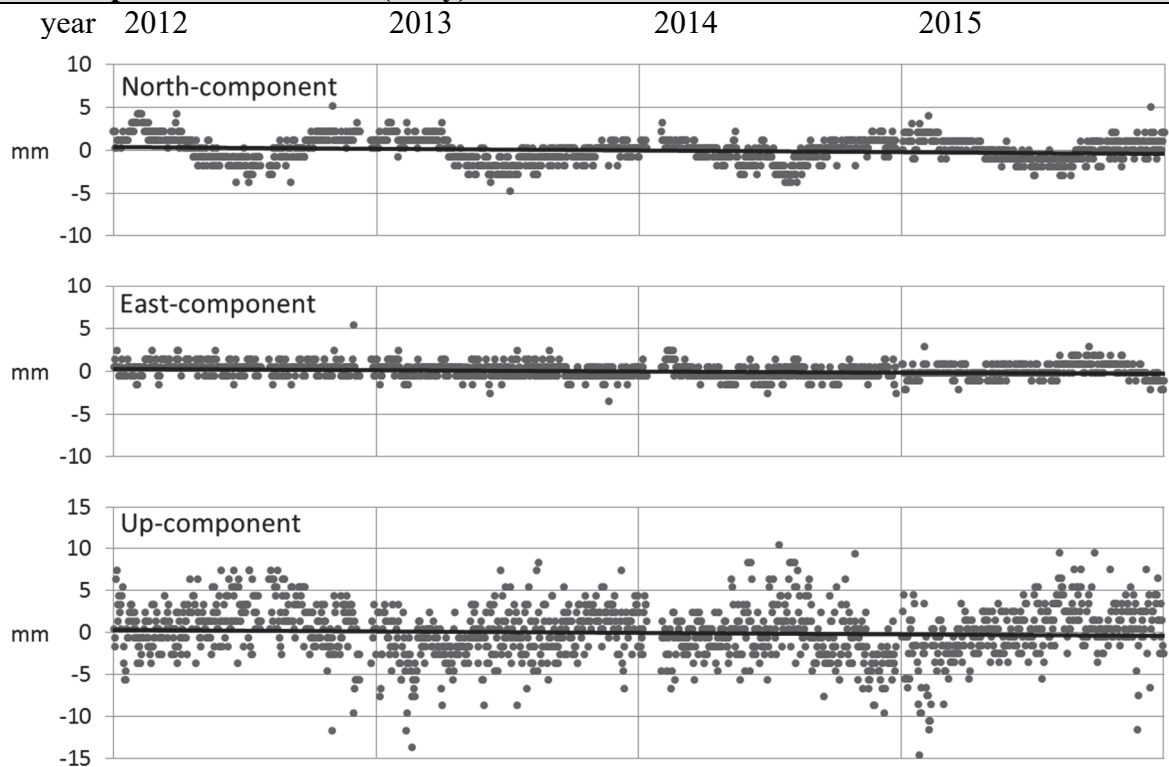
Site type: b1-007

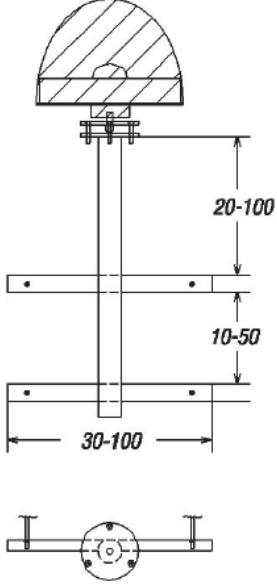
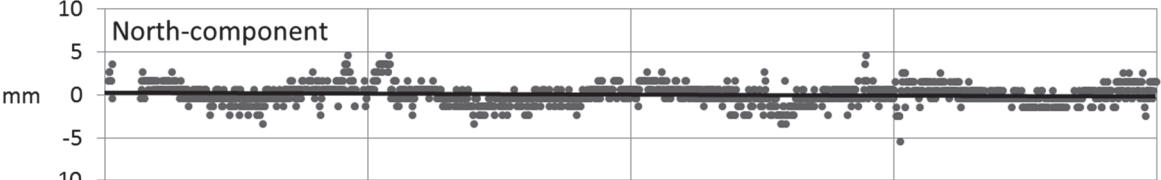
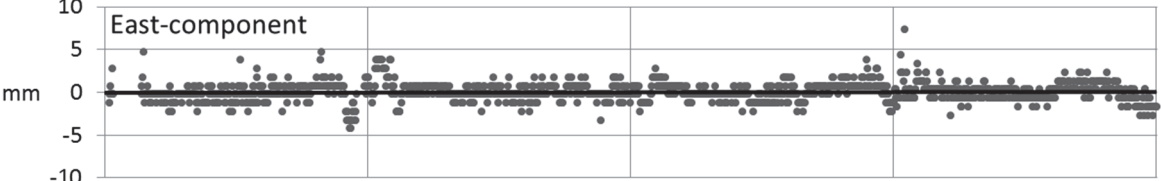
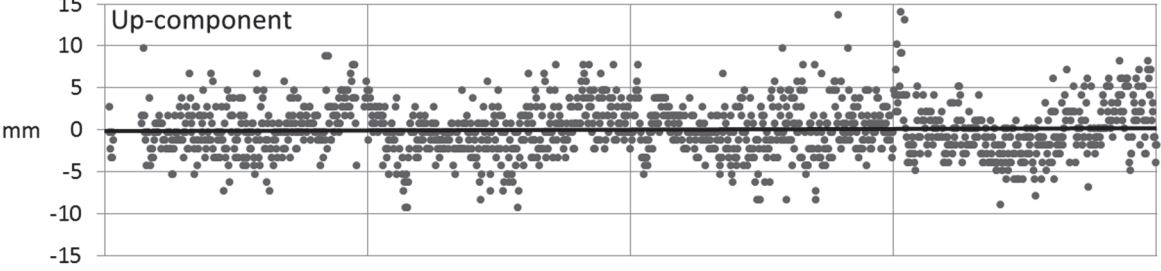
Installation year: 2010

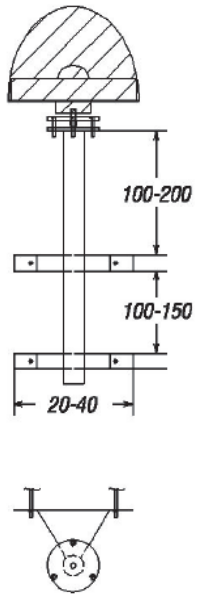
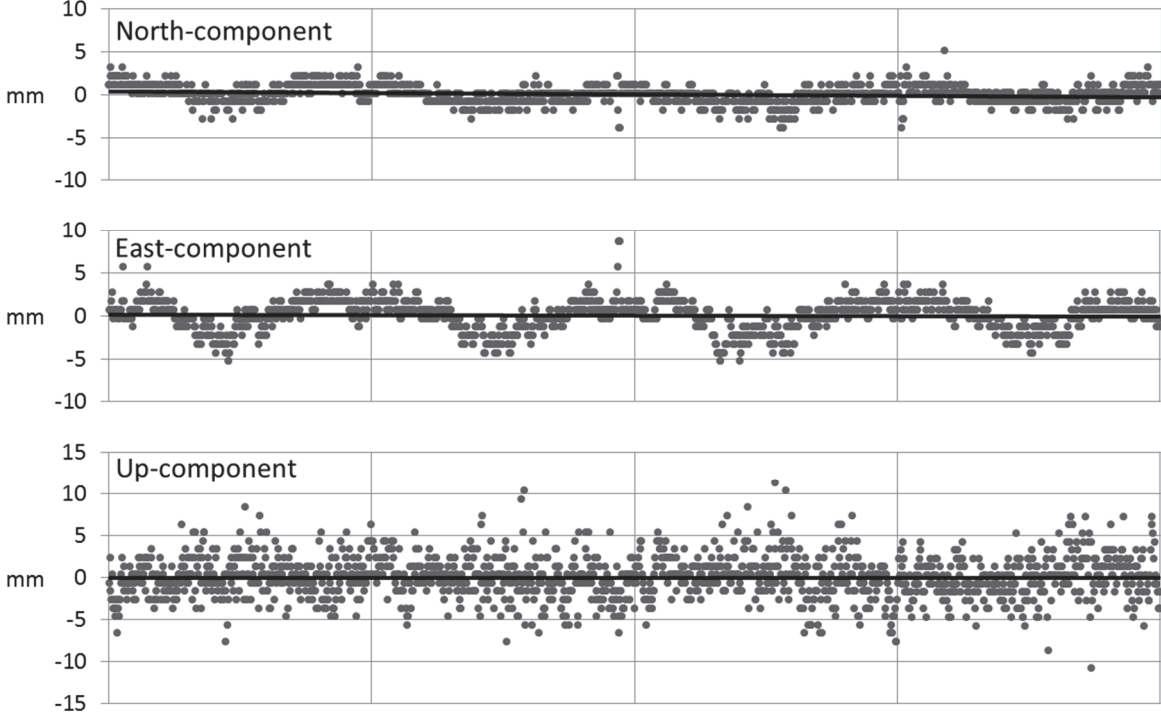
Location



Residual position time series (daily)				
--	--	--	--	--

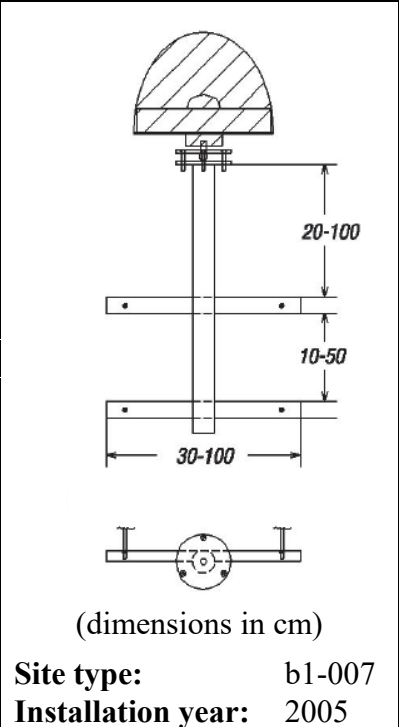


Station name: SIGU	Address: Zinātnes iela 7, Sigulda			
Network: LatPos	Coordinates: X Y Z			
<i>Reference frame: ETRF2000 at epoch 2015.5</i> 3145951.771 1459815.081 5335020.953				
Monument		Antenna mounting		
 		 <p>(dimensions in cm)</p>		
Location		Site type: b1-007 Installation year: 2005		
				
Residual position time series (daily)				
year	2012	2013	2014	2015
mm				
mm				
mm				

Station name: SLD1	Address: Striķu iela 36, Saldus			
Network: LatPos	Coordinates: X	Y	Z	
<i>Reference frame: ETRF2000 at epoch 2015.5</i> 3246339.053 1344595.907 5305291.930				
Monument		Antenna mounting		
		 <p>(dimensions in cm)</p>		
Location		Site type: b1-004		
		Installation year: 2011		
Residual position time series (daily)				
year	2012	2013	2014	2015
mm				

Station name: TALS	Address: Kareivju iela 7, Talsi		
Network: LatPos	Coordinates: X	Y	Z
<i>Reference frame: ETRF2000 at epoch 2015.5</i> 3193687.674 1328546.504 5340896.991			

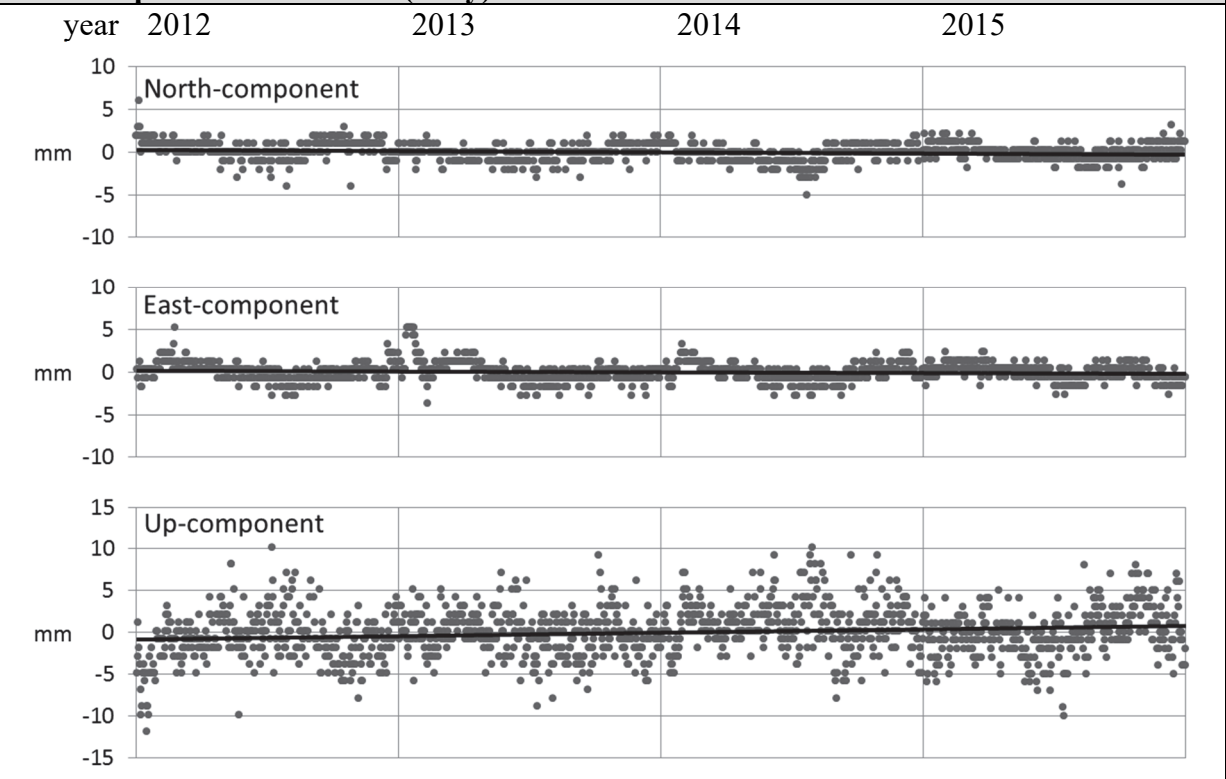
Monument	Antenna mounting
-----------------	-------------------------



Location

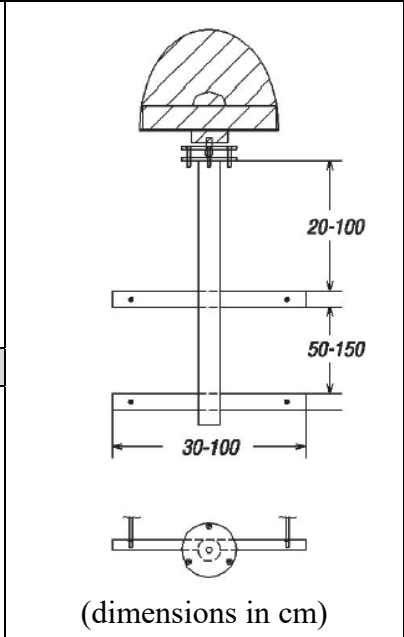


Residual position time series (daily)
--



Station name: TKMS	Address: Pils iela 22, Tukums
Network: LatPos	Coordinates: X Y Z
<i>Reference frame: ETRF2000 at epoch 2015.5</i> 3204261.450 1370807.820 5323945.989	

Monument	Antenna mounting
----------	------------------

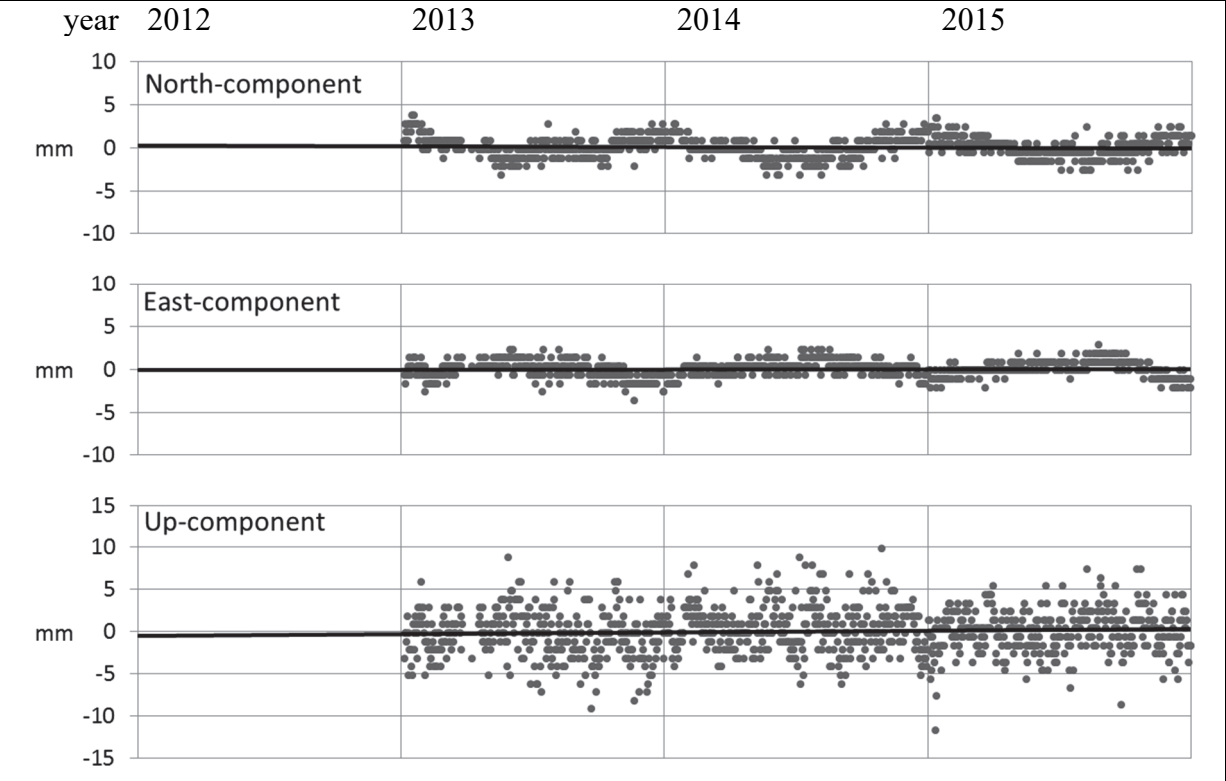


Location



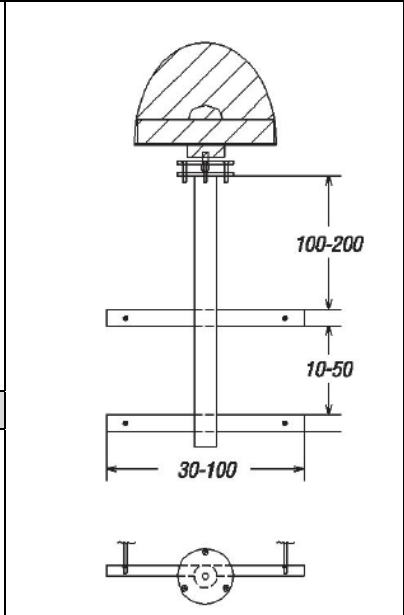
Site type: b1-008
Installation year: 2012

Residual position time series (daily)				
---------------------------------------	--	--	--	--



Station name: VAL1	Address: Rīgas iela 47, Valmiera		
Network: LatPos	Coordinates: X	Y	Z
<i>Reference frame: ETRF2000 at epoch 2015.5</i>			
	3099933.577	1472349.420	5358237.290

Monument	Antenna mounting
-----------------	-------------------------



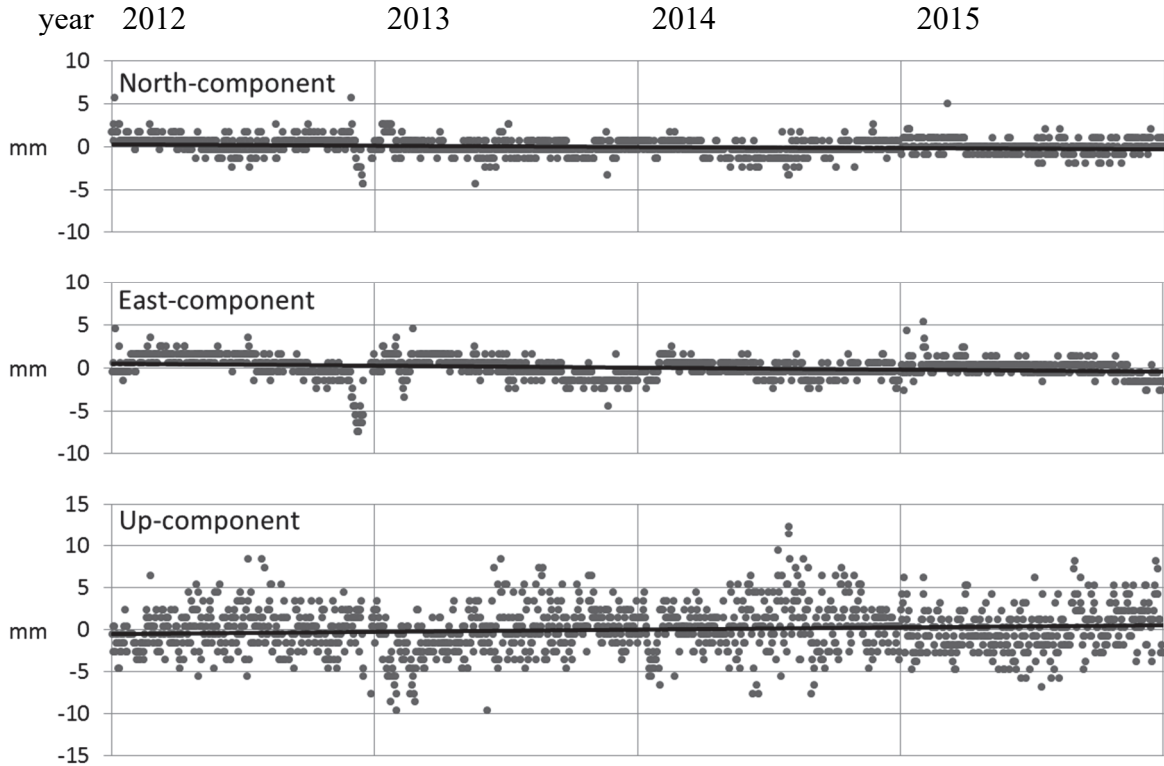
(dimensions in cm)

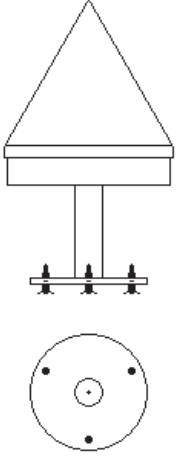
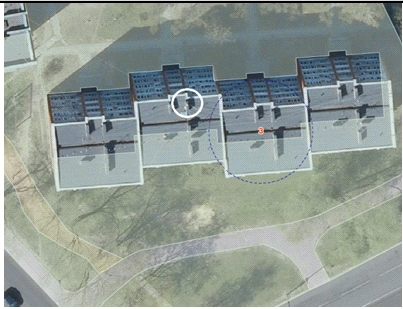
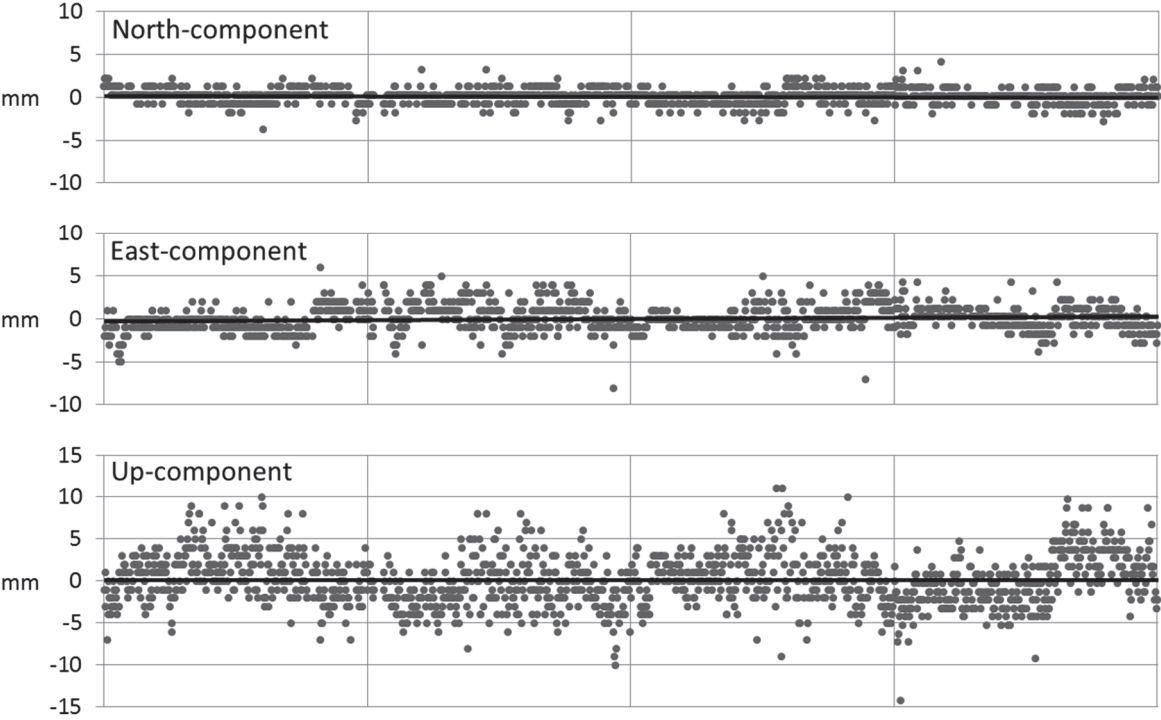
Site type: b1-006
Installation year: 2011

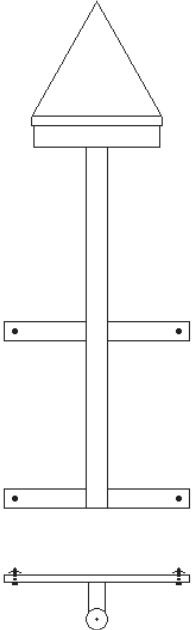
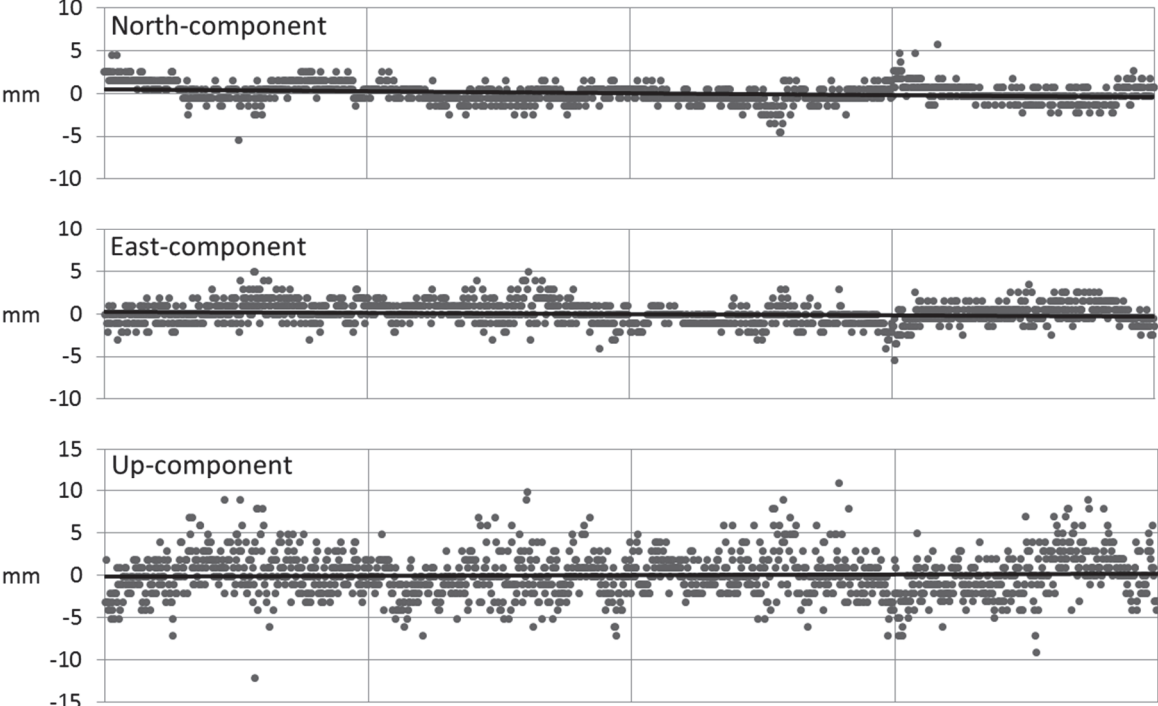
Location

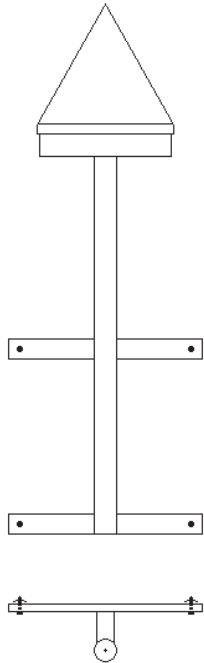


Residual position time series (daily)

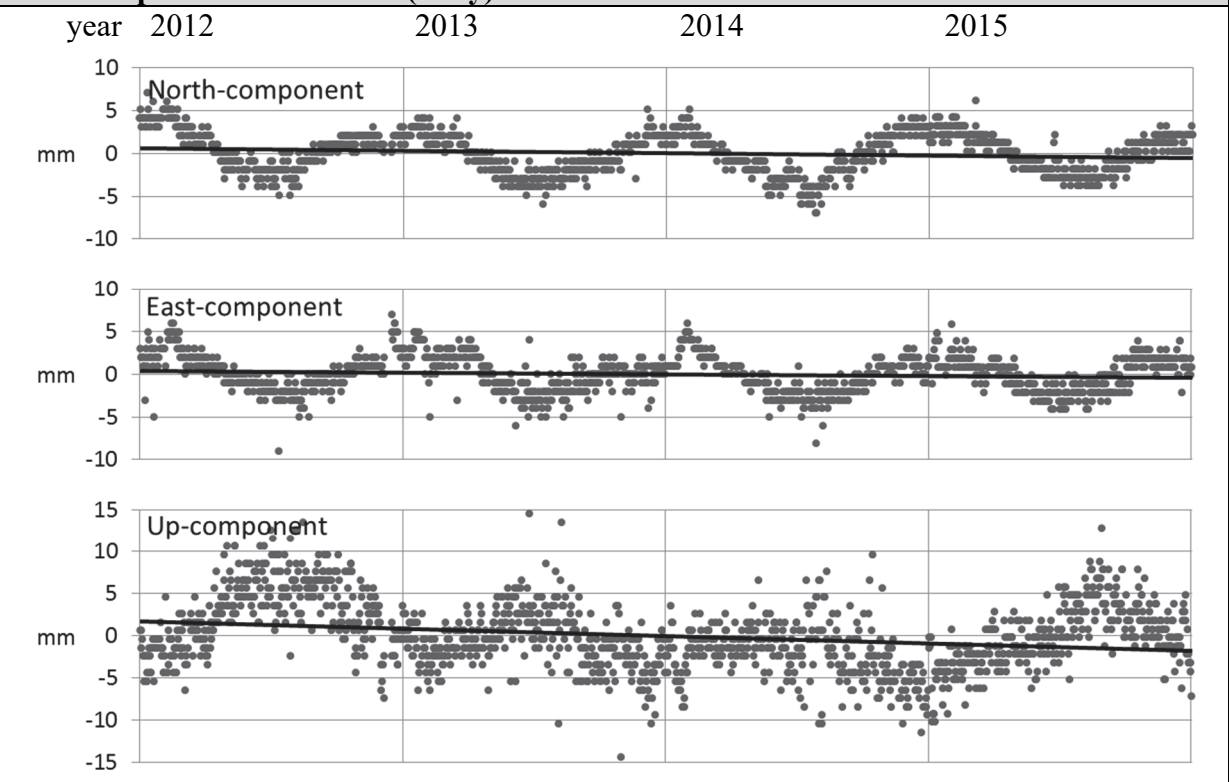


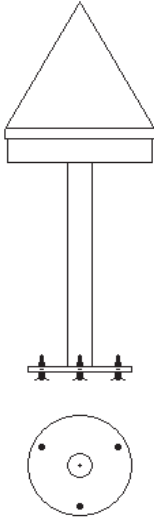
Station name: KREI	Address: Kreimeņu iela 3, Rīga			
Network: EUPOS-Riga	Coordinates: X	Y	Z	
<i>Reference frame: ETRF2000 at epoch 2015.5</i> 3175810.584 1419886.848 5328038.039				
Monument		Antenna mounting		
				
Location				
		Site type: - Installation year: 2006		
Residual position time series (daily)				
year	2012	2013	2014	2015
mm				

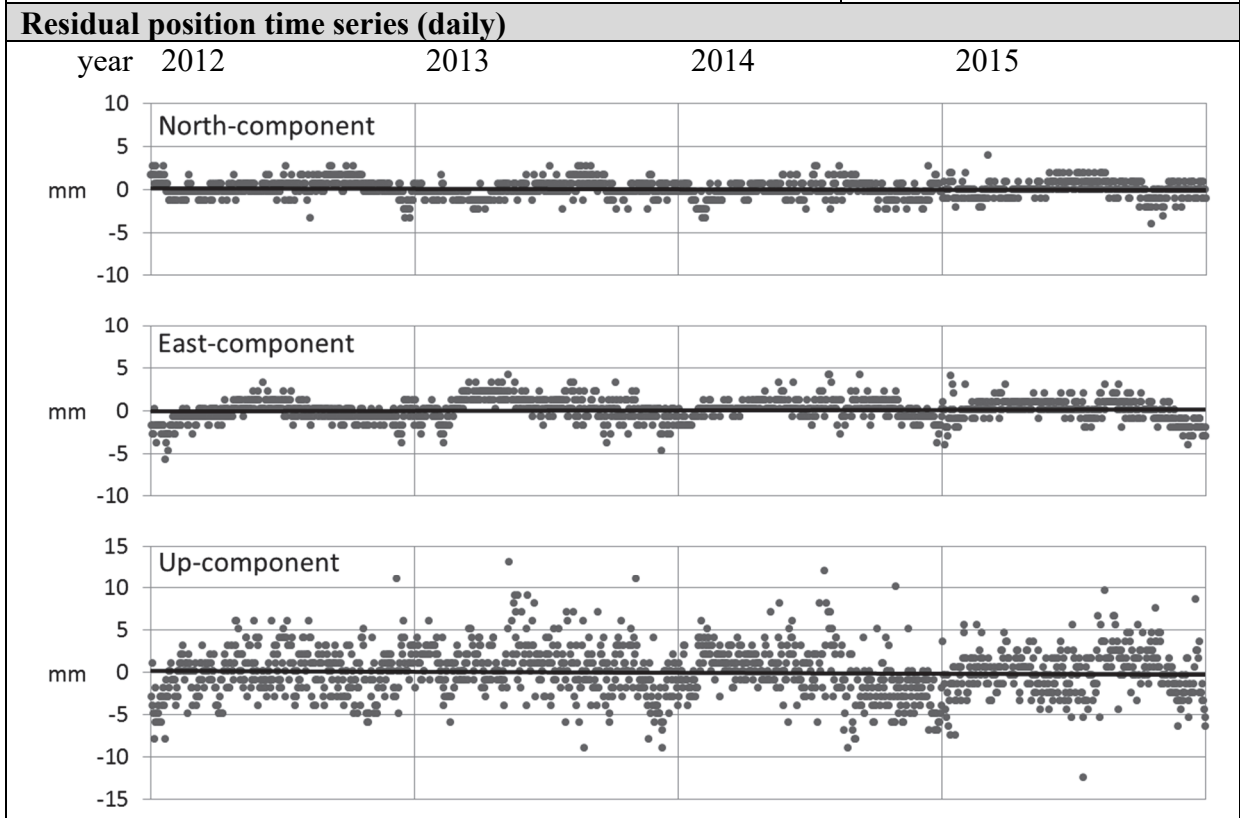
Station name: LUNI	Address: Raiņa bulvāris 19, Rīga			
Network: EUPOS-Riga	Coordinates: X	Y	Z	
<i>Reference frame: ETRF2000 at epoch 2015.5</i> 3182302.476 1424614.575 5322944.643				
Monument		Antenna mounting		
				
Location		Site type: - Installation year: 2006		
				
Residual position time series (daily)				
year	2012	2013	2014	2015
mm				

Station name: SALP	Address: Miera iela 32, Salaspils		
Network: EUPOS-Riga	Coordinates: X Y Z		
<i>Reference frame: ETRF2000 at epoch 2015.5</i> 3182384.922 1443462.220 5317877.533			
Monument		Antenna mounting	
			
Location		Site type: - Installation year: 2011	
			

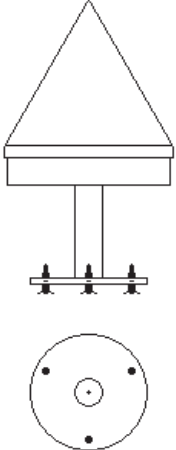
Residual position time series (daily)

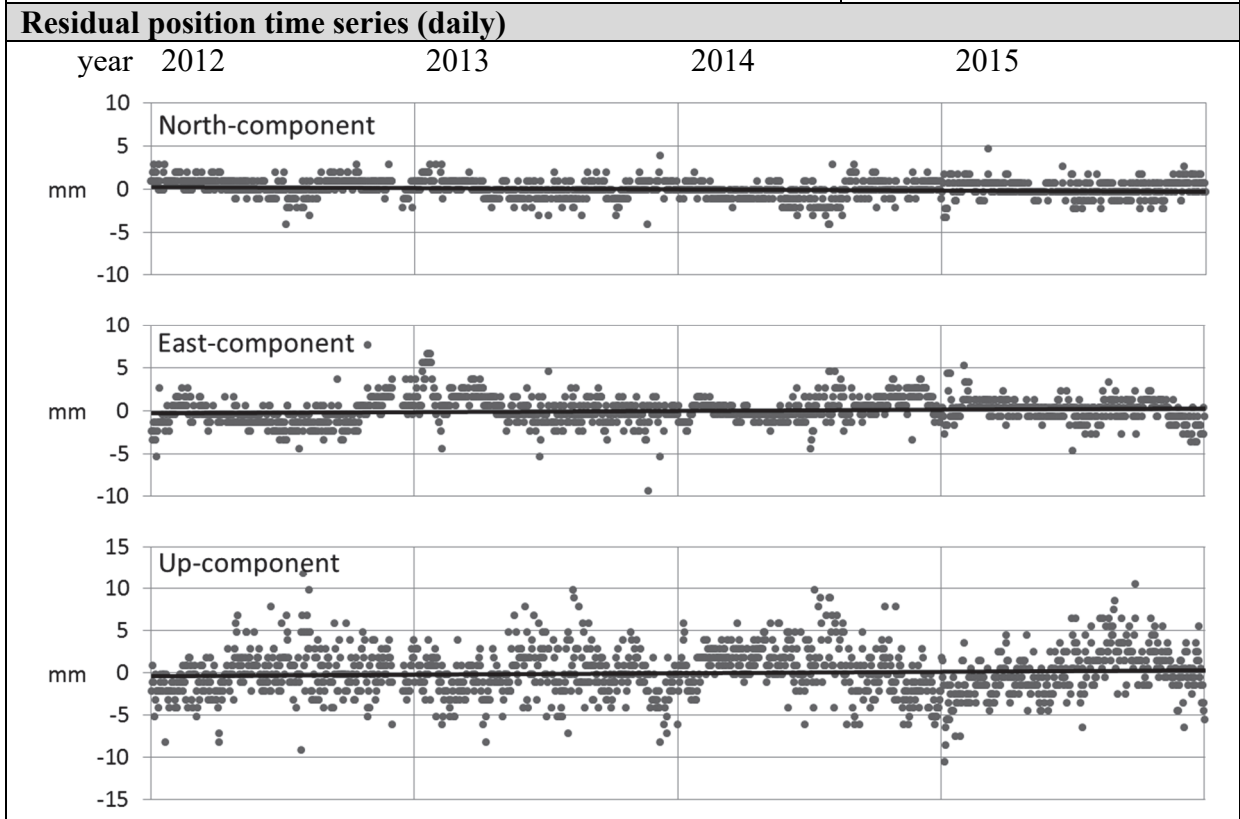


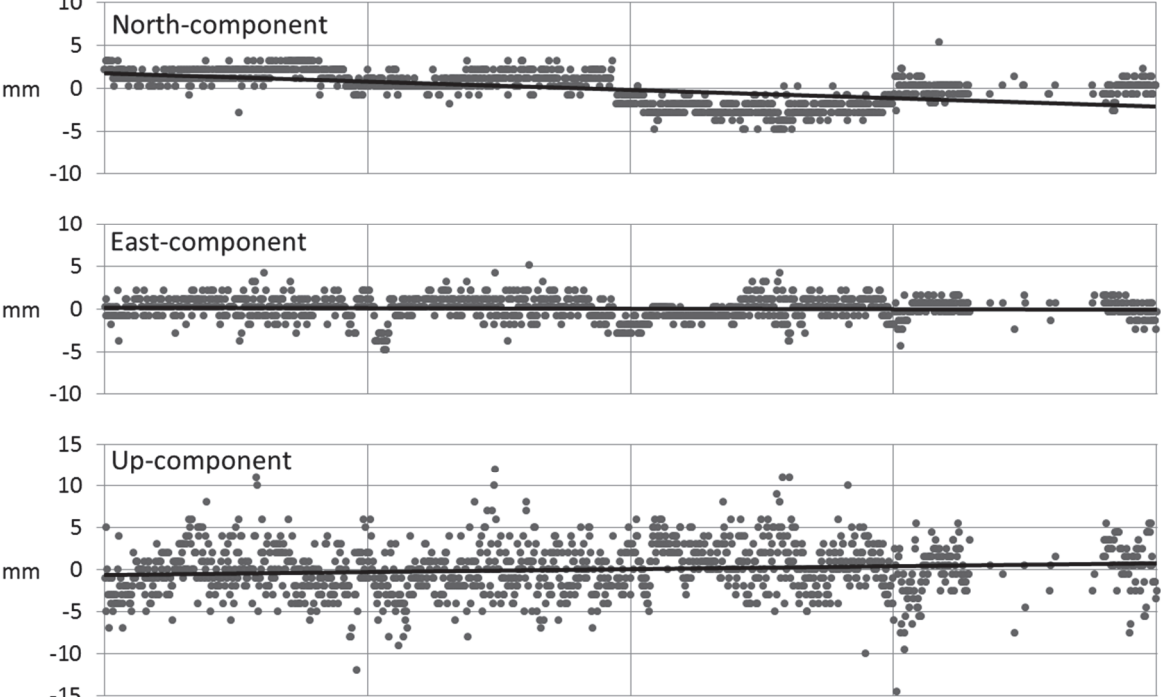
Station name: VAIV	Address: Asaru prospekts 61, Jūrmala		
Network: EUPOS-Riga	Coordinates: X	Y	Z
<i>Reference frame: ETRF2000 at epoch 2015.5</i> 3192633.699 1399321.045 5323475.672			
Monument		Antenna mounting	
			
Location			
		<p>Site type: -</p> <p>Installation year: 2011</p>	



Station name: VANG	Address: Vangažu iela 32, Rīga
Network: EUPOS-Riga	Coordinates: X Y Z
<i>Reference frame: ETRF2000 at epoch 2015.5</i>	3176404.598 1429570.695 5325144.063

Monument	Antenna mounting
 	
Location	
	<p>Site type: -</p> <p>Installation year: 2006</p>



Station name: RIGA	Address: Botanical Gardens of the University of Latvia, Riga			
Network: EPN, IGS	Coordinates: X Y Z			
<i>Reference frame: ETRF2000 at epoch 2015.5</i> 3183899.547 1421478.316 5322810.626				
Monument		Antenna mounting		
				
Location				
		Site type: - Installation year: -		
Residual position time series (daily)				
year	2012	2013	2014	2015
mm				

LIST OF REFERENCES OF THE THESIS

- Abele, M., Balodis, J., Balodis, K., Normand, M., Janpaule, I., Mitrofanovs, I., Rubans, A., Silabriedis, G. and Zarins, A., 2008. Implementation of New Positioning System in Riga. *Int. Symp. EUREF*, 18–20 June 2008, Brussels: 6 pages.
- Abele, M., Balodis, J., Janpaule, I., Lasmane, I., Rubans, A. and Zarins, A., 2012. Digital zenith camera for vertical deflection determination, *Geodesy and Cartography* 38(4): 123–129.
- Agnew, D. C. *Baytap08 User's Manual*, 2013: 30.
- Ågren, J. and Svensson, R. Postglacial land uplift model and system definition for the new Swedish height system RH 2000. LMV-Rapport 2007: 4. *Reports in Geodesy and Geographical Information Systems*, Gävle, 2007: 124.
- Altamimi, Z., Sillard, P. and Boucher, C., 2003. The impact of a No-Net-Rotation Condition on ITRF2000. *Geophysical Research Letters* 30 (2): 1064.
- Balodis, J., Haritonova, D., Janpaule, I., Normand, M., Silabriedis, G., Zarins, A., Rubans, A., Kalinka, M., Jumare, I. and Lasmane, I., 2013. On the geodynamics in Latvia. *Proc. of ESA Living Planet Symposium*, ESA SP-722: 8 pages.
- Balodis, J., Silabriedis, G., Haritonova, D., Kalinka, M., Janpaule, I., Morozova, K., Jumare, I., Mitrofanovs, I., Zvirgzds, J., Kaminskis, J. and Liepiņš, I., 2015a. Development of the one centimeter accuracy geoid model of Latvia for GNSS measurements. Proc. of the 2nd International Conference on Innovative Materials, Structures and Technologies. *IOP Conf. Series: Materials Science and Engineering* 96: 9 pages.
- Balodis, J., Silabriedis, G., Haritonova, D., Morozova, K., Zarins, A. and Rubans, A., 2016. Recent research activities at the Institute of Geodesy and Geoinformatics. *Proc. of ESA Living Planet Symposium*, ESA SP-740: 5 pages.
- Balodis, J., Zarins, A., Haritonova, D. and Janpaule, I., 2014. Parameters for automated star identification. *Geodesy and Cartography* 40 (4): 163–170.
- Balodis, J., Zarins, A., Rubans, A., Haritonova, D. and Kaminskis, J. (b). Digital zenith camera – a new astrometric instrument for precision measurements in geodesy. *The FOTONIKA-LV conference “Achievements and Future prospects”*, 23–24 April 2015, Riga: presentation.
- Available at: <https://fotonikalv.wordpress.com/fotonika-lv-5th-anniversary-conference/>

- Berglund, M., 2004. Holocene shore displacement and chronology in Ångermanland, eastern Sweden, the Scandinavian glacio-isostatic uplift centre. *Boreas* 33 (1): 48–60.
- Beutler, G., Bock, H., Brockmann, E. et al. *User manual of the Bernese GPS Software Version 4.2*, University of Berne, 2000.
- Beutler, G., Bock, H., Dach, R. et al. *User manual of the Bernese GPS Software Version 5.0*, Astronomical Institute, University of Bern, 2007: 612.
- Boucher, C. and Altamimi, Z. *Memo: Specifications for reference frame fixing in the analysis of a EUREF GPS campaign*, 2011: 10.
Available at: <http://etrs89.ensg.ign.fr/memo-V8.pdf>
- Boucher, C., Altamimi, Z. and Duhem, L. ITRF 91 and its associated velocity field. *IERS Technical Note 12*, Paris: Central Bureau of IERS – Observatoire de Paris, 1992: 143.
- Boucher, C., Altamimi, Z. and Sillard, P. The 1997 International Terrestrial Reference Frame (ITRF97). *IERS Technical Note 27*, Paris: Central Bureau of IERS – Observatoire de Paris, 1999: 192.
- Braasch, M., 1996: Multipath Effects. *Parkinson, Spilker (eds.)* 1: 547–568.
- Bruyninx, C., Altamimi, Z., Caporali, A. et al. *Guidelines for EUREF Densifications*, EUREF, 2013: 9.
Available at ftp://epncb.oma.be/pub/general/Guidelines_for_EUREF_Densifications.pdf
- CODE data – available at: <ftp://ftp.unibe.ch/aiub/CODE>
- Dach, R., Andritsch, F., Arnold, D. et al. *User manual of the Bernese GNSS Software Version 5.2*, Astronomical Institute, University of Bern, 2015: 852.
- Doan, M.-L. and Brodsky, E. E. *Tidal analysis of water level in continental boreholes, version 2.2*, Santa Cruz: University of California, 2006: 60.
- Einstein, N. Map of the Baltic Sea, 2006.
Available at: https://commons.wikimedia.org/wiki/File:Baltic_Sea_map.png
- Ekman, M. *The Changing Level of the Baltic Sea during 300 Years: A Clue to Understanding the Earth*, Åland Islands: Summer Institute for Historical Geophysics, 2009: 155.
- Ekman, M., 1998. Secular change of the seasonal sea level variation in the Baltic Sea and secular change of the winter climate. *Geophysica* 34 (3): 131–140.
- Ekman, M., 1996. A consistent map of the postglacial uplift of Fennoscandia. *Terra Nova* 8(2): 158-165.

- Elken, J. and Matthäus, W., 2008. Annex A: physical system description. *The BALTEX Assessment of Climate Change for the Baltic Sea Basin*, Springer-Verlag: 379–398.
- EPN Coordination Group and the EPN Central Bureau. *Guidelines for the EPN Analysis Centres*, EPN Guidelines, 2013: 8.
Available at: <http://www.epncb.oma.be/documentation/guidelines/>
- EUPOS[®] home page. Available at: <http://www.eupos.org/>
- EUPOS[®] ISC. *EUPOS Technical Standards*: Revised 3rd Edition, Resolution 23.2, Tbilisi, Georgia, 7–8 May 2013: 17.
- EUPOS[®]-Riga home page.
Available at: <http://www.rdpad.lv/geotelpiska-informacija/eupos-riga/>
- EUREF. *Terms of Reference*, EUREF 2008 Symposium: Brussels, Belgium, 18–21 June 2008: 3.
- EPN home page. Available at: <http://epncb.oma.be/>
- Fosu, C., 1998. Astrogeodetic Levelling by the Combination of GPS and CCD Zenith Camera. *Studiengang Vermessungswesen, Schriftenreihe UniBw München* 62.
- Gregorius, T. *GIPSY-OASIS II: How it works*, Pasadena: California Institute of Technology, NASA Jet Propulsion Laboratory, 1996.
- Grewal, M. S., Weill, L. R. and Andrews, A. P. *Global Positioning Systems, Inertial Navigation, and Integration, 2nd Edition*, Wiley, New York, 2007: 525.
- Haritonova, D., 2016. Sea level variations at the Latvian coastal hydrologic stations. *Geodesy and Cartography* 42 (2): 31–38.
- Haritonova, D. Earth tide observations and analysis methods. *73rd Annual Scientific Conference of the University of Latvia*, Section: The Project “FOTONIKA-LV – FP7-REGPOT-CT-2011-285912” – the third year scientific outcomes, 6 February 2015, Riga: poster.
Available at: <https://ortus.rtu.lv/science/lv/publications/20130>
- Haritonova, D. GNSS station kinematic coordinate analysis. *71st annual scientific conference of University of Latvia*, Natural sciences photonics, 1 February 2013, Riga: abstract.
Available at: <https://ortus.rtu.lv/science/lv/publications/16131>
- Haritonova, D. (a). GNSS station kinematic coordinate analysis. *Riga Technical University 53rd International Scientific Conference*, dedicated to the 150th Anniversary, the 1st Congress of World Engineers and Riga Polytechnical Institute / RTU Alumni, 11–12 October 2012, Riga: abstract.
Available at: <https://ortus.rtu.lv/science/lv/publications/16138>

- Haritonova, D. (b). The impact of solid Earth tides on the DGNSS positioning results. *United Nations / Latvia Workshop on the Applications of Global Navigation Satellite Systems*, 14–18 May 2012, Riga: presentation.
- Available at:
<http://www.unoosa.org/documents/pdf/psa/activities/2012/un-latvia/ppt/2-11.pdf>
- Haritonova, D., 2012c. Solid Earth tides in the territory of Latvia. *RTU Scientific Proceedings “ĢEOMĀTIKA”*, Riga: 5 pages.
- Haritonova, D. and Balodis, J., 2012. History of tidal effect observations [in Latvian]. In: 53. *RTU Studentu zinātniskās un tehniskās konferences materiāli*: 169–170.
- Available at: <https://ortus.rtu.lv/science/en/publications/18174>
- Haritonova, D., Balodis, J., Janpaule, I., Jumare, I. and Normand, M. (a). Earth’s surface movements in Latvia. *72nd annual scientific conference of University of Latvia*, Section: The Project “FOTONIKA-LV – FP7-REGPOT-CT-2011-285912” – the second year scientific outcomes, 7 February 2014, Riga: poster.
- Available at:
<http://publikacijas.lu.lv/zinatniskie-instituti/lu-geodezijas-un-geoinformatikas-instituts/earths-surface-movements-latvia/>
- Haritonova, D., Balodis, J., Janpaule, I. and Morozova, K., 2015a. Earth’s surface displacements from the GPS time series. *Proc. of the 2nd International Conference on Innovative Materials, Structures and Technologies. IOP Conf. Series: Materials Science and Engineering* 96: 10 pages.
- Haritonova, D., Balodis, J., Janpaule, I. and Normand, M., 2013a. Displacements at the GNSS stations. *Proc. of 4th International Scientific Conference “Civil Engineering’13”*, Latvia University of Agriculture: 5 pages.
- Haritonova, D., Balodis, J., Janpaule, I. and Normand, M. (b). GNSS station displacement analysis. *EGU General Assembly*, 7–12 April 2013, Vienna: poster.
- Available at: <http://meetingorganizer.copernicus.org/EGU2013/posters/11671>
- Haritonova, D., Balodis, J., Zarins, A. and Rubans, A. High precision techniques for Earth’s crust movement observations in Latvia. *EUREF Symposium*, 25–27 May 2016, Donostia – San Sebastian: poster.
- Available at: <http://euref.eu/symposia/2016SanSebastian/p-03-01-Haritonova.pdf>

- Haritonova, D., Balodis, J., Zarins, A., Rubans, A. and Janpaule, I. (b). Application of GNSS observation results to determination of the ground deformations. *EUREF Symposium*, 3–7 June 2014, Vilnius: abstract.
Available at: http://www.nzt.lt/euref2014/Abstracts_book.pdf
- Haritonova, D., Janpaule, I., Rubans, A. and Zarins, A., 2015b. Project of multi-purpose optical tracking system. *EGU General Assembly*, 12–17 April 2015, Vienna: poster.
Available at: http://presentations.copernicus.org/EGU2015-14980_presentation.pdf
- Haritonova, D., Kaminskis, J. and Lasmane, I. (c). Analysis of kinematic coordinates from GNSS stations in Latvia. *NKG Science Week*, 12–14 March 2013, Reykjavik: presentation.
Available at: <https://ortus.rtu.lv/science/lv/publications/22473>
- Haritonova, D., Zarins, A., Rubans, A. and Janpaule, I. (c). Project of multi-purpose optical tracking system: design and deformations of optical system's transmitting path. *1st International Conference "Nocturnal Atmosphere, Remote Sensing and Laser Ranging: NOCTURNAL – Riga 2014"*, 16–22 October 2014, Riga: poster.
Available at: <https://ortus.rtu.lv/science/lv/publications/18936>
- Hirt, C., 2001. Automatic determination of vertical deflections in real-time by combining GPS and digital zenith camera for solving the "GPS-height-problem". *Proc. of the 14th International Technical Meeting of the Satellite Division of the Institute of Navigation*, Salt Lake City: 2540–2551.
- Hofmann-Wellenhof, B., Lichtenegger, H. and Wasle, E. *GNSS – Global Navigation Satellite Systems: GPS, GLONASS, Galileo, and more*, SpringerWienNewYork, 2008: 516.
IGS data – available at: <ftp://igscb.jpl.nasa.gov/igscb/product>
- ILRS / Technology / Modeling [online], [cited November 2015].
Available at: <http://ilrs.gsfc.nasa.gov/technology/modeling/index.html>
- Janpaule, I., Haritonova, D., Balodis, J., Zarins, A., Silabriedis, G. and Kaminskis, J., 2015. Improvement of Latvian geoid model using GNSS/levelling, GOCE data and vertical deflection measurements. *Proc. of 5th International GOCE User Workshop*, ESA SP-728: 4 pages.
- Jenkins, G. M. and Watts, D. G. *Spectral analysis and its applications*, Holden-Day, 1968: 525.

- Jivall, L., 2014. The Maintenance of SWEREF99, including the use of a deformation model. *EUREF Symposium*, 3–7 June 2014, Vilnius: presentation.
Available at: <http://www.euref.eu/symposia/2014Vilnius/Symposium2014-Vilnius.html>
- Jivall, L., Kaminskis, J. and Paršeliūnas, E., 2007. Improvement and extension of ETRS89 in Latvia and Lithuania based on the NKG 2003 GPS campaign. *Geodesy and Cartography* 33 (1): 13–20.
- Kakkuri, J., ed. *Geodesy and geophysics* 115, Finnish Geodetic Institute, Helsinki, 1993: 200.
- Kaminskis, J., Zarins, A., Rothacher, M., Rubans, A., Silabriedis, G., Balodis, J. and Haritonova, D. Astrometric instruments of GGI for geodetic tasks. *EUREF Symposium*, 3–5 June 2015, Leipzig: poster.
- Kenyeres, A. EUPOS Combination centre now extended as EPN densification. *EUPOS ISC meeting*, 6–7 May 2014, Riga: presentation.
- Kenyeres, A. Maintenance of the EPN ETRS89 coordinates. *EUREF TWG Spring Meeting*, 26–27 February 2009, Budapest: presentation.
Available at:
http://www.euref.eu/TWG/EUREF%20TWG%20minutes/49-Budapest2009/03-e-ETRSmaint_TWGregBP.pdf
- Kenyeres, A. and Bruyninx, C., 2009. Noise and Periodic Terms in the EPN Time Series. *Geodetic Reference Frames*, IAG Symposia 134, Springer-Verlag Berlin Heidelberg: 143–148.
- Keruss, M. and Sennikovs, J., 1999. Determination of tides in Gulf of Riga and Baltic Sea. *Proc. International Scientific Colloquium “Modelling of Material Processing”*, 28–29 May 1999, Riga.
- Khan, S. A. *Surface deformations analyzed using GPS time series*, Thesis for PhD degree, University of Copenhagen, Niels Bohr Institute for Astronomy, Physics and Geophysics, 2005: 120.
- Kierulf, H. P., Steffen, H., Simpson, M. J. R., Lidberg, M., Wu, P. and Wang, H., 2014. A GPS velocity field for Fennoscandia and a consistent comparison to glacial isostatic adjustment models. *J. Geophys. Res.: Solid Earth* 119 (8): 6613–6629.
- Lambeck, K., Smither, C. and Ekman, M., 1998. Test of glacial rebound models for Fennoscandia based on instrumented sea- and lake-level records, *Geophys. J. Int.* 135 (2): 375–387.

LatPos home page. Available at: <http://www.latpos.lgia.gov.lv/SpiderWeb/>

LEGMC sea level observations are available at:

<https://www.meteo.lv/en/hidrologija-datu-pieejamiba/?nid=912>

LGIA home page. Available at: <http://map.lgia.gov.lv/>

LGIA National Geodetic Network Database is available at:

<http://geodezija.lgia.gov.lv/start.php>

Lidberg, M. *Motions in the Geodetic Reference Frames – GPS observations*, Technical Report No. 517, Licentiate Thesis, Chalmers University of Technology, Department of Radio and Space Science with Onsala Space Observatory, Göteborg, 2004.

Lidberg, M., Johansson, J. M., Scherneck, H. G. and Davis, J. L., 2007. An improved and extended GPS-derived 3-D velocity field of the glacial isostatic adjustment (GIA) in Fennoscandia, *Journal of Geodesy* 81 (3): 213–230.

Lisitzin, E., 1959. Uninodal seiches in the oscillation system Baltic proper – Gulf of Finland, *Tellus* 11 (4): 459–466.

Madsen, F. and Madsen, B., 1993. A new GPS-network in the Baltic countries. *Symp. of the IAG Subcommission for Europe (EUREF)*, 17–19 May 1993, Budapest: 83–91.

Matthäus, W. *The History of Investigation of Salt Water Inflows into the Baltic Sea – from the Early Beginning to Recent Results*, Marine Science Reports 65, Baltic Sea Research Institute, Warnemünde, 2006: 73.

Medvedsky, M. and Pap, V., 2008. The new pointing model of telescope based on tracking data. *Proc. of the 16th International Workshop on Laser Ranging*, 12–17 October 2008, Poznan: 483–488.

Medvedsky, M. and Suberlak, V., 2002. Mount errors model for the Kyiv SLR station. *Artificial Satellites* 37: 3–16.

Meier, H. E. M., 2006. Baltic Sea climate in the late twenty-first century: a dynamical downscaling approach using two global models and two emission scenarios. *Climate Dynamics* 27 (1): 39–68.

Milne, G. A., Davis, J. L., Mitrovica, J. X., Scherneck, H.-G., Johansson, J. M., Vermeer, M. and Koivula, H., 2001. Space-geodetic constraints on glacial isostatic adjustments in Fennoscandia. *Science* 291 (5512): 2381–2385.

- Nordman, M. *Improving GPS time series for geodynamic studies*, Thesis for PhD degree, Finnish Geodetic Institute, Kirkkonummi, 2010: 59.
- Nordman, M., Poutanen, M., Kairus, A. and Virtanen, J., 2014. Using the Nordic Geodetic Observing System for land uplift studies. *Solid Earth* 5 (2): 673–681.
- Nordman, M., Virtanen, H., Nyberg, S. and Mäkinen, J., 2015. Non-tidal loading by the Baltic Sea: Comparison of modelled deformation with GNSS time series. *GeoResJ* 7: 14–21.
- Ocean tide loading provider. Available at: <http://holt.oso.chalmers.se/loading>
- Omstedt, A., Elken, J., Lehmann, A., Leppäranta, M., Meier, H. E. M., Myrberg, K. and Rutgersson, A., 2014. Progress in physical oceanography of the Baltic Sea during the 2003–2014 period. *Progress in Oceanography* 128: 139–171.
- Peltier, W. R., 1994. Ice age paleotopography. *Science* 265 (5169), 195–201.
- Petit, G. and Luzum, B. IERS Conventions (2010). *IERS Technical Note 36*, Frankfurt am Main: Verlag des Bundesamts für Kartographie und Geodäsie, 2010: 179.
- Podobed, V. V. and Nesterov, V. V. *General Astrometry* [in Russian], Nauka, Moscow, 1975: 552.
- Poutanen, M. and Steffen, H., 2014. Land Uplift at Kvarken Archipelago / High Coast UNESCO World Heritage area. Geophysical Society of Finland, *Geophysica* 50 (2): 49–64.
- Rebischung, P. Upcoming switch to IGS08/igs08.atx [IGSMail-6354], 2011.
Available at: <http://igs08.jpl.nasa.gov/pipermail/igsmail/2011/006346.html>
- Rosenthal, G. European Position Determination System Status and Activities. *3rd Meeting of the International Committee on Global Navigation Satellite Systems*, 8–12 December 2008, Pasadena.
- Ruotsalainen, H., Nordman, M., Virtanen, J. and Virtanen, H., 2015. Ocean tide, Baltic Sea and atmospheric loading model tilt comparisons with interferometric geodynamic tilt observation – case study at Lohja2 geodynamic station, southern Finland. *Journal of Geodetic Science* 5 (1): 156–162.
- Schildknecht, T., 1994. Optical astrometry of fast moving objects using CCD detectors. *Geod. Geophys. Arb. Schweiz* 49.
- Seeber, G. *Satellite Geodesy, 2nd completely revised and extended edition*, Walter de Gruyter, Berlin, New York, 2003: 589.

- Seeber, G. *Satellite Geodesy*, de Gruyter, Berlin, 1993.
- Spada, G. and Melini, D. *SELEN User Manual for Version 2.9*, Computational Infrastructure for Geodynamics, 2013: 60.
Available at: <https://geodynamics.org/cig/software/selen>
- Spilker, J., 1980. GPS signal structure and performance characteristics. *Navigation* 25 (2) (1978), In: *Janiczek (ed.)* (1986) 1: 29–54.
- Steffen, H. Glacial isostatic adjustment: Introduction – Part 1. *SCAR GIA Summer School*, 13–19 September 2015, Gibraltar Island: presentation (by Whitehouse, P. and Bentley, M.).
- Steffen, H. and Wu, P. 2011. Glacial isostatic adjustment in Fennoscandia – a review of data and modeling. *Journal of Geodynamics* 52 (3–4): 169–204.
- Vestøl, O., 2006. Determination of postglacial land uplift in Fennoscandia from leveling, tide-gauges and continuous GPS stations using least squares collocation. *Journal of Geodesy* 80 (5): 248–258.
- Vestøl, O., Ågren, J., Kall, T., Aleksejenko, I., Paršeliūnas, E. and Rūdja, A. A new updated empirical land uplift model. *NKG General Assembly*, 1–4 September 2014, Göteborg: presentation.
Available at:
https://www.lantmateriet.se/globalassets/kartor-och-geografisk-information/gps-och-matning/nkg2014/26_vestol_nkg-general_assembly.pdf
- Virtanen, H. and Mäkinen, J., 2003a. The effect of the Baltic Sea level on gravity at the Metsähovi station. *Journal of Geodynamics* 35 (4–5): 553–565.
- Wübbena, G., 1991. Zur Modellierung von GPS Beobachtungen für die hochgenaue Positionsbestimmung. *Wiss. Arb. Univ. Hannover*, Nr. 168, Hannover.
- Wübbler, Ch. and Krauss, W., 1979. The two-dimensional seiches of the Baltic Sea. *Oceanologica Acta* 2 (4): 435–446.
- Zariņš, A., Haritonova, D., Rubans, A., Silabriedis, G. and Zvirgzds, J., 2016. Field tests of astrometric subsystem. *Geodesy and Cartography* 42 (1): 1–6.
- Zariņš, A., Janpaule, I. and Kaminskis, J., 2014. On reference star recognition and identification. *Geodesy and Cartography* 40 (4): 143–147.

Zarins, A., Rubans, A., Janpaule, I., Haritonova, D., Silabriedis, G. and Barzdis, A. Project of multipurpose optical tracking device – progress report. *73rd Annual Scientific Conference of the University of Latvia*, Section: The Project “FOTONIKA-LV – FP7-REGPOT-CT-2011-285912” – the third year scientific outcomes, 6 February 2015, Riga: abstract.

Available at:

http://www.lu.lv/fileadmin/user_upload/lu_portal/projekti/fotonika-lv/book_of_abstracts_lu73.pdf

Zhaborovsky, V. P., Pap, V. O., Medvedsky, M. M. and Choliy, V., 2012. Error budget model for SLR station 1824 Kyiv-Golosieve telescope. *Bulletin of Ukrainian Earth Orientation Parameters Laboratory* 7: 27–29.

Zvirgzds, J. *Rational system LatPos* [in Latvian], Thesis for PhD degree, Riga Technical University, Department of Geomatics, Riga, 2012: 264.

Zvirgzds, J., 2007. Geodetic measurements using GPS base station system LatPos. *Geomatics* 11, RTU, Riga: 81–89.

CONFIRMATION / APSTIPRINĀJUMS

I hereby declare that the Doctoral Thesis “Evaluation of High-Precision Technique Application for Observations of Earth’s Crust Movements in Latvia” submitted for the review to Riga Technical University for the promotion to the scientific degree of Doctor of Engineering Sciences is my own. I confirm that this Thesis has not been submitted to any other university for the promotion to other scientific degree.

Apstiprinu, ka esmu izstrādājusi promocijas darbu “Augstas precizitātes tehnoloģiju pielietojuma novērtējums Zemes garozas kustību novērojumiem Latvijā”, kas iesniegts izskatīšanai Rīgas Tehniskajā universitātē inženierzinātņu doktora grāda iegūšanai. Promocijas darbs zinātniskā grāda iegūšanai nav iesniegts nevienā citā universitātē.

Diāna HARITONOVA
(signature / paraksts)

.....
(date / datums)